NASA Contractor Report 195415

Analysis of the Progressive Failure of Brittle Matrix Composites

David J. Thomas
S.U.N.Y. at Buffalo
Buffalo, New York

February 1995

Prepared for
Lewis Research Center
Under Grant NAG3–862

National Aeronautics and
Space Administration

ABSTRACT

This report investigates two of the most common modes of localized failures; namely, periodic fiber-bridged matrix cracks, and transverse matrix cracks. A modification of Daniels' bundle theory is combined with Weibull's weakest link theory to model the statistical distribution of the periodic matrix cracking strength for an individual layer. Results of the model predictions are compared with experimental data from the open literature. Extensions to the model are made to account for possible imperfections within the layer (i.e., non-uniform fiber lengths, irregular crack spacing, and degraded in-situ fiber properties), and the results of these studies are presented. A generalized shear-lag analysis is derived which is capable of modeling the development of transverse matrix cracks in material systems having a general multilayer configuration and under states of full in-plane load. A method for computing the effective elastic properties for the damaged layer at the global level is detailed based upon the solution for the effects of the damage at the local level. This methodology is general in nature and is therefore also applicable to $[0_m/90_n]_s$ systems. The characteristic stress-strain response for more general cases is shown to be qualitatively correct (experimental data is not available for a quantitative evaluation), and the damage evolution is recorded in terms of the matrix crack density as a function of the applied strain. Probabilistic effects are introduced to account for the statistical nature of the material strengths, thus allowing cumulative distribution curves for the probability of failure to be generated for each of the example laminates. Additionally,

Oh and Finney's classic work on fracture location in brittle materials is extended and combined with the shear-lag analysis. The result is an analytical form for predicting the probability density function for the location of the next transverse crack occurrence within a crack bounded region. The results of this study verified qualitatively the validity of assuming a uniform crack spacing (as was done in the shear-lag model).

TABLE OF CONTENTS

LIST OF FIGURES

LIST OF TABLES

CHAPTER 1

Introduction

Laminated composite materials can be engineered to exhibit gradual (or progressive) failure as opposed to the less desirable catastrophic failure. Localized failures begin to occur early in the loading history of a laminate, but due to the laminate's ability to redistribute its load internally, the laminate as a whole remains unfailed and continues to perform its load-carrying function. As the loading of the laminate continues, the number of localized failures accumulate and begin to degrade the overall laminate properties, eventually reaching the point at which total laminate failure occurs.

In trying to model laminate failure, it is important to recognize the progressive nature of the failure process in order to obtain a correct strength prediction. Ignoring this behavior, as is done in first ply failure (FPF) theories, leads to failure predictions which are too conservative. When implementing a progressive failure scheme, the unit of failure which is to be considered must be defined. At the macroscopic level, this unit can be assumed to either represent the entire load bearing capacity of a ply ("ply failure"); or this ply can be further sub-divided into smaller units, each corresponding to a particular load bearing mode ("modal failure"). Techniques allowing for such behavior have been pursued

as an improvement over FPF (Petit and Waddoups, 1969; Thomas and Wetherhold, 1991(b)). However, these methods also are conservative because they do not allow for any load carrying capacity of the damaged layer away from the localized failure zone. The load redistribution scheme utilized in this report employs the modal approach with the belief that it better represents the progressive failure nature of the composite. A non-interactive failure function is used in which the individual stresses are assumed to act independently of one another in the failure process. Four potential modes of failure are recognized within each layer (see Figure 1.1). In the longitudinal direction a two-stage failure process is considered. Both of these modes of failure are associated with the in-plane normal stress in the fiber direction, σ_1. The first stage is representative of the periodic matrix cracking (cracks running perpendicular to the fiber direction and bridged by the fibers) predicted by ACK theory. Failure of this mode degrades the stiffness properties of the layer, but the survival of the fibers which bridge these cracks allows continued loading. The second stage of failure deals with the fracture of these bridging fibers. In the transverse direction, a single mode of failure models the occurrence of transverse matrix cracking (through-the-thickness cracks running parallel to the fiber direction). This failure mode is a function of the normal stress, σ_2. The fourth and final mode is an in-plane shear failure associated with the stress τ_{12} (σ_6 in Voigt-contracted notation). The failure functions for each of these modes are given below in equations (1.1) through (1.4).

$$f_{1m} = \frac{\langle \sigma_1 \rangle}{X_{1m}^T} + \frac{\langle -\sigma_1 \rangle}{X_{1m}^C} \tag{1.1}$$

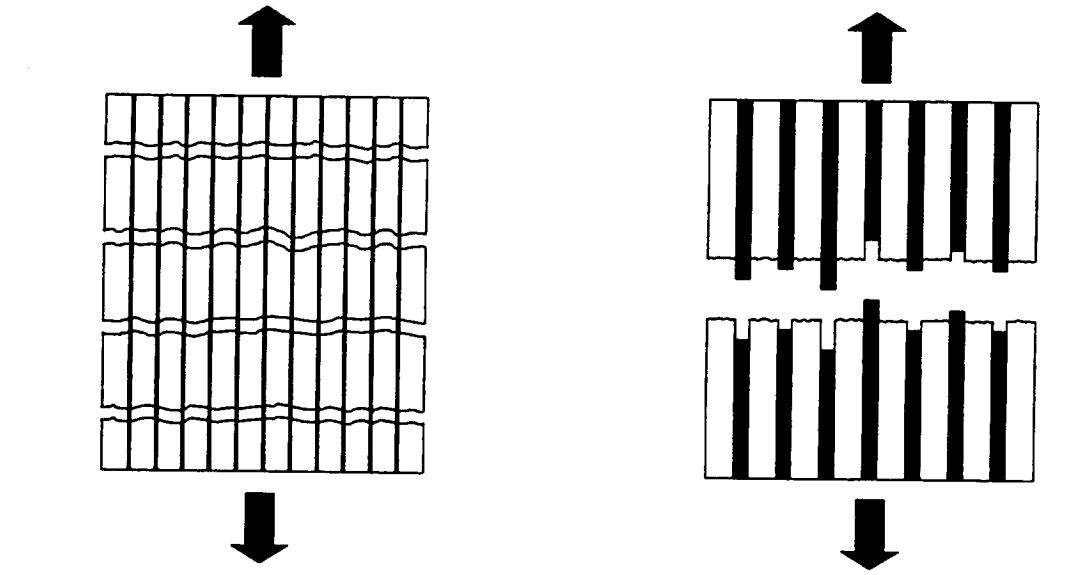

Periodic, bridged matrix cracks

Fiber failure

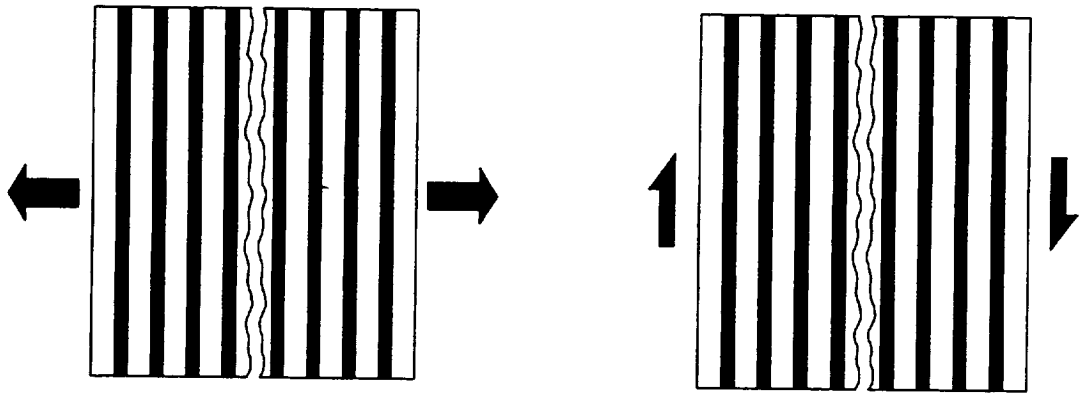

Transverse matrix cracking

Shear failure

Figure 1.1: Potential failure modes for an individual layer.

$$f_{1f} = \frac{\langle \sigma_1 \rangle}{X_{1f}^T} + \frac{\langle -\sigma_1 \rangle}{X_{1f}^C} \tag{1.2}$$

$$f_2 = \frac{\langle \sigma_2 \rangle}{X_2^T} + \frac{\langle -\sigma_2 \rangle}{X_2^C} \tag{1.3}$$

$$f_6 = \frac{\langle \sigma_6 \rangle}{X_6^T} + \frac{\langle -\sigma_6 \rangle}{X_6^C} \tag{1.4}$$

where

$$\langle x \rangle \equiv x \cdot u[x] = \begin{cases} 0 , & x \le 0 \\ x , & x > 0 \end{cases} \tag{1.5}$$

and X_i^T and X_i^C are the tensile and compressive strengths, respectively. Values of f less than one ($f < 1$) designate the safe loading regime, and values of f equal to one($f = 1$) denote failure. (Keep in mind that the shear strengths must be equal, $X_6^T = X_6^C$).

Unlike conventional engineering materials (i.e., metals), where local failures can be relieved by plastic deformation thus allowing their strengths to be considered deterministically, composite materials' brittle nature results in their being characterized by a high variability of material strengths. Therefore, in order for efficient application of these materials, design methods using probabilistic failure analyses must be advanced. As a result, rather than having a clearly defined *fail/no fail* situation as described in the previous paragraph, the situation becomes a matter of evaluating the *probability of failure/survival* (i.e., $Pr(f \le 1)$) for a given system where the material's strengths are

considered to be random variables. Within this report, investigations will be made into modeling both the progressive and probabilistic aspects of failure.

With regard to failure in the form of periodic matrix cracking, the use of a *modified bundle* theory to model the post-matrix cracking state predicted by ACK theory has been proposed (Walls, 1986; Evans and Marshall, 1989). Chapter 2 will present a scheme for incorporating this method into a laminate analysis algorithm which utilizes Monte Carlo simulations to evaluate reliability. Example calculations using this method will be demonstrated and compared with experimental results from the open literature. Some of the problems encountered with the method will be discussed and potential causes will be investigated.

The onset of transverse matrix cracking has been found to be a key occurrence in the laminate failure process, and as a result much research has been devoted to its modeling. Continuum damage models (Talreja, 1985; Nuismer and Tan, 1988) as well as many shear-lag approaches (Garret and Bailey, 1977; Reifsnider, 1978; Laws and Dvorak, 1988; Lee and Daniel, 1990) have been proposed for analyzing cross-ply laminates. Chapter 3 extends the shear-lag method of Lee and Daniel from a two-layer cross-ply system to a general symmetric multilayer system. In Chapter 4, the elasticity problem for the region of the laminate between two parallel matrix cracks having a general off-axis orientation is posed from equilibrium considerations. This is done in terms of the average (through-the-thickness) stresses and solved using the generalized shear-lag relation and the appropriate boundary conditions. A method for modeling the effective elastic behavior of the damaged material based on this solution is detailed. This model is then included in a computer program designed for probabilistic laminate analysis and the results are compared to those

determined using the ply drop-off technique.

In Chapter 5, a cross-ply laminate experiencing transverse matrix cracking under uniaxial longitudinal loading is studied. Combining the solution for the stress state in the damaged layer (determined in Chapter 4) with Oh and Finnie's results for fracture location in brittle solids (Oh and Finnie, 1970) an expression is determined for the probability density function for the location of the occurrence of the next transverse matrix crack. Example problems are presented, and the validity of assuming a uniform crack spacing in models such as that of Chapter 4 is examined qualitatively.

CHAPTER 2

Periodic, Bridged Matrix Cracks

The use of a *modified bundle* theory to model the post-matrix cracking state predicted by ACK theory has been proposed (Walls, 1986; Evans and Marshall, 1989). In this chapter the suitability of this method is examined by incorporating it into a load sharing algorithm for the progressive failure study of composite laminates. Example problems will be presented where both the modified bundle approach as well as a previous version of the load sharing algorithm (Thomas and Wetherhold, 1991(b)) which did not permit separate consideration of periodic matrix cracking have been used. The results of these analyses will be compared to experimental results from the open literature. Some of the problems encountered with the method will be discussed and potential causes will be investigated.

LAMINATE ANALYSIS

Consider an n-layer composite laminate with $4n$ potential failure modes. As a ramp loading is slowly applied some of these modes will begin to fail in some layers. As a

result of these failures, internal loads must be redistributed and stiffnesses reduced. In order to model these occurrences, load sharing rules must be adopted that are both physically plausible and computationally manageable. Failure is assumed to be governed by equations (1.1) through (1.4) of Chapter 1. In the following discussion, a local load sharing scheme will be applied by which the load previously carried by the now-failed mode will be distributed evenly between the two immediately adjacent layers within the laminate. If either of these layers has already failed or contain modes which have failed, that portion of the load is globally redistributed in accordance with the laminate constitutive law (see Jones (1975) for a review composite mechanics). Upon the occurrence of periodic matrix cracking in a particular layer, the Q_{11} and Q_{12} terms of the layer's stiffnesses matrix must be reduced. It is proposed that this reduction be made by the ratio of corresponding strengths for that layer, i.e.,

$$(Q_{1j})_{reduced} = Q_{1j}\left(1-\frac{X_{1m}}{X_{1f}}\right) \qquad ; \quad j = 1,2 \tag{2.1}$$

For all other modes of failure, the appropriate stiffnesses are conservatively reduced to zero. That is to say, in the case of fiber failure Q_{11} and Q_{12} are set to zero, for transverse matrix cracking Q_{22} and Q_{12} are set equal to zero, and finally for the case of in-plane shear failure Q_{66} is set to zero.

STRENGTH EVALUATION

At this point the ideal approach would be to state the problem in terms of a failure tree. However, the number of different branches quickly becomes too large, and any change in

the laminate configuration would require the entire tree to be rebuilt. The use of computer simulations is a more viable alternative method of solution. A sample population of laminates may be created within the computer's memory using realizations. That is, hypothetical sample values of the modal strengths whose frequency of occurrence is weighted in accordance with their distribution. The reliability of the laminate can then be determined for a specified load via a *Monte Carlo* analysis.

The strengths X_{1m}, X_2 and X_6 are random variables assumed to be characterized by a two-parameter Weibull distribution, the parameters of which must be determined experimentally. By inverting these distribution functions and sampling a uniform random variable on $[0,1]$ the needed realizations for these strengths can be obtained. A similar method could also be employed for the strength X_{1f}. However, it has been proposed that the characterization of this strength can be arrived at through more physically based arguments via the application of a modified bundle theory.

After matrix cracking has occurred, the longitudinal strength of the ply is governed by the intact fibers which bridge the matrix crack sites. Daniels (1945) has characterized the strength of a bundle of fibers under a tensile axial load as having a normal distribution with

$$S_u = n s_f \left[1 - b(s_f)\right] \tag{2.2}$$

$$\hat{\sigma} = s_f \sqrt{n b(s_f)\left[1 - b(s_f)\right]} \tag{2.3}$$

where S_u and $\hat{\sigma}$ are the average ultimate load and standard deviation of load, respectively, for the bundle; with n being the number of fibers, $b(s)$ the cumulative distribution function for the failure of a single fiber under load s, and s_f is the fiber load which

maximizes the expression $s[1 - b(s)]$. For the problem at hand, a modification to this theory has been proposed (Walls, 1986; Evans and Marshall, 1989) in which the bridging fibers are taken to be analogous to Daniels' fiber bundle, with the added complexity of the fibers' being embedded in a periodically cracked matrix, thus producing an axial variation in the fiber stress.

Assuming the stress to be constant over the cross sectional area of the fiber, A, the probability of failure for the fiber may be described by a Weibull distribution:

$$b(s) = 1 - \exp\left[-\int_L \left(\frac{\sigma(s,x)}{\beta_l}\right)^{\alpha} dx\right] \tag{2.4}$$

where α is called the Weibull shape parameter and is dimensionless, and β_l is a scale parameter based on length. The value of β_l is not generally measured directly from experiment. Conventionally, tensile failure data is obtained for fiber specimens all having the same experimental test volume, V_0, and with each specimen under a state of uniform uniaxial tensile stress. This data is fit to a Weibull distribution of the form

$$b(\sigma) = 1 - \exp\left[-\left(\frac{\sigma}{\beta}\right)^{\alpha}\right] \quad ; \alpha, \beta > 0 \tag{2.5}$$

The Weibull scale parameter in equation (2.5) is based on the experimental volume, and is inferred directly from the experimental data. From this value of β, the parameter β_l can be obtained from the expression below.

$$\beta_l = \beta\left(\frac{V_0}{A}\right)^{\frac{1}{\alpha}} \tag{2.6}$$

The parameter β has dimensions of [stress] and those of β_l are [stress]$\cdot$[length]$^{1/\alpha}$.

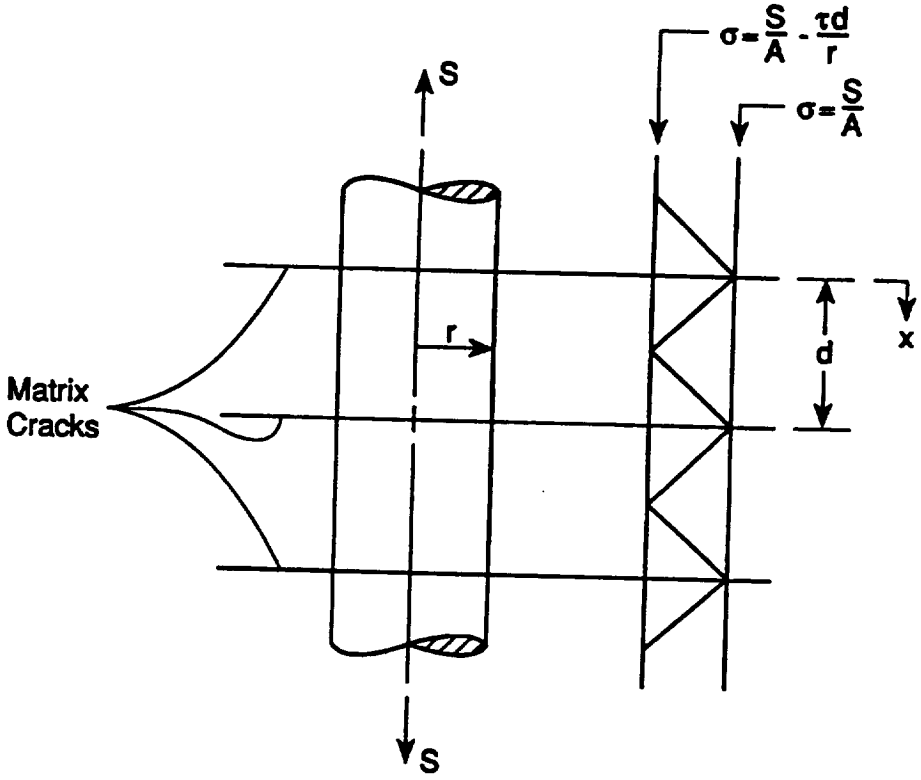

Figure 2.1: Axial normal stress distribution within fiber.

For the case of a fiber which bridges a matrix crack (see Figure 2.1), with the shear stress (τ) at the debonded fiber/matrix interface assumed to be constant, the axial stress distribution within the fiber will be linear. The maximum values will occur at the matrix crack faces and minimum values midway between the cracks. Evaluating the stress through a force balance,

$$\sigma(s,x) = \frac{s}{A} - \frac{2\tau}{r}x \qquad ; \qquad 0 \le x \le \frac{d}{2} \tag{2.7}$$

Here s is defined to be the fiber load at the matrix crack face, x is the longitudinal position measured from the crack face, r is the fiber radius and d is the crack spacing. The value of d must be between x' and $2x'$ (Aveston et al., 1971), where

$$x' = \left(\frac{V_m}{V_f}\right)\frac{\sigma_{mu}r}{2\tau} \tag{2.8}$$

with (V_f, V_m) being the (fiber,matrix) volume fraction and σ_{mu} the critical matrix cracking stress. It will be conservatively assumed that the value of d maintains a uniform value of x'. Using the above expression (equation (2.7)) for the fiber stress in equation (2.4) leads to the following form of the cumulative distribution function for a single fiber.

$$b(s) = 1 - \exp\left\{\frac{\beta_l L r}{\tau d(\alpha+1)}\left[\left(\frac{s}{A\beta_l} - \frac{\tau d}{r\beta_l}\right)^{\alpha+1} - \left(\frac{s}{A\beta_l}\right)^{\alpha+1}\right]\right\} \tag{2.9}$$

Performing the necessary maximization results in an implicit expression for s_f, equation (2.10), which may be solved numerically.

$$s_f = A\beta_l\left\{\frac{\beta_l L r}{\tau d}\left[1 - \left(1 - \frac{\tau A d}{s_f r}\right)^{\alpha}\right]\right\}^{\frac{-1}{\alpha+1}} \tag{2.10}$$

This may in turn be used in equations (2.2) and (2.3) for the mean strength and standard deviation to characterize X_{1f}, the post-matrix-cracking ply strength.

EXAMPLES

The material system for the example problems was a silicon carbide fiber-reinforced / reaction-bonded silicon nitride (SiC/RBSN) tested by Bhatt and Phillips (1990). The test specimens measured 12.7 mm wide, had a gage length of 25 mm, and layer thicknesses

TABLE 2.1
Weibull Strength Parameters for SiC/RBSN
(Bhatt and Phillips, 1990)

Modal strength, X_i	α	β(*MPa*)
X_{1m}	6.5	244.
$(X_1)_{alt}$	5.2	741.
X_2	10.9	28.
X_6^*	7.5	56.

* assumed values

TABLE 2.2
Elastic Material Properties for SiC/RBSN
(Bhatt and Phillips, 1990)

E_1	193. *GPa*
E_2	69. *GPa*
G_{12}	31. *GPa*
ν_{12}	0.21

of 0.25 mm. The fiber volume fraction was 0.3 and the fiber radius was 71×10^{-6} m. The Weibull strength parameters are printed in Table 2.1. They were calculated mathematically from the published values of the respective means and standard deviations. Table 2.2 contains information regarding the elastic material properties. Data was also given for the individual fibers. Twenty (20) separate tensile tests were performed on individual nitrogen-treated SiC fibers at a gage length of 25 mm. The average tensile strength was calculated to be 2860 MPa with a standard deviation of 440 MPa and a Weibull shape parameter of 8.2. From these results a value of 3043 MPa may be inferred for the

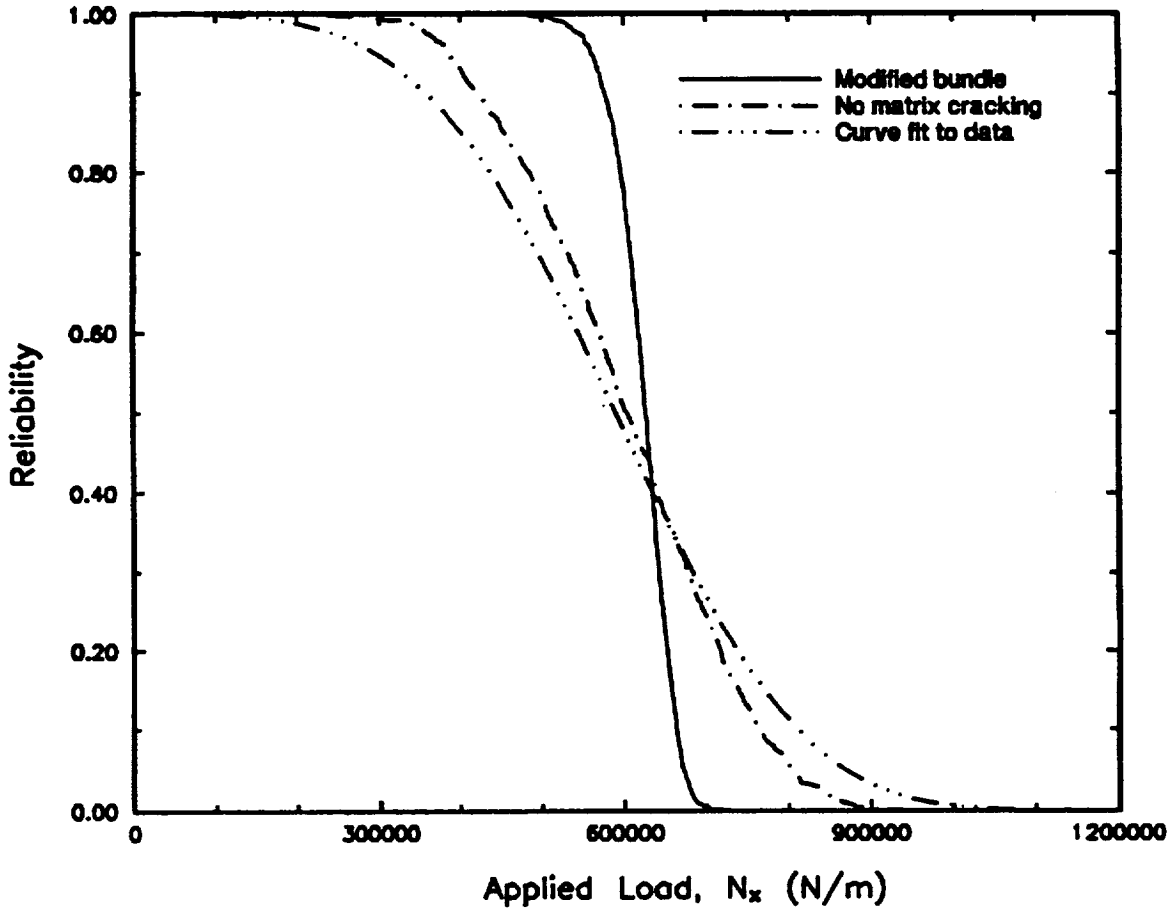

Figure 2.2: Comparison of failure models for $[0_2/90_2]_s$ laminate.

Weibull scale parameter on a unit volume basis, β.

The results of including the modified bundle model in a laminate analysis are shown in Figure 2.2 for a $[0_2/90_2]_s$ laminate and in Figure 2.3 for a $[+45_2/-45_2]_s$ laminate. In addition to these results, each figure also contains results from a similar analysis with the exception that periodic matrix cracking was neglected (i.e., only three potential modes of failure per layer, corresponding strengths were $(X_1)_{ult}, X_2, X_6$), as well as a curve fit to experimentally measured values of the laminate's mean strength and standard deviation (Bhatt and Phillips, 1990). For the $[0_2/90_2]_s$ laminate, the curve for the modified bundle technique shows a very tight distribution and does not agree well with the other two

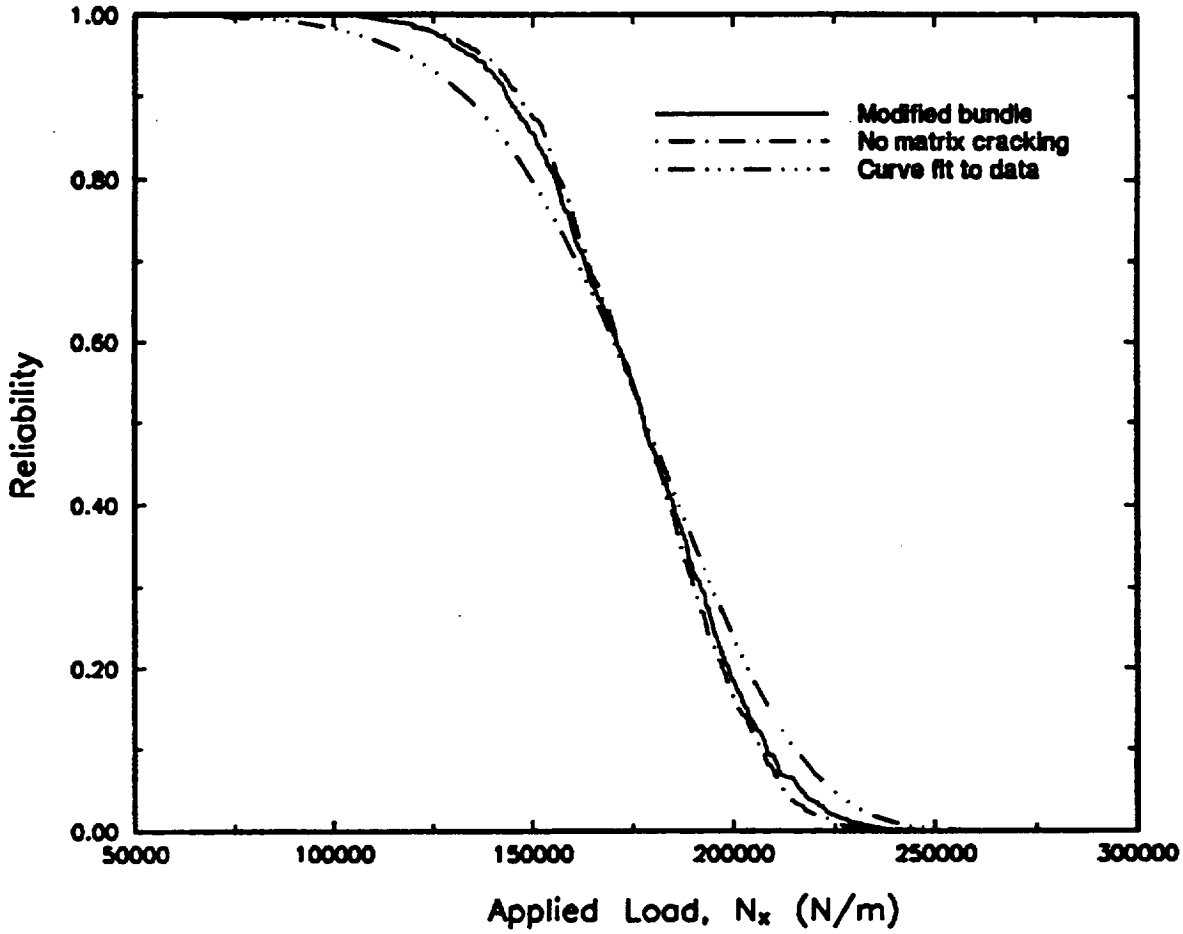

Figure 2.3: Comparison of failure models for $[+45_2/-45_2]_s$ laminate.

curves. A close examination of the results of the simulation that produced this curve found that the mode of failure which ultimately governed the overall failure of the laminate was the longitudinal fiber failure of the 0° layers. Furthermore, the modified bundle prediction for the coefficient of variation (COV) of X_{1f} was approximately 0.05. This value is much lower than the COV value of 0.22 observed experimentally for $(X_1)_{ult}$. The combination of these two factors led to the steep slope of Figure 2.2. For the $[+45_2/-45_2]_s$ laminate the mode of failure which governed the laminate failure was the in-plane shear failure of the layers. Thus the low predicted COV of X_{1f} did not effect these results. No experimental values for the Weibull parameters describing the distribution of the shear

strength X_6 were available. The value of the Weibull scale parameter for X_6 was chosen to be twice that of the scale parameter for X_2, and a parametric study was done using *"reasonable"* values for the Weibull shape parameter. The shape parameter value that gave the best fit, as compared against the experimental data, of the reliability curve for the $[+45_2/-45_2]_s$ laminate was used in Figure 2.3 and is the value listed in Table 2.1.

NON-IDEAL BUNDLE

In an effort to explain the low predicted value for the coefficient of variation of X_{1f} obtained using the modified bundle theory, the effects of certain non-ideal conditions which may have existed, but were not considered in the model, are investigated. While the present theory has accounted for a variability in the strength from fiber to fiber, it has not allowed for any variability in the geometry of the problem. Kerans (1988) has stated that all composite fibers are not identical and that these non-uniformities can produce unintended but desirable characteristics such as increased toughness. Specifically, Kerans studied the effect of non-uniform fiber lengths on the bundle's stress-strain behavior. To find the effect non-uniform fiber lengths would have on the COV of the layer's ultimate strength, a computer program was used to simulate a strain controlled test on a bundle of such fibers. The number of fibers in the bundle was the same as in the experimental test specimens, $n=60$. It was assumed that the bundle represented the complete load bearing capacity of the damaged layer, and thus the layer's strength was calculated by dividing the maximum bundle load by the area of the layer. A series of *Monte Carlo* analyses was performed. A sample population of fiber lengths was simulated for each analysis. Each

sample had a normal distribution which was truncated at arbitrarily imposed minimum and maximum values lying five (5) standard deviations away from the mean. For each case the minimum value was taken to be the nominal bundle length, and various percentages of this value were used for the maximums. The results are shown in Figure (2.4) and in Table 2.3. It can be seen that while non-uniform fiber lengths do increase the coefficient of variation, the magnitude achieved is still much smaller than that observed experimentally and at the same time an adverse effect on the mean strength prediction is experienced.

Until now it has been assumed that the damaged layer has a regular crack spacing of x'. More realistically the crack spacings will be uniformly distributed between the minimum and maximum values of x' and $2x'$ allowed by ACK theory. To study what effect this would have, simulations were conducted keeping the same gage length (L) as in the other analyses but allowing the crack spacings (d_i) to take on random values uniformly distributed between x' and $2x'$. That is to say,

$$L = \sum_{i=1}^{n} d_i \quad ; \quad d_i \in (x', 2x') \tag{2.11}$$

where n is the number of segments necessary to span the entire gage length. Applying the modified bundle theory to a simulation of such a crack field lowered the COV of X_{1f} from 0.0453 to 0.0449. Based on this negligible change, it appears that the assumption of a uniform crack spacing of x' is reasonable and errs on the conservative side.

Lastly, the effect of a degraded in-situ Weibull shape parameter for the fiber was investigated. A parametric study was done over a range of values of from a minimum of 2.0 to a maximum value of 8.2 which was measured experimentally. The COV of X_{1f}

TABLE 2.3
Effect of non-uniform fiber length on bundle strength
Number of fibers = 60 Number of trials = 500

$\frac{L_{max}-L_{min}}{L_{min}} \times 100$	Mean Strength, X_{1f} (MPa)	*cov*	α^*	$\beta^*(MPa)$
0.0	630.1	0.0438	23.79	643.3
0.5	615.8	0.0442	24.51	628.7
1.0	573.8	0.0464	22.36	586.5
2.0	471.4	0.0689	15.61	486.4
3.0	385.0	0.0850	12.68	399.9

* Weibull parameters estimated using maximum likelihood method

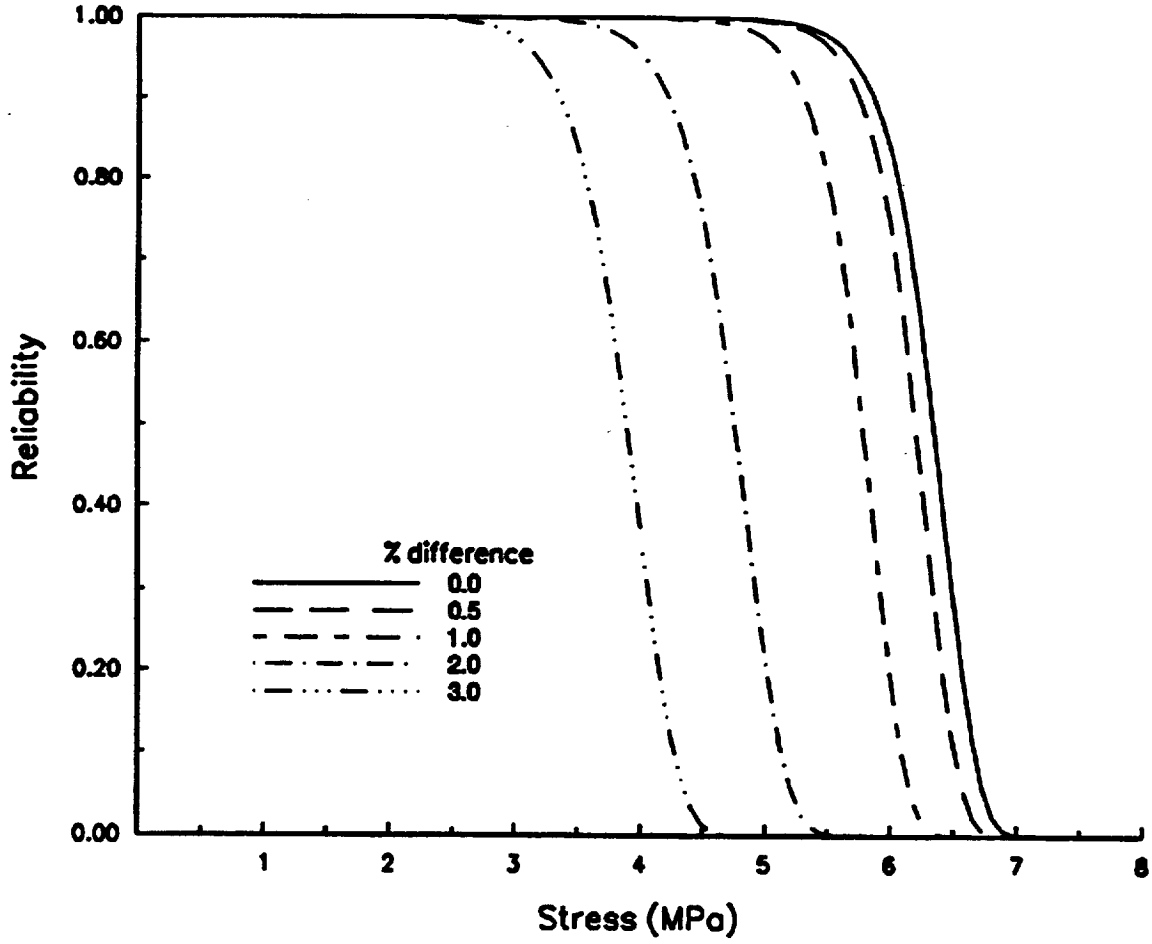

Figure 2.4: Effect of non-uniform fiber lengths on bundle strength.

TABLE 2.4
Modified bundle strength predictions for X_{1f}

α_f	Mean Strength (MPa)	Coefficient of Variation
8.2	658.	0.045
6.0	605.	0.053
4.0	533.	0.067
2.0	416.	0.100
experiment:		
$(X_1)_{ult}$	682.	0.220

increased moderately and the mean strength decreased for a decreasing value in the shape parameter. Complete results are given in Table 2.4.

SUMMARY

The modified bundle theory, even with the irregularities which have been introduced in the previous section, does not adequately predict the variation which is seen experimentally for the post-matrix-cracking longitudinal strength of a layer, X_{1f}. This suggests that the model is ignoring one or more important mechanisms. One possible area to be focused on is the fiber/matrix interface; the interfacial shear stress is not truly a constant, stress concentrations are present on the fiber at the crack face, also the matrix environment makes the reloading of failed fibers away from the failure location possible. However, while there are problems with the modified bundle analysis in its present form, the results of the analyses which simply allow for a complete all-at-once failure in the longitudinal

direction are generally good. This is encouraging for the basic modal analysis and load redistribution scheme.

CHAPTER 3

Generalized Shear-Lag Analysis

The onset of transverse matrix cracking has been found to be a key occurrence in the laminate failure process, and as a result much research has been devoted to its modeling. Continuum damage models (Talreja, 1985; Nuismer and Tan, 1988) as well as many shear-lag approaches (Garret and Bailey, 1977; Reifsnider, 1978; Laws and Dvorak, 1988; Lee and Daniel, 1991) have been proposed for analyzing transverse cracking in cross-ply laminates, but very little work has addressed the problem for layers of arbitrary orientation. In this chapter, the method developed by Lee and Daniel for determining the shear-lag parameters is reviewed and extended. Their original application of the method was for a cross-ply $[0_m/90_n]_s$ laminate; here, the shear-lag relationship will be developed for a generalized system comprised of three arbitrarily oriented layers of the form $[\theta/\phi/\psi]_s$. This generalized shear-lag analysis will then be used in Chapter 4 to aid in the solution of the elasticity problem for the region of a general symmetric laminate between two parallel transverse matrix cracks.

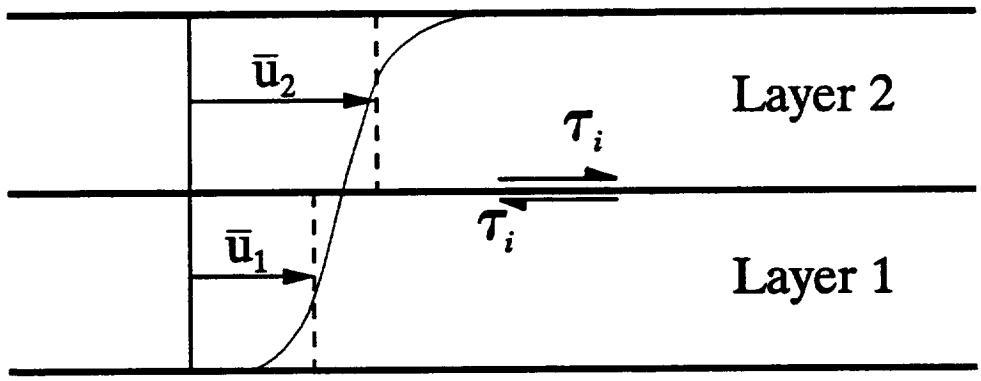

Figure 3.1: Traditional shear-lag model.

SHEAR-LAG METHODOLOGY

Shear-lag analyses are generally set up to relate the shear stress present at the interface between two contiguous bodies to the difference in their respective average displacements. That is to say, for the bodies shown in Figure 3.1, a shear-lag rule applied in the traditional manner would define the shear stress (τ_i) present at the interface between bodies 1 and 2 to be proportional to the difference in the average displacements $(\bar{u}_1$ and $\bar{u}_2)$ observed in each of these bodies.

$$\tau_i = H(\bar{u}_1 - \bar{u}_2) \tag{3.1}$$

The proportionality constant H in the above equation is referred to as the *shear-lag parameter*, and is a property of the entire system.

In regard to the application of shear-lag methods to composite laminates, layers 1 and 2 of Figure 3.1 generally refer to two orthogonal layers which comprise one half of a symmetric laminate system. One of these layers is considered to have undergone some

form of damage, typically transverse matrix cracking, which results in the displacement variation between the layers. If it were not for the damage being present, laminated plate theory would predict a uniform displacement field through the thickness of the system! - in the absence of bending moments and non-symmetric configurations. Various methods exist to evaluate H, employing mechanics, energy principles, hindsight, and combinations of the above. The most methodical and robust approach, in this author's opinion, was proposed by Lee and Daniel (1991) and expanded to two dimensions by Tsai, Daniel and Lee (1990). This is the method which will be adopted for this report, and the remainder of this chapter is devoted to extending this method to a three layer system.

MODEL DERIVATION

The derivation is begun by explicitly defining the system of interest. The laminate is assumed to be symmetric, and therefore attention can be focused on only those layers lying on one side of the laminate's mid-surface. Thus, a six layer laminate reduces to only a three layer system. Considering the case where the middle layer of this three layer system has experienced transverse cracking, the overall goal for this chapter and the next is to determine the effects of this damage on the layer's behavior. That is to say, that the middle layer is the main focus of interest, and therefore, the definition of the problem is setup with this layer in mind. The layer numbering scheme is established in a manner such that the damaged layer is referred to as layer 1, and the two adjacent layers as layers 2 and 3. This is shown in Figure 3.2.

The solution of the problem will be conducted in the material coordinate system of layer

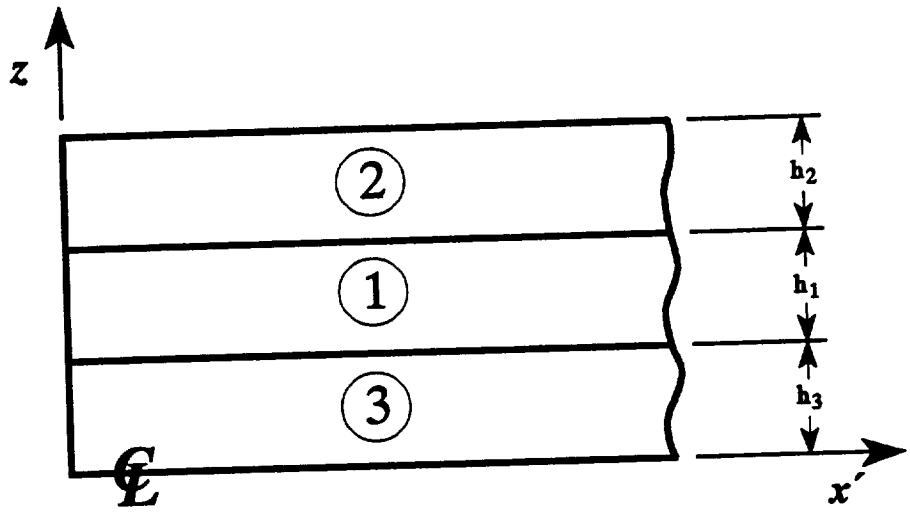

Figure 3.2: Three-layer system.

1. This requires a transformation from the global $x-y$ coordinates of the laminate to the $x'-y'$ coordinates of layer 1 (note that this is an orthogonal transformation about the z axis such that $z'=z$). The system is now sufficiently defined for the derivation to proceed.

Key to this derivation is the assumption that the out-of-plane shear stresses vary linearly through the thickness within each layer. As a result, a quadratic displacement field through the thickness direction for each of the layers is proposed

$$u'_1(x',y',z) = a_1 z^2 + a_2 z + a_3 \tag{3.2}$$

$$v'_1(x',y',z) = a_4 z^2 + a_5 z + a_6 \tag{3.3}$$

$$u'_2(x',y',z) = a_7 z^2 + a_8 z + a_9 \tag{3.4}$$

$$v'_2(x',y',z) = a_{10} z^2 + a_{11} z + a_{12} \tag{3.5}$$

$$u'_3(x',y',z) = a_{13} z^2 + a_{14} z + a_{15} \tag{3.6}$$

$$v'_3(x',y',z) = a_{16} z^2 + a_{17} z + a_{18} \tag{3.7}$$

with u'_i and v'_i designating displacement in the x' and y' directions, respectively, for layer i (where $i=1,2,3$), and the coefficients $a_1, \ldots a_{18}$ representing undetermined

functions of x' and y'.

The constitutive relation for transverse stresses and strains for layer i is given below.

$$\begin{Bmatrix}\tau_{x'z}\\ \tau_{y'z}\end{Bmatrix}_i = \begin{bmatrix}Q'_{55} & Q'_{45}\\ Q'_{45} & Q'_{44}\end{bmatrix}_i \begin{Bmatrix}\gamma_{x'z}\\ \gamma_{y'z}\end{Bmatrix}_i \qquad i=1,2,3 \tag{3.8}$$

(No summation is implied by the repeated subscript in equation (3.8)). The primes on the stiffness terms are present to signify that they have been transformed to the x'-y' coordinate system. These equations can be considered separately from the in-plane constitutive equations because of the assumed orthotropy of the layers (Reismann/Wetherhold, 1988).

The appropriate strain-displacement relations are given in equation (3.9).

$$\gamma^{(i)}_{x'z} = \frac{\partial u'_i}{\partial z} \quad ; \quad \gamma^{(i)}_{y'z} = \frac{\partial v'_i}{\partial z} \tag{3.9a,b}$$

These equations neglect the influence of deformation in the out-of-plane direction, i.e., $\frac{\partial w}{\partial x'}$ and $\frac{\partial w}{\partial y'}$. Utilizing the displacement equations (3.2 - 3.7) as well as the strain-displacement relations (3.9a,b) in the constitutive law yields the following system of equations relating the out-of-plane shear stresses to the unknown coefficients of the displacement equations.

$$\begin{Bmatrix}\tau_{x'z}\\ \tau_{y'z}\end{Bmatrix}_1 = [Q]_1 \begin{Bmatrix}2a_1z+a_2\\ 2a_4z+a_5\end{Bmatrix} \tag{3.10}$$

$$\begin{Bmatrix}\tau_{x'z}\\ \tau_{y'z}\end{Bmatrix}_2 = [Q']_2 \begin{Bmatrix}2a_7z+a_8\\ 2a_{10}z+a_{11}\end{Bmatrix} \tag{3.11}$$

$$\begin{Bmatrix}\tau_{x'z}\\ \tau_{y'z}\end{Bmatrix}_3 = [Q']_3 \begin{Bmatrix}2a_{13}z+a_{14}\\ 2a_{16}z+a_{17}\end{Bmatrix} \tag{3.12}$$

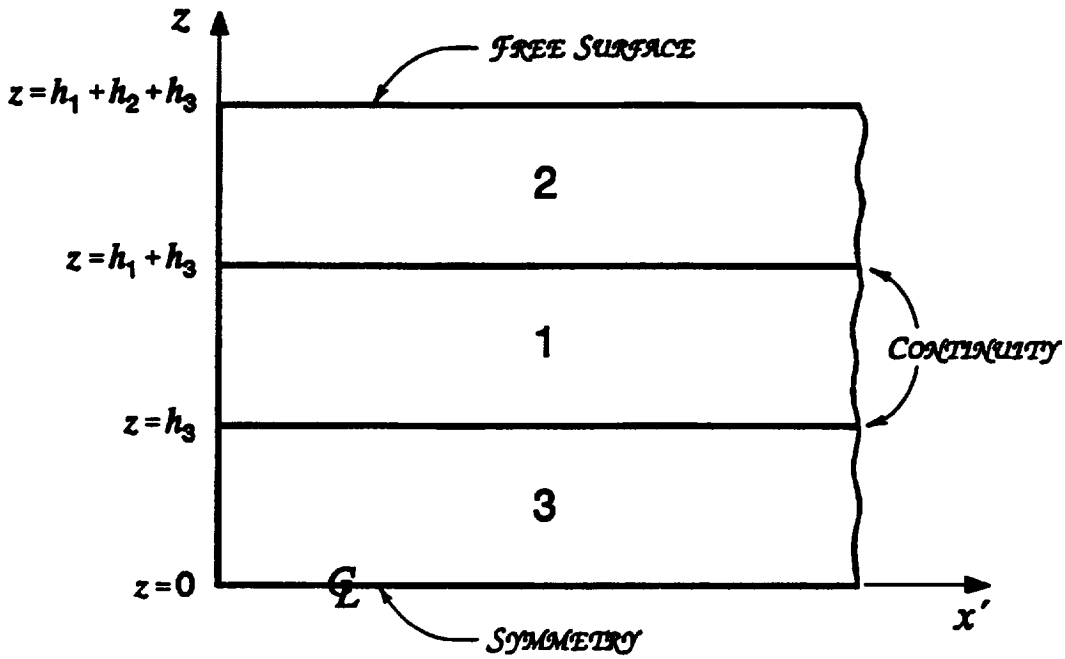

Figure 3.3: Boundary conditions for three-layer system.

Note that use has been made of the fact that the transformed coordinates are aligned with the material coordinates of layer 1, and thus $[Q']_1 = [Q]_1$.

Considering the boundary conditions (see Figure 3.3), states of zero shear exist on the top face of the laminate $(z = h_1+h_2+h_3)$ and at the mid-plane $(z = 0)$,

$$\begin{Bmatrix}\tau_{x'z}(z=h_1+h_2+h_3)\\ \tau_{y'z}(z=h_1+h_2+h_3)\end{Bmatrix}_2 = \begin{Bmatrix}0\\0\end{Bmatrix} \tag{3.13}$$

$$\begin{Bmatrix}\tau_{x'z}(z=0)\\ \tau_{y'z}(z=0)\end{Bmatrix}_3 = \begin{Bmatrix}0\\0\end{Bmatrix} \tag{3.14}$$

and conditions of continuity exist at the two layer interfaces $(z=h_1+h_3,\ z=h_3)$,

$$\begin{Bmatrix}\tau_{x'z}(z=h_1+h_3)\\ \tau_{y'z}(z=h_1+h_3)\end{Bmatrix}_2 = \begin{Bmatrix}\tau_{x'z}(z=h_1+h_3)\\ \tau_{y'z}(z=h_1+h_3)\end{Bmatrix}_1 \equiv \begin{Bmatrix}\tau_{x'z}^{(1-2)}\\ \tau_{y'z}^{(1-2)}\end{Bmatrix} \tag{3.15}$$

$$\begin{Bmatrix} \tau_{x'z}(z=h_3) \\ \tau_{y'z}(z=h_3) \end{Bmatrix}_3 = \begin{Bmatrix} \tau_{x'z}(z=h_3) \\ \tau_{y'z}(z=h_3) \end{Bmatrix}_1 \equiv \begin{Bmatrix} \tau_{x'z}^{(1-3)} \\ \tau_{y'z}^{(1-3)} \end{Bmatrix} \tag{3.16}$$

We have introduced the variable definition $\tau_{x'z}^{(1-2)}$, $\tau_{y'z}^{(1-2)}$, $\tau_{x'z}^{(1-3)}$ and $\tau_{y'z}^{(1-3)}$ to designate the shear stresses present at the interfaces. These stresses are undetermined functions of x' and y'. Applying the above boundary conditions to equations (3.10 - 3.12), the coefficients for the linear and quadratic z terms can be solved for as functions of the interfacial shear stresses, and layer stiffnesses and thicknesses. This results in displacement equations containing the shear stresses and the "a" coefficients of the zero-order z terms as unknowns.

$$\begin{Bmatrix} u' \\ v' \end{Bmatrix}_1 = [Q]_1^{-1} \left[\begin{Bmatrix} \tau_{x'z}^{(1-2)} \\ \tau_{y'z}^{(1-2)} \end{Bmatrix} \frac{z^2 - 2h_3 z}{2h_1} - \begin{Bmatrix} \tau_{x'z}^{(1-3)} \\ \tau_{y'z}^{(1-3)} \end{Bmatrix} \frac{z^2 - 2(h_1+h_3)z}{2h_1} \right] + \begin{Bmatrix} a_3 \\ a_6 \end{Bmatrix} \tag{3.17}$$

$$\begin{Bmatrix} u' \\ v' \end{Bmatrix}_2 = [Q']_2^{-1} \begin{Bmatrix} \tau_{x'z}^{(1-2)} \\ \tau_{y'z}^{(1-2)} \end{Bmatrix} \frac{-z^2 + 2(h_1+h_2+h_3)z}{2h_2} + \begin{Bmatrix} a_9 \\ a_{12} \end{Bmatrix} \tag{3.18}$$

$$\begin{Bmatrix} u' \\ v' \end{Bmatrix}_3 = [Q']_3^{-1} \begin{Bmatrix} \tau_{x'z}^{(1-3)} \\ \tau_{y'z}^{(1-3)} \end{Bmatrix} \frac{z^2}{2h_3} + \begin{Bmatrix} a_{15} \\ a_{18} \end{Bmatrix} \tag{3.19}$$

Requiring displacement continuity for u' and v' at the (1-2) and (1-3) interfaces yields expressions for the last remaining unknown coefficients,

$$\begin{Bmatrix} a_3 - a_9 \\ a_6 - a_{12} \end{Bmatrix} = \left[[Q]_1^{-1} R_1 + [Q']_2^{-1} R_2 \right] \begin{Bmatrix} \tau_{x'z}^{(1-2)} \\ \tau_{y'z}^{(1-2)} \end{Bmatrix} + [Q]_1^{-1} R_3 \begin{Bmatrix} \tau_{x'z}^{(1-3)} \\ \tau_{y'z}^{(1-3)} \end{Bmatrix} \tag{3.20}$$

$$\begin{Bmatrix} a_3 - a_{15} \\ a_6 - a_{18} \end{Bmatrix} = [Q]_1^{-1} R_4 \begin{Bmatrix} \tau_{x'z}^{(1-2)} \\ \tau_{y'z}^{(1-2)} \end{Bmatrix} + \left[[Q]_1^{-1} R_5 + [Q']_2^{-1} R_6 \right] \begin{Bmatrix} \tau_{x'z}^{(1-3)} \\ \tau_{y'z}^{(1-3)} \end{Bmatrix} \tag{3.21}$$

where

$$R_1 = -\frac{(h_1+h_3)(h_1-h_3)}{2h_1} \qquad R_4 = \frac{h_3^2}{2h_1}$$

$$R_2 = \frac{(h_1+h_3)(h_1+2h_2+h_3)}{2h_2} \qquad R_5 = \frac{h_3^2 - 2(h_1+h_3)h_3}{2h_1}$$

$$R_3 = -\frac{(h_1+h_3)^2}{2h_1} \qquad R_6 = \frac{h_3}{2}$$

Equations (3.20) and (3.21) represent a system of four independent equations in terms of six unknowns (a_3, a_6, a_9, a_{12}, a_{15} and a_{18}). There is not sufficient information available to explicitly solve for each of the unknown terms. However, by averaging the displacement equations and subtracting (in order to find the difference in average displacements required for a shear lag analysis), all the unknown coefficients will drop out of the analysis.

The average displacement within each of the layers can be determined by integrating the corresponding displacement equation (i.e., equations (3.17) through (3.19)) over z and dividing by the respective layer thickness. This procedure results in the following set of equations for the average through-the-thickness displacements (note: these displacements are still functions of x' and y').

$$\begin{Bmatrix} \bar{u}'_1 \\ \bar{v}'_1 \end{Bmatrix} = [Q]_1^{-1} \left[R_7 \begin{Bmatrix} \tau_{x'z}^{(1-2)} \\ \tau_{y'z}^{(1-2)} \end{Bmatrix} + R_8 \begin{Bmatrix} \tau_{x'z}^{(1-3)} \\ \tau_{y'z}^{(1-3)} \end{Bmatrix} \right] + \begin{Bmatrix} a_3 \\ a_6 \end{Bmatrix} \tag{3.22}$$

$$\begin{Bmatrix} \bar{u}'_2 \\ \bar{v}'_2 \end{Bmatrix} = [Q']_2^{-1} \begin{Bmatrix} \tau_{x'z}^{(1-2)} \\ \tau_{y'z}^{(1-2)} \end{Bmatrix} R_9 + \begin{Bmatrix} a_9 \\ a_{12} \end{Bmatrix} \tag{3.23}$$

$$\begin{Bmatrix} \bar{u}'_3 \\ \bar{v}'_3 \end{Bmatrix} = [Q']_3^{-1} \begin{Bmatrix} \tau_{x'z}^{(1-3)} \\ \tau_{y'z}^{(1-3)} \end{Bmatrix} R_{10} + \begin{Bmatrix} a_{15} \\ a_{18} \end{Bmatrix} \tag{3.24}$$

where

$$R_7 = \frac{\frac{1}{3}\left[(h_1+h_3)^3 - h_3^3\right] - h_3(h_1+h_3)^2 + h_3^3}{2h_1^2}$$

$$R_8 = -\frac{\frac{1}{3}\left[(h_1+h_3)^3 - h_3^3\right] - (h_1+h_3)^3 + (h_1+h_3)h_3^2}{2h_1^2}$$

$$R_9 = -\frac{\frac{1}{3}\left[(h_1+h_2+h_3)^3 - (h_1+h_3)^3\right] - (h_1+h_2+h_3)^3 + (h_1+h_2+h_3)(h_1+h_3)^2}{2h_2^2}$$

$$R_{10} = \frac{h_3}{6}$$

Subtracting to find the appropriate "differences" in the average displacements results in equations which are functions of the layer stiffness and thickness terms (which are known), the interfacial shear stresses (which are unknown), and the expressions $\begin{Bmatrix} a_3 - a_9 \\ a_6 - a_{12} \end{Bmatrix}$ and $\begin{Bmatrix} a_3 - a_{15} \\ a_6 - a_{18} \end{Bmatrix}$ involving the remaining coefficients from the displacement equations (these are known from equations (3.20) and (3.21)). The final forms of these difference in displacement equations are given below:

$$\begin{Bmatrix} \bar{u}'_1 - \bar{u}'_2 \\ \bar{v}'_1 - \bar{v}'_2 \end{Bmatrix} = [A] \begin{Bmatrix} \tau_{x'z}^{(1-2)} \\ \tau_{y'z}^{(1-2)} \end{Bmatrix} + [B] \begin{Bmatrix} \tau_{x'z}^{(1-3)} \\ \tau_{y'z}^{(1-3)} \end{Bmatrix} \tag{3.25}$$

$$\begin{Bmatrix} \bar{u}'_1 - \bar{u}'_3 \\ \bar{v}'_1 - \bar{v}'_3 \end{Bmatrix} = [C] \begin{Bmatrix} \tau_{x'z}^{(1-2)} \\ \tau_{y'z}^{(1-2)} \end{Bmatrix} + [D] \begin{Bmatrix} \tau_{x'z}^{(1-3)} \\ \tau_{y'z}^{(1-3)} \end{Bmatrix} \tag{3.26}$$

where

$$[A] = -\frac{h_1}{3}[Q]_1^{-1} - \frac{h_2}{3}[Q']_2^{-1}$$

$$[B] = -\frac{h_1}{6}[Q]_1^{-1}$$

$$[C] = \frac{h_1}{6}[Q]_1^{-1}$$

$$[D] = \frac{h_1}{3}[Q]_1^{-1} + \frac{h_3}{3}[Q']_3^{-1}$$

At this point, as a check, the three layer model can be compared to Tsai, Daniel and Lee's two layer model. If layer 3 were no longer present, the (1-3) interface would become the laminate's mid-surface, and as a result the shear stresses $\tau_{x'z}^{(1-3)}$ and $\tau_{y'z}^{(1-3)}$ would be equal to zero due to symmetry considerations. Under these conditions, equation (3.25) becomes

$$\begin{Bmatrix} \bar{u}'_1 - \bar{u}'_2 \\ \bar{v}'_1 - \bar{v}'_2 \end{Bmatrix} = -\left[[Q]_1^{-1} \frac{h_1}{3} + [Q']_2^{-1} \frac{h_2}{3} \right] \begin{Bmatrix} \tau_{x'z}^{(1-2)} \\ \tau_{y'z}^{(1-2)} \end{Bmatrix}$$

which agrees with the published solution (Tsai, et al., 1990) for a two layer system.

Equations (3.25) and (3.26) can be inverted to solve for the shear stresses as a function of the difference in the average in-plane displacements for each of the layers

$$\begin{Bmatrix} \tau_{x'z}^{(1-2)} \\ \tau_{y'z}^{(1-2)} \end{Bmatrix} = [H] \begin{Bmatrix} \bar{u}'_1 - \bar{u}'_2 \\ \bar{v}'_1 - \bar{v}'_2 \end{Bmatrix} + [J] \begin{Bmatrix} \bar{u}'_1 - \bar{u}'_3 \\ \bar{v}'_1 - \bar{v}'_3 \end{Bmatrix} \tag{3.26}$$

$$\begin{Bmatrix} \tau_{x'z}^{(1-3)} \\ \tau_{y'z}^{(1-3)} \end{Bmatrix} = [K] \begin{Bmatrix} \bar{u}'_1 - \bar{u}'_2 \\ \bar{v}'_1 - \bar{v}'_2 \end{Bmatrix} + [L] \begin{Bmatrix} \bar{u}'_1 - \bar{u}'_3 \\ \bar{v}'_1 - \bar{v}'_3 \end{Bmatrix} \tag{3.27}$$

where

$$[L] = \left[[D] - [C][A]^{-1}[B] \right]^{-1} \tag{3.28}$$

$$[H] = [A]^{-1} + [A]^{-1}[B][L][C][A]^{-1} \tag{3.29}$$

$$[J] = -[A]^{-1}[B][L] \tag{3.30}$$

$$[K] = -[L][C][A]^{-1} \tag{3.31}$$

In this form, resemblance to traditional shear-lag analyses can be seen, with the out-of-plane shear stresses at the interfaces being stated explicitly in terms of the differences in the average in-plane displacements. The matrices $[H]$, $[J]$, $[K]$ and $[L]$ are the shear-lag parameters for the system. These parameters are constants which are completely defined by the equations above, and contain only elastic constants and layer thicknesses.

SUMMARY

In this chapter a generalized shear-lag analysis has been developed to model a system comprised of three arbitrarily oriented layers (and thus, a six layer symmetric laminate). The only assumptions made in the development of this model were the linear variation in the out-of-plane shear stresses through the thickness of each layer, and the form of the stress-strain constitutive relationship. These assumptions along with stress and displacement continuity considerations then led to the shear-lag relationship of equations (3.26) and (3.27). This relationship shows the system to be coupled: the shear stresses at the interface

between layer 1 and layer 2 are a function of not only of the displacements in layers 1 and 2, but also the displacement of layer 3. Similarly, the shear stress at the (1-3) interface is coupled to the displacements in all three layers. Were it not for a methodical approach to the derivation of the shear-lag relationship, this coupling effect might very easily be overlooked, and the functional form of the effect would most certainly not be otherwise intuitively determined.

CHAPTER 4

Elasticity Solution of the Three-Layer Problem

As discussed in the Introduction, the failure process in composite laminates often initiates with the onset of transverse matrix cracking within the individual layers. The initiation of transverse cracking within a layer occurs when the transverse stress present within the layer reaches the local strength. This strength value is typically referred to as the *first matrix cracking strength*. When dealing with brittle materials (e.g., ceramics) the purpose of designing with composite materials as opposed to monolithic materials is to reduce the flaw sensitivity of the material system. While this desired effect is realized in a relative sense, brittle matrix composite materials still possess an inherent flaw sensitivity, and as a result the observed strength characteristics for the composite contain scatter. In this report the material strengths are considered to be random variables represented by Weibull distributions. However, even after transverse cracking has occurred within individual layers, the system as a whole can continue to survive due to the in-situ constraints of the laminate system on these individual layers. In fact, due to

shearing effects between neighboring undamaged and damaged layers, the damaged layers themselves can still continue to carry load! In this chapter, the reloading of a damaged layer in the region between two parallel transverse matrix cracks is investigated in detail. This analysis will be carried out for a system of three arbitrarily oriented layers under general in-plane applied load conditions. It will be shown through homogenization techniques that this solution is sufficient to model the damage effects of transverse matrix cracks in ***any*** symmetric laminate.

DEFINING THE PROBLEM

The investigation begins by considering a general symmetric multilayered laminate having a total of $2n$ layers. The corresponding layer thicknesses and orientations are designated by h_j and θ_j, respectively, for $j=1$ to $2n$. It is assumed that the laminate is subjected to a general in-plane load of $(2P_x, 2P_y, 2P_{xy})$. Owing to the laminate's symmetry, attention is restricted to only those layers above the mid-surface (i.e., layers 1 through n), thereby reducing the complexity of the problem by a factor of two. As a result of the applied load, transverse matrix cracking begins to develop in one of the inner layers, namely, layer i. Figure 4.1 depicts a schematic representation of the system just described.

The goal is to determine how the formation of these transverse cracks effects the load-carrying capabilities of the damaged layer, and thus in turn the global level behavior of the entire laminate. To achieve this, the stress state for the region between two parallel transverse cracks of the damaged layer needs to be determined at the local level. This

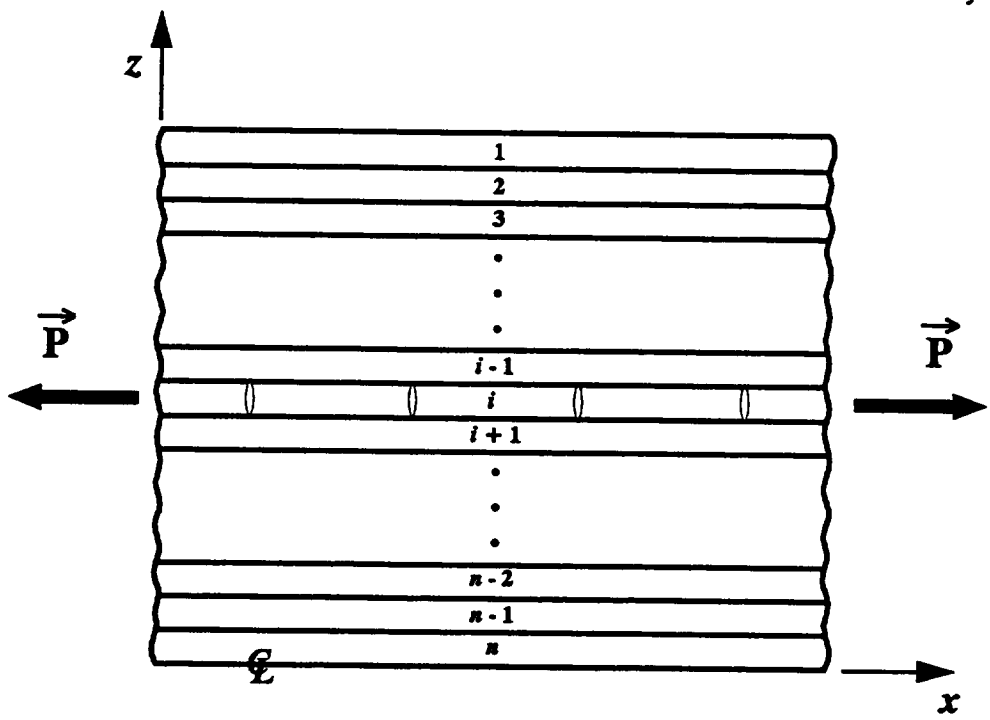

Figure 4.1: Laminate undergoing transverse matrix cracking in layer i.

stress state is a function of position in all three spatial coordinates, i.e. $\{\sigma\}_i = \{\sigma(x,y,z)\}_i$. However, because interested is focused on the in-plane effects of this damage (i.e., the problem deals with a thin plate within the analytical confines of classical laminated plate theory), only functional relationships with respect to x and y are of main interest. Thus, the solution for the average through-the-thickness stress within the layer, $\{\bar{\sigma}\}_i = \{\bar{\sigma}(x,y)\}_i$, is pursued. As a note, throughout the remainder of this chapter, reference to a variable as an *average value* or the use of the *over bar* symbol will always refer to a through-the-thickness average unless otherwise specifically stated.

At the local perspective from which this problem is being approached, only the stress solution for the area in the damaged layer between the two transverse cracks is of concern. The knowledge of the stress state throughout the remainder of the laminate is only of

interest as it affects the damaged region. Thus, in an effort to reduce the complexity of the problem, it is proposed that all layers, other than the damaged layer of interest, be homogenized. This action results in a system which is elastically equivalent at the global level, and has been effectively reduced from n-layers to only 3-layers. This new homogenized system is shown in Figure 4.2. In the new system, the layer numbering scheme has been reordered such that layer $\tilde{1}$ refers to the damaged layer and layers $\tilde{2}$ and $\tilde{3}$ designate the two adjacent layers, with the tildes (~) used to differentiate between the homogenized and original systems. The elastic properties and layer thickness for the damaged layer in the new system, layer $\tilde{1}$, and in the original system, layer i, remain the same, i.e.,

$$[S]_{\tilde{1}} = [S]_i \tag{4.1}$$

$$h_{\tilde{1}} = h_i \tag{4.2}$$

The properties for layers $\tilde{2}$ and $\tilde{3}$ are now given by a thickness weighted average expressed as

$$\left[\bar{S}\right]_{\tilde{2}} = \left[\bar{S}\right]_{\tilde{3}} = \frac{1}{\sum_{j=1}^{n} h_j}\left(\sum_{j=1}^{n} h_j\left[\bar{S}\right]_j\right) \quad ; \quad j \neq i \tag{4.3}$$

$$h_{\tilde{2}} = \sum_{j=1}^{j=i-1} h_j \quad ; \quad h_{\tilde{3}} = \sum_{j=i+1}^{j=n} h_j \tag{4.4}$$

Here $h_{\tilde{2}}$ and $h_{\tilde{3}}$ are the layer thicknesses in the new system, and $\left[\bar{S}\right]_{\tilde{2}}$ and $\left[\bar{S}\right]_{\tilde{3}}$ are the compliance matrices for the homogenized layers. The $\left[\bar{S}\right]$ notation signifies that the compliance matrices have been transformed from the local material coordinates of the layer to the global coordinates of the laminate. Since layers $\tilde{2}$ and $\tilde{3}$ possess the same elastic

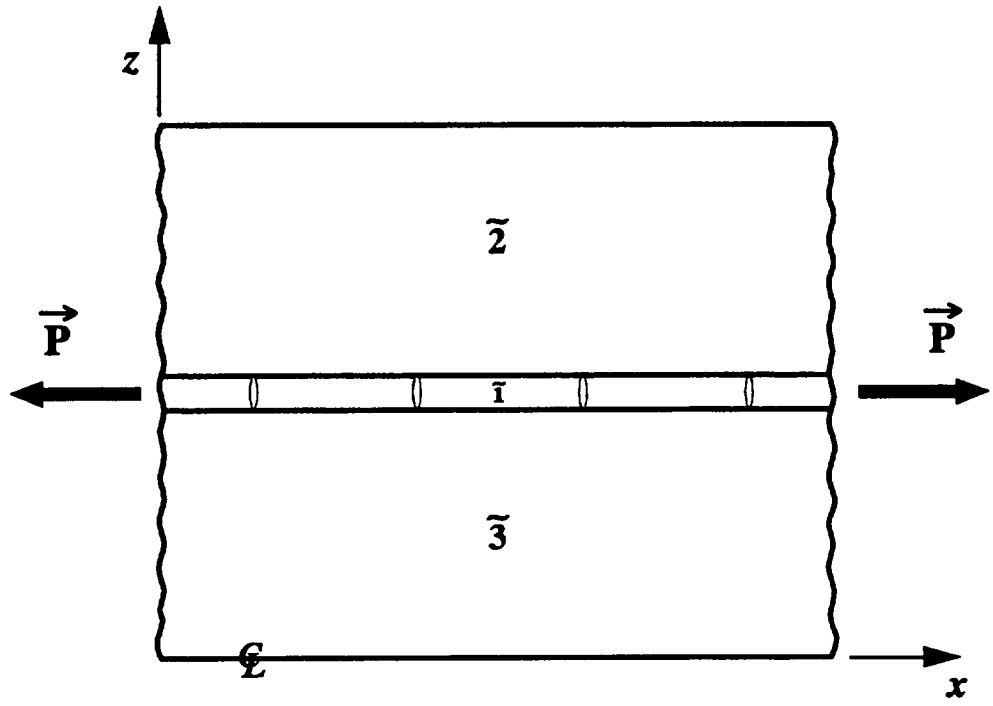

Figure 4.2: Elastically equivalent three layer system.

properties in the homogenized system, the problem to be solved is further simplified.

Figure 4.3(a) shows a top view of the laminate. The matrix cracks in layer $\tilde{1}$ are designated by the dashed lines. It becomes apparent from this view of the problem that the natural coordinate system in which to pursue the solution is the local material coordinate system of the damaged layer. Thus, the problem is set up in the x'-y' coordinates of layer $\tilde{1}$. Note that this is an orthogonal transformation about the z axis such that $z' = z$. A detailed view of the representative system for this problem is shown in Figure 4.3(b). From this point on, all analysis will be conducted for the homogenized system. Therefore, no ambiguity should result from dropping the tildes ($\sim$) from the layer designations in order to ease notation.

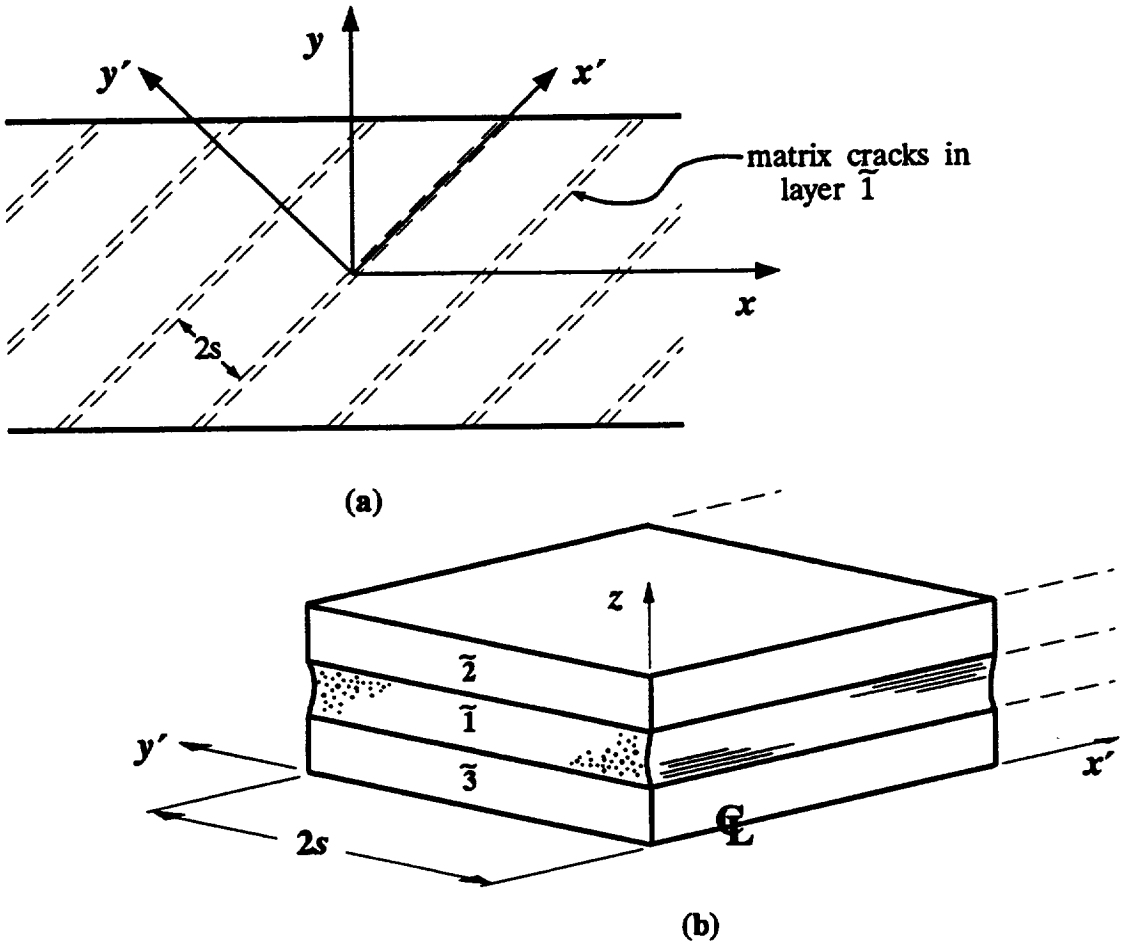

Figure 4.3 (a) Top view of the laminate. (b) Detailed view of the representative volume element to be solved.

PROBLEM SOLUTION

The solution begins with a formulation of the in-plane equilibrium equations for the three-layer system. Consider blocks of differential size in the in-plane directions and with finite thicknesses corresponding to the individual layer thicknesses in the out-of-plane direction (see Figure 4.4). Summation of forces in the x' and y' directions for layer 1 yields,

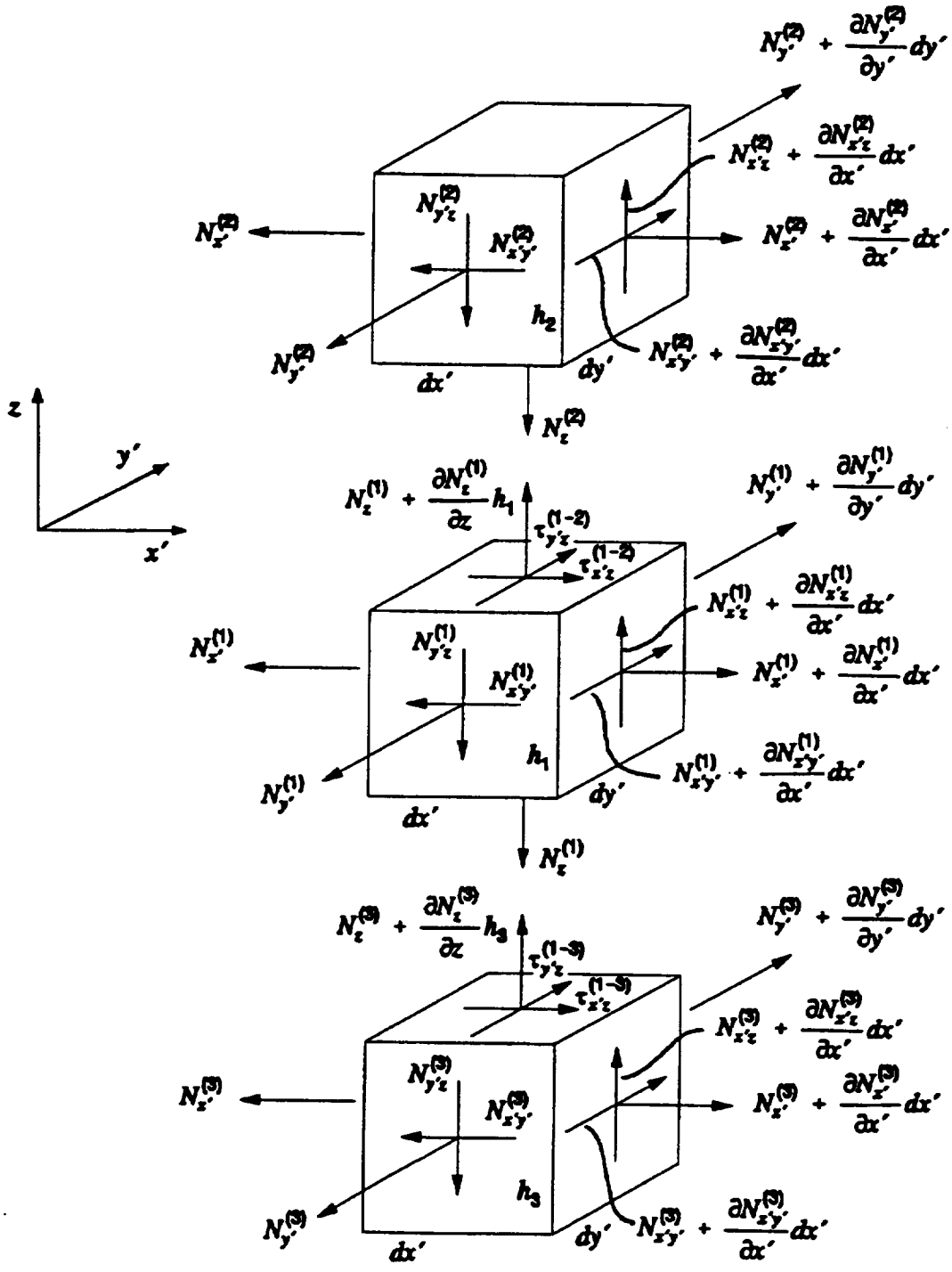

Figure 4.4: Free body diagrams for individual layers in a three-layer system.

$$\sum F_{x'}^{(1)} = 0 = -N_{x'}^{(1)}dy' + \left(N_{x'}^{(1)} + \frac{\partial N_{x'}^{(1)}}{\partial x'}dx'\right)dy' - N_{x'y'}^{(1)}dx' + \left(N_{x'y'}^{(1)} + \frac{\partial N_{x'y'}^{(1)}}{\partial y'}dy'\right)dx' + \tau_{x'z}^{(1-2)}dx'dy' - \tau_{x'z}^{(1-3)}dx'dy' \tag{4.5a}$$

$$\tau_{x'z}^{(1-3)} - \tau_{x'z}^{(1-2)} = \frac{\partial N_{x'}^{(1)}}{\partial x'} + \frac{\partial N_{x'y'}^{(1)}}{\partial y'} \tag{4.5b}$$

$$\sum F_{y'}^{(1)} = 0 = -N_{y'}^{(1)}dx' + \left(N_{y'}^{(1)} + \frac{\partial N_{y'}^{(1)}}{\partial y'}dy'\right)dx' - N_{x'y'}^{(1)}dy' + \left(N_{x'y'}^{(1)} + \frac{\partial N_{x'y'}^{(1)}}{\partial x'}dx'\right)dy' + \tau_{y'z}^{(1-2)}dx'dy' - \tau_{y'z}^{(1-3)}dx'dy' \tag{4.6a}$$

$$\tau_{y'z}^{(1-3)} - \tau_{y'z}^{(1-2)} = \frac{\partial N_{x'y'}^{(1)}}{\partial x'} + \frac{\partial N_{y'}^{(1)}}{\partial y'} \tag{4.6b}$$

In a similar manner, the forces acting on layers 2 and 3 may be summed. The resulting local equilibrium equations for all of the layers are grouped together and presented in equations (4.7) through (4.12) below.

$$\tau_{x'z}^{(1-2)} = \frac{\partial N_{x'}^{(2)}}{\partial x'} + \frac{\partial N_{x'y'}^{(2)}}{\partial y'} \tag{4.7}$$

$$\tau_{y'z}^{(1-2)} = \frac{\partial N_{x'y'}^{(2)}}{\partial x'} + \frac{\partial N_{y'}^{(2)}}{\partial y'} \tag{4.8}$$

$$\tau_{x'z}^{(1-3)} - \tau_{x'z}^{(1-2)} = \frac{\partial N_{x'}^{(1)}}{\partial x'} + \frac{\partial N_{x'y'}^{(1)}}{\partial y'} \tag{4.9}$$

$$\tau_{y'z}^{(1-3)} - \tau_{y'z}^{(1-2)} = \frac{\partial N_{x'y'}^{(1)}}{\partial x'} + \frac{\partial N_{y'}^{(1)}}{\partial y'} \tag{4.10}$$

$$-\tau_{x'z}^{(1-3)} = \frac{\partial N_{x'}^{(3)}}{\partial x'} + \frac{\partial N_{x'y'}^{(3)}}{\partial y'} \tag{4.11}$$

$$-\tau_{y'z}^{(1-3)} = \frac{\partial N_{x'y'}^{(3)}}{\partial x'} + \frac{\partial N_{y'}^{(3)}}{\partial y'} \tag{4.12}$$

We make the assumption that the effects of the transverse cracking are direction-specific. That is to say, the influence of this form of damage is seen as the observer moves in a direction perpendicular to the matrix crack face (y' direction); and if the observer moves parallel to the fiber (x' direction), no damage influence is detected. Thus, all parameters are constant with respect to x' (i.e., $\frac{\partial(\cdot)}{\partial x'}=0$). This simplifies the local equilibrium equations, resulting in ordinary differential equations with independent variable x' only.

$$\tau_{x'z}^{(1-2)} = \frac{dN_{x'y'}^{(2)}}{dy'} \tag{4.13}$$

$$\tau_{y'z}^{(1-2)} = \frac{dN_{y'}^{(2)}}{dy'} \tag{4.14}$$

$$\tau_{x'z}^{(1-3)} - \tau_{x'z}^{(1-2)} = \frac{dN_{x'y'}^{(1)}}{dy'} \tag{4.15}$$

$$\tau_{y'z}^{(1-3)} - \tau_{y'z}^{(1-2)} = \frac{dN_{y'}^{(1)}}{dy'} \tag{4.16}$$

$$-\tau_{x'z}^{(1-3)} = \frac{dN_{x'y'}^{(3)}}{dy'} \tag{4.17}$$

$$-\tau_{y'z}^{(1-3)} = \frac{dN_{y'}^{(3)}}{dy'} \tag{4.18}$$

A further result of this assumption is that displacement continuity between each of the

layers in the x' direction is maintained. Thus,

$$\bar{u}'_1 = \bar{u}'_2 = \bar{u}'_3 \tag{4.19}$$

The objective is to determine the stress state for layer 1. Therefore it is reasonable to look at equations (4.15) and (4.16), which relate the interfacial shear stresses to the in-plane loads for layer 1. Begin with equation (4.16) which specifically deals with the rate change of normal loading in the y' direction as we move away from the crack face.

$$\frac{dN_{y'}^{(1)}}{dy'} = \tau_{y'z}^{(1-3)} - \tau_{y'z}^{(1-2)}$$

This equation contains both in-plane effects (i.e., the loads) and out-of-plane effects (i.e., the shear stresses), but can be written entirely in terms of in-plane effects by making use of the shear-lag equations (3.26) and (3.27). Using these equations, the interfacial shear stresses appearing in this equilibrium equation can be written in terms of the in-plane displacements.

$$\tau_{y'z}^{(1-2)} = H_{12}\left(\bar{u}'_1 - \bar{u}'_2\right) + H_{22}\left(\bar{v}'_1 - \bar{v}'_2\right) + J_{12}\left(\bar{u}'_1 - \bar{u}'_3\right) + J_{22}\left(\bar{v}'_1 - \bar{v}'_3\right) \tag{4.20}$$

$$\tau_{y'z}^{(1-3)} = K_{12}\left(\bar{u}'_1 - \bar{u}'_2\right) + K_{22}\left(\bar{v}'_1 - \bar{v}'_2\right) + L_{12}\left(\bar{u}'_1 - \bar{u}'_3\right) + L_{22}\left(\bar{v}'_1 - \bar{v}'_3\right) \tag{4.21}$$

From the displacement continuity assumption, the difference in the displacement in the x' direction between each layer must be zero, i.e. $\left(\bar{u}'_1 - \bar{u}'_2\right) = \left(\bar{u}'_1 - \bar{u}'_3\right) = 0$. The local equilibrium equation thereby becomes,

$$\frac{dN_{y'}^{(1)}}{dy'} = \left(K_{22} - H_{22}\right)\left(\bar{v}'_1 - \bar{v}'_2\right) + \left(L_{22} - J_{22}\right)\left(\bar{v}'_1 - \bar{v}'_3\right) \tag{4.22}$$

Differentiating this equation with respect to y', and applying the strain-displacement

relation

$$\bar{\epsilon}_{y'} = \frac{d\bar{v}'}{dy'} \tag{4.23}$$

yields a governing differential equation containing both unknown load and strain terms.

$$\frac{d^2 N_{y'}^{(1)}}{dy'^2} = \left(K_{22} - H_{22}\right)\left(\bar{\epsilon}_{y'}^{(1)} - \bar{\epsilon}_{y'}^{(2)}\right) + \left(L_{22} - J_{22}\right)\left(\bar{\epsilon}_{y'}^{(1)} - \bar{\epsilon}_{y'}^{(3)}\right) \tag{4.24}$$

LAYER THICKNESS EFFECT

Thus far the governing equation has been modified from one with mixed in-plane and out-of-plane effects to an equation solely in terms of in-plane terms. The next step involves a further modification to this equation such that the unknowns represent the same physical phenomena (i.e., either strains or loads). By utilizing the constitutive relation for the individual layers, the strains appearing in equation (4.24) can be expressed in terms of the in-plane loads.

$$\bar{\epsilon}_{y'}^{(1)} = \frac{1}{h_1}\left[S_{12}^{(1)} N_{x'}^{(1)} + S_{22}^{(1)} N_{y'}^{(1)} + S_{26}^{(1)} N_{x'y'}^{(1)}\right] \tag{4.25}$$

$$\bar{\epsilon}_{y'}^{(2)} = \frac{1}{h_2}\left[S'^{(2)}_{12} N_{x'}^{(2)} + S'^{(2)}_{22} N_{y'}^{(2)} + S'^{(2)}_{26} N_{x'y'}^{(2)}\right] \tag{4.26}$$

$$\bar{\epsilon}_{y'}^{(3)} = \frac{1}{h_3}\left[S'^{(3)}_{12} N_{x'}^{(3)} + S'^{(3)}_{22} N_{y'}^{(3)} + S'^{(3)}_{26} N_{x'y'}^{(3)}\right] \tag{4.27}$$

It is important to note that though the only stresses contained in these equations are in-plane, this does not imply that a plane stress state is being assumed. Because the individual layers are orthotropic, the in-plane strain and out-of-plane stress are uncoupled.

Therefore, equations (4.25) through (4.27) do not preclude the existence of out-of-plane shear stresses; this is indeed important due to the role they play in the reloading scheme. The primes on the compliance terms are present to signify that they have been transformed to the $x'-y'$ coordinate system (note that no transformations for the compliance terms for layer 1 are necessary).

At this point, two specific examples (one for a two-layer case and another for a three-layer case, see Figure 4.5) and an inconsistency is detected. In the two-layer case, a layer containing transverse cracks is faced on one side by an undamaged layer which provides for reloading the damaged layer. The related three-layer case has been created by basically "splitting up" the undamaged layer from the two-layer case into two separate layers and placing one on each face of the damaged layer. The governing differential equation for the two-layer case is given below,

$$\left(\frac{d^2 N_{y'}^{(1)}}{dy'^2}\right)_{2\text{-layer case}} = \hat{H}\left(\bar{\epsilon}_{y'}^{(1)} - \bar{\epsilon}_{y'}^{(2)}\right)_{2\text{-layer case}} \tag{4.28}$$

where $\hat{H}$ designates the shear-lag parameter for the two layer case (Lee and Daniel, 1991); the governing equation for the three-layer case is given in equation (4.24).

The elastic properties are the same for the two cases, therefore the loads are related as follows,

$$\left(N^{(1)}\right)_{3\text{-layer case}} = \left(N^{(1)}\right)_{2\text{-layer case}} \tag{4.29}$$

$$\left(N^{(2)}\right)_{3\text{-layer case}} = \frac{1}{2}\left(N^{(2)}\right)_{2\text{-layer case}} \tag{4.30}$$

Calculation of the strains using the constitutive relations above leads to the incorrect prediction that the difference between the strains of layer 1 and layer 2 are the same for

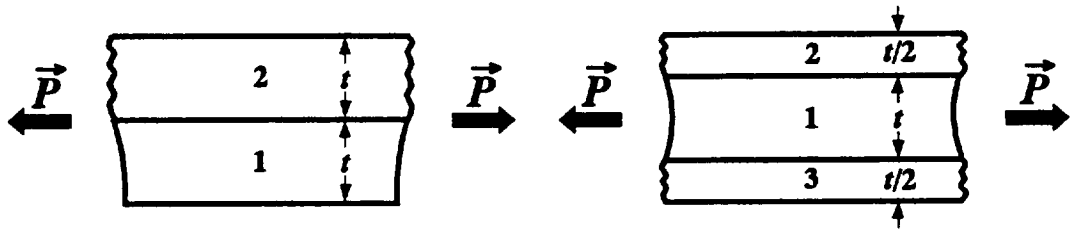

Figure 4.5: Related two-layer and three-layer cases.

both cases. In actuality, it is known that there is a thickness effect present such that as the thickness of the facing layer decreases, the difference in the strains also decreases. Thus, the relationship sought to predict is:

$$\left(\bar{\epsilon}_{y'}^{(1)} - \bar{\epsilon}_{y'}^{(2)}\right)_{2\text{-layer case}} > \left(\bar{\epsilon}_{y'}^{(1)} - \bar{\epsilon}_{y'}^{(2)}\right)_{3\text{-layer case}} \tag{4.31}$$

In order to achieve this prediction, the introduction of a correction term becomes necessary.

In proposing the form of the thickness correction terms, terms are defined such that the rate of reloading is the same in both cases. Thus the following relationship is required to hold true,

$$\left(\frac{d^2 N_{y'}^{(1)}}{dy'^2}\right)_{2\text{-layer case}} = \left(\frac{d^2 N_{y'}^{(1)}}{dy'^2}\right)_{3\text{-layer case}} \tag{4.32}$$

This condition may be restated using the shear-lag relationships,

$$\begin{aligned} \hat{H}\left(\bar{\epsilon}_{y'}^{(1)} - \bar{\epsilon}_{y'}^{(2)}\right)_{2\text{-layer}} = {} & \delta_2 (K_{22} - H_{22}) \left(\bar{\epsilon}_{y'}^{(1)} - \bar{\epsilon}_{y'}^{(2)}\right)_{3\text{-layer}} \\ & + \delta_3 (L_{22} - J_{22}) \left(\bar{\epsilon}_{y'}^{(1)} - \bar{\epsilon}_{y'}^{(3)}\right)_{3\text{-layer}} \end{aligned} \tag{4.33}$$

where thickness correction terms, δ_2 and δ_3, for layers 2 and 3 respectively, have been introduced to modify the difference in strain terms. For this example case, upon evaluating the shear-lag parameters, we find

$$(K_{22}-H_{22}) = (L_{22}-J_{22}) = 2\times\hat{H} \tag{4.34}$$

Additionally, because the elastic properties are the same in the two facing layers, the strains in these layers are the same.

$$\bar{\epsilon}_y^{(2)} = \bar{\epsilon}_y^{(3)} \tag{4.35}$$

Substituting this information into equation (4.33) results in the following condition on the thickness correction terms,

$$\delta_2 + \delta_3 = \frac{1}{2} \tag{4.36}$$

The ensuing additional conditions are imposed,

$$\delta_2 = \delta_3 = \frac{1}{4} \qquad \text{if} \quad h_2 = h_3 \tag{4.37}$$

$$\delta_2 = 0 \;;\; \delta_3 = \frac{1}{2} \qquad \text{if} \quad h_2 = 0 \tag{4.38}$$

$$\delta_2 = \frac{1}{2} \;;\; \delta_3 = 0 \qquad \text{if} \quad h_3 = 0 \tag{4.39}$$

The following forms which satisfy the above conditions are proposed for the correction terms.

$$\delta_2 = \frac{h_2}{2(h_2+h_3)} \quad ; \quad \delta_3 = \frac{h_3}{2(h_2+h_3)} \tag{4.40}$$

An alternative interpretation (Tsai, 1993) to the discrepancy between the two-layer and three-layer formulations is that a facing layer, regardless of its thickness (or lack thereof),

provides reloading support to the system; and thus the fact that the solution for predicted shear force transmitted to the damaged layer is discontinuous at the transition point from a two-layer to a three-layer system should not be unexpected.

This author believes that "real life" lies somewhere in between these two interpretations. That is to say, that a three-layer configuration provides a more efficient reloading mechanism, yet there still must be some thickness effect present. The perspective of Tsai would over-predict the reloading capability of the system, and thus err unconservatively. Whereas the interpretation of the thickness effect presented in this section approaches the correct solution in the limit, while erring on the conservative side. Thus, it is this thickness effect model which is adopted for the remainder of this body of work.

SOLUTION (continued)

In the homogenized system, the elastic parameters for layers 2 and 3 are the same, and as a result $\bar{\epsilon}_{y'}^{(2)} = \bar{\epsilon}_{y'}^{(3)}$. The governing differential equation for the three-layer case thus becomes

$$\frac{d^2 N_{y'}^{(1)}}{dy'^2} = \psi_{22}\left(\bar{\epsilon}_{y'}^{(2)} - \bar{\epsilon}_{y'}^{(1)}\right) \tag{4.41}$$

where ψ_{22} is a known constant which is a function of the shear-lag parameters and the layer thicknesses.

$$\psi_{22} = \frac{1}{2(h_2 + h_3)}\left[h_2\left(H_{22} - K_{22}\right) + h_3\left(J_{22} - L_{22}\right)\right] \tag{4.42}$$

Substitution for the strains using the constitutive relations (equations 4.25-4.27) produces

a governing differential equation entirely expressed in terms of in-plane loads.

$$\frac{d^2 N_{y'}^{(1)}}{dy'^2} = \psi_{22}\left\{\frac{1}{h_2}\left[S'^{(2)}_{12}N_{x'}^{(2)} + S'^{(2)}_{22}N_{y'}^{(2)} + S'^{(2)}_{26}N_{x'y'}^{(2)}\right] - \frac{1}{h_1}\left[S_{12}^{(1)}N_{x'}^{(1)} + S_{22}^{(1)}N_{y'}^{(1)} + S_{26}^{(1)}N_{x'y'}^{(1)}\right]\right\} \quad (4.43)$$

However, as it stands this one equation contains six unknowns and thus five additional independent equations must be found. From global equilibrium considerations (see Appendix A) three of the necessary equations are obtained.

$$P_{x'} = N_{x'}^{(1)} + N_{x'}^{(2)} + N_{x'}^{(3)} = N_{x'}^{(1)} + \left(1 + \frac{h_3}{h_2}\right)N_{x'}^{(2)} \quad (4.44)$$

$$P_{y'} = N_{y'}^{(1)} + N_{y'}^{(2)} + N_{y'}^{(3)} = N_{y'}^{(1)} + \left(1 + \frac{h_3}{h_2}\right)N_{y'}^{(2)} \quad (4.45)$$

$$P_{x'y'} = N_{x'y'}^{(1)} + N_{x'y'}^{(2)} + N_{x'y'}^{(3)} = N_{x'y'}^{(1)} + \left(1 + \frac{h_3}{h_2}\right)N_{x'y'}^{(2)} \quad (4.46)$$

These can be used to solve for the in-plane loads of layer 2 in terms of the in-plane loads of layer 1 and the loads $P_{x'}, P_{y'}$ and $P_{x'y'}$ (transformed from the known applied loads P_x, P_y and P_{xy}, see Appendix B). Continuing the previously made assumption of displacement continuity in the x' direction implies that the normal strains in this direction for each layer are equal.

$$\bar{\epsilon}_{x'}^{(1)} = \bar{\epsilon}_{x'}^{(2)} \quad (4.47)$$

This equation can be used to solve for $N_{x'}^{(1)}$ in terms of the remaining unknown terms. Substitution of these results into equation (4.43) produces a second order, ordinary differential equation with only two remaining unknowns, $N_{y'}^{(1)}$ and $N_{x'y'}^{(1)}$.

$$\frac{d^2 N_{y'}^{(1)}}{dy'^2} = \psi_{22}\left(\alpha N_{y'}^{(1)} + \eta N_{x'y'}^{(1)} + \beta\right) \quad (4.48)$$

The coefficients α, η and β are constants which are algebraic functions of the elastic and shear-lag parameters, and β also contains the applied loading terms,

$$\alpha = \left[\left(\frac{S_{11}^{(1)}}{h_1} + \frac{S'^{(2)}_{11}}{h_2+h_3}\right)^{-1}\left(\frac{S_{12}^{(1)}}{h_1} + \frac{S'^{(2)}_{12}}{h_2+h_3}\right)^2 - \left(\frac{S_{22}^{(1)}}{h_1} + \frac{S'^{(2)}_{22}}{h_2+h_3}\right)\right] \tag{4.49}$$

$$\eta = \left[\left(\frac{S_{11}^{(1)}}{h_1} + \frac{S'^{(2)}_{11}}{h_2+h_3}\right)^{-1}\left(\frac{S_{12}^{(1)}}{h_1} + \frac{S'^{(2)}_{12}}{h_2+h_3}\right)\left(\frac{S_{16}^{(1)}}{h_1} + \frac{S'^{(2)}_{16}}{h_2+h_3}\right) - \left(\frac{S_{26}^{(1)}}{h_1} + \frac{S'^{(2)}_{26}}{h_2+h_3}\right)\right] \tag{4.50}$$

$$\beta = A_1 P_{x'} + A_2 P_{y'} + A_3 P_{x'y'} \tag{4.51}$$

where

$$A_1 = \frac{1}{h_2+h_3}\left[S'^{(2)}_{12} - S'^{(2)}_{11}\left(\frac{S_{11}^{(1)}}{h_1} + \frac{S'^{(2)}_{11}}{h_2+h_3}\right)^{-1}\left(\frac{S_{12}^{(1)}}{h_1} + \frac{S'^{(2)}_{12}}{h_2+h_3}\right)\right] \tag{4.52a}$$

$$A_2 = \frac{1}{h_2+h_3}\left[S'^{(2)}_{22} - S'^{(2)}_{12}\left(\frac{S_{11}^{(1)}}{h_1} + \frac{S'^{(2)}_{11}}{h_2+h_3}\right)^{-1}\left(\frac{S_{12}^{(1)}}{h_1} + \frac{S'^{(2)}_{12}}{h_2+h_3}\right)\right] \tag{4.52b}$$

$$A_3 = \frac{1}{h_2+h_3}\left[S'^{(2)}_{26} - S'^{(2)}_{16}\left(\frac{S_{11}^{(1)}}{h_1} + \frac{S'^{(2)}_{11}}{h_2+h_3}\right)^{-1}\left(\frac{S_{12}^{(1)}}{h_1} + \frac{S'^{(2)}_{12}}{h_2+h_3}\right)\right] \tag{4.52c}$$

The last required equation comes from the set of local equilibrium equations. Using equation (4.15), and applying the shear-lag relations along with the necessary thickness correction terms, a second order ordinary differential equation for $N_{x'y'}^{(1)}$ is achieved which is similar in form to equation (4.41).

$$\frac{d^2 N_{x'y'}^{(1)}}{dy'^2} = \psi_{12}\left(\bar{\epsilon}_{y'}^{(2)} - \bar{\epsilon}_{y'}^{(1)}\right) \tag{4.53}$$

where

$$\psi_{12} = \frac{1}{2(h_2 + h_3)}\left[h_2(H_{12} - K_{12}) + h_3(J_{12} - L_{12})\right] \tag{4.54}$$

Following a procedure similar to the one outlined above, this differential equation can be reformulated such that it contains the known constants ψ_{12}, α, η and β, and the unknown loads $N_{y'}^{(1)}$ and $N_{x'y'}^{(1)}$.

$$\frac{d^2 N_{x'y'}^{(1)}}{dy'^2} = \psi_{12}\left(\alpha N_{y'}^{(1)} + \eta N_{x'y'}^{(1)} + \beta\right) \tag{4.55}$$

Thus with equations (4.48) and (4.55) a system of two coupled, second order, ordinary differential equations is obtained. The boundary conditions for this problem are homogeneous owing to the traction-free crack surfaces,

$$N_{y'}^{(1)}(y'=0) = N_{y'}^{(1)}(y'=2s) = 0 \tag{4.56}$$

$$N_{x'y'}^{(1)}(y'=0) = N_{x'y'}^{(1)}(y'=2s) = 0 \tag{4.57}$$

where $2s$ is the distance between two parallel matrix cracks. This system can be uncoupled at the expense of increasing the order of differentiation, resulting in the following fourth order, homogeneous differential equation,

$$\frac{d^4 N_{y'}^{(1)}}{dy'^4} - \left(\alpha\psi_{22} + \eta\psi_{12}\right)\frac{d^2 N_{y'}^{(1)}}{dy'^2} = 0 \tag{4.58}$$

with the new boundary conditions,

$$N_{y'}^{(1)}(0) = N_{y'}^{(1)}(2s) = 0 \tag{4.59}$$

and

$$\frac{d^2N_{y'}^{(1)}(0)}{dy'^2} = \frac{d^2N_{y'}^{(1)}(2s)}{dy'^2} = \beta\psi_{22} \tag{4.60}$$

The solution of this equation for $N_{y'}^{(1)}(y')$ then leads directly to $N_{x'}^{(1)}(y')$ and $N_{x'y'}^{(1)}(y')$ being known as well. The final forms of the solution for all three in-plane loads of layer 1 can now be written as

$$N_{x'}^{(1)}(y') = B_1\sinh(\lambda y') + B_2\cosh(\lambda y') + B_3 \tag{4.61}$$

$$N_{y'}^{(1)}(y') = B_4\sinh(\lambda y') + B_5\cosh(\lambda y') + B_6 \tag{4.62}$$

$$N_{x'y'}^{(1)}(y') = B_7\sinh(\lambda y') + B_8\cosh(\lambda y') + B_9 \tag{4.63}$$

with expressions for λ and the coefficients B_1 through B_9 given below:

$$\lambda = +\sqrt{\alpha\psi_{22} + \eta\psi_{12}}$$

$$B_4 = \frac{\beta\psi_{22}}{\lambda^2}\,\frac{1-\cosh(2\lambda s)}{\sinh(2\lambda s)} \qquad B_7 = \left(\frac{\lambda^2}{\psi_{22}} - \alpha\right)\frac{B_4}{\eta}$$

$$B_5 = \frac{\beta\psi_{22}}{\lambda^2} \qquad B_8 = \left(\frac{\lambda^2}{\psi_{22}} - \alpha\right)\frac{B_5}{\eta}$$

$$B_6 = -B_5 \qquad B_9 = -B_8$$

$$B_1 = \left(\frac{S_{11}^{(1)}}{h_1} + \frac{S'^{(2)}_{11}}{h_2+h_3}\right)^{-1}\left[-B_4\left(\frac{S_{12}^{(1)}}{h_1} + \frac{S'^{(2)}_{12}}{h_2+h_3}\right) - B_7\left(\frac{S_{16}^{(1)}}{h_1} + \frac{S'^{(2)}_{16}}{h_2+h_3}\right)\right]$$

$$B_2 = \left(\frac{S_{11}^{(1)}}{h_1} + \frac{S'^{(2)}_{11}}{h_2+h_3}\right)^{-1}\left[-B_5\left(\frac{S_{12}^{(1)}}{h_1} + \frac{S'^{(2)}_{12}}{h_2+h_3}\right) - B_8\left(\frac{S_{16}^{(1)}}{h_1} + \frac{S'^{(2)}_{16}}{h_2+h_3}\right)\right]$$

$$B_3 = \left(\frac{S_{11}^{(1)}}{h_1} + \frac{S'^{(2)}_{11}}{h_2+h_3}\right)^{-1}\left[-B_6\left(\frac{S_{12}^{(1)}}{h_1} + \frac{S'^{(2)}_{12}}{h_2+h_3}\right) - B_9\left(\frac{S_{16}^{(1)}}{h_1} + \frac{S'^{(2)}_{16}}{h_2+h_3}\right) + \frac{S'^{(2)}_{11}P_{x'} + S'^{(2)}_{12}P_{y'} + S'^{(2)}_{16}P_{x'y'}}{h_2+h_3}\right]$$

This solution for cases where a full general in-plane loading is applied is dependent upon a non-zero value for the shear-lag terms ψ_{22} and ψ_{12}. The value of ψ_{22} will always be non-zero; however, for certain laminate configurations $\psi_{12} = 0$. Further details are discussed in Appendix C.

Finally, the shear stresses at the interfaces can be calculated. From the local equilibrium equations, the shear stresses at the (1-2) interface are known in terms of the in-plane loads of layer 2,

$$\tau_{x'z}^{(1-2)} = \frac{dN_{x'y'}^{(2)}}{dy'} \tag{4.64}$$

$$\tau_{y'z}^{(1-2)} = \frac{dN_{y'}^{(2)}}{dy'} \tag{4.65}$$

Combining the solutions for the in-plane loads of layer 1 with the overall equilibrium equations (4.44) through (4.46), the loads for layer 2 may be determined and equations (4.64) and (4.65) can be evaluated.

$$\tau_{x'z}^{(1-2)} = \frac{h_2}{h_2+h_3}\left[-B_7\lambda\cosh(\lambda y') - B_8\lambda\sinh(\lambda y')\right] \tag{4.66}$$

$$\tau_{y'z}^{(1-2)} = \frac{h_2}{h_2+h_3}\left[-B_4\lambda\cosh(\lambda y') - B_5\lambda\sinh(\lambda y')\right] \tag{4.67}$$

Similarly, from the local equilibrium equations for layer 1,

$$\tau_{x'z}^{(1-3)} - \tau_{x'z}^{(1-2)} = \frac{dN_{x'y'}^{(1)}}{dy'} \tag{4.68}$$

$$\tau_{y'z}^{(1-3)} - \tau_{y'z}^{(1-2)} = \frac{dN_{y'}^{(1)}}{dy'} \tag{4.69}$$

These equations yield expressions for the shear stresses at the (1-3) interface.

$$\tau_{x'z}^{(1-3)} = \left(1 - \frac{h_2}{h_2 + h_3}\right)\left[B_7 \lambda \cosh(\lambda y') + B_8 \lambda \sinh(\lambda y')\right] \tag{4.70}$$

$$\tau_{y'z}^{(1-3)} = \left(1 - \frac{h_2}{h_2 + h_3}\right)\left[B_4 \lambda \cosh(\lambda y') + B_5 \lambda \sinh(\lambda y')\right] \tag{4.71}$$

EFFECTIVE ELASTIC BEHAVIOR

The in-plane loads of a damaged layer within the region between two transverse matrix cracks have now been completely solved for. The next step is to determine how this layer will effectively behave, from a macro-level viewpoint, within the laminate. In examining this behavior, the interest is in the in-plane-average responses (in contrast to the average through-the-thickness that has been discussed up to this point). In order to emphasize that the averages being considered in this section are with regard to both the thickness of the layer as well as the in-plane length, a *double over bar* notation $\bar{\bar{(\cdot)}}$ is introduced to signify that the average is with respect to both dimensions, and the *single over bar* notation is continued to denote averages taken with respect to thickness only.

The effective compliance of layer 1, $[\hat{S}]_1$, is defined by the relationship between the

in-plane-average strain of the layer, $\{\bar{\bar{\epsilon}}\}_1$, and the in-plane-average stress, $\{\bar{\bar{\sigma}}\}_1$, as shown below,

$$\begin{Bmatrix} \bar{\bar{\epsilon}}_{x'} \\ \bar{\bar{\epsilon}}_{y'} \\ \bar{\bar{\gamma}}_{x'y'} \end{Bmatrix}_1 = \begin{bmatrix} \hat{S}_{11} & \hat{S}_{12} & 0 \\ \hat{S}_{12} & \hat{S}_{22} & 0 \\ 0 & 0 & \hat{S}_{66} \end{bmatrix}_1 \begin{Bmatrix} \bar{\bar{\sigma}}_{x'} \\ \bar{\bar{\sigma}}_{y'} \\ \bar{\bar{\tau}}_{x'y'} \end{Bmatrix}_1 \tag{4.72}$$

Modeling the material in this fashion provides a measure of the effective "secant" (as opposed to "tangential") behavior of the layer. That is, if the applied strain is assumed to be removed from the layer, the layer's load will decrease to zero (the origin of the stress-strain diagram) linearly. Upon reloading, the layer will again behave linearly until reaching the previous load state. Further straining beyond this point can result in additional damage accumulation and a reduction in the effective modulus as just described. Expressions for the in-plane-average stress can be determined by integrating the stress equations (found by dividing equations 4.61 through 4.63 for the in-plane loads by the layer thickness; i.e., $\bar{\sigma}^{(i)} = N^{(i)}/h_i$) over the crack bounded region. Note that these equations are independent of x'; as a result, averaging is only necessary over y'. For the average stress of layer 1 in the x' direction, this yields

$$\begin{aligned} \bar{\bar{\sigma}}_{x'}^{(1)} &= \frac{1}{2s}\int_0^{2s} \frac{N_{x'}^{(1)}(y')}{h_1}\,dy' \\ &= \frac{B_1}{2h_1\lambda s}[\cosh(2\lambda s)-1] + \frac{B_2}{2h_1\lambda s}\sinh(2\lambda s) + \frac{B_3}{h_1} \end{aligned} \tag{4.73}$$

and similarly for the remaining stress terms,

$$\bar{\bar{\sigma}}^{(1)}_{y'} = \frac{B_4}{2h_1\lambda s}[\cosh(2\lambda s)-1] + \frac{B_5}{2h_1\lambda s}\sinh(2\lambda s) + \frac{B_6}{h_1} \tag{4.74}$$

$$\bar{\bar{\tau}}^{(1)}_{x'y'} = \frac{B_7}{2h_1\lambda s}[\cosh(2\lambda s)-1] + \frac{B_8}{2h_1\lambda s}\sinh(2\lambda s) + \frac{B_9}{h_1} \tag{4.75}$$

The above equations can be used to determine the average in-plane stresses based on the far-field applied loads (which the coefficients B_1 through B_9 depend on) and the crack spacing ($2s$). The size of this crack spacing can be determined in an iterative manner. Transverse cracking occurs when the in-plane transverse stress ($\bar{\sigma}_{y'}$) reaches the material's transverse strength (X_2). From the form of equation (4.62), it can be seen that the transverse stress reaches its maximum value at the midpoint of the crack spacing. Therefore, by iterating on the value of the half crack spacing, s, until the calculated value of the stress at the midpoint reaches the strength value, i.e. $\bar{\sigma}_{y'}(y'=s) = X_2$, the crack spacing can be determined.

Remembering that it is the effective global behavior of the layer within the laminate that is being modeled, it is reasonable to assume that the average strains appearing in equation (4.72) are equal to the mid-plane strains of the laminate.

$$\begin{Bmatrix} \bar{\bar{\epsilon}}_{x'} \\ \bar{\bar{\epsilon}}_{y'} \\ \bar{\bar{\gamma}}_{x'y'} \end{Bmatrix}_1 = \begin{Bmatrix} \epsilon^o_{x'} \\ \epsilon^o_{y'} \\ \gamma^o_{x'y'} \end{Bmatrix} \tag{4.76}$$

With this assumption, equation (4.72) relates the in-plane average stress of the layer (which can be calculated) to the strains of the laminate (which can either be measured or

calculated), all of which are known. The only unknowns are the four compliance terms.

The assumption has previously been made that the damage effects due to transverse matrix cracking are restricted to the y' direction. This implies that the effective Young's modulus in the x' direction should remain unchanged,

$$\hat{E}_1 = E_1 \tag{4.77}$$

and as a result the effective compliance term $\hat{S}_{11}$ can be solved for.

$$\hat{S}_{11} = \frac{1}{\hat{E}_1} = \frac{1}{E_1} = S_{11} \tag{4.78}$$

This leaves only three remaining unknown terms in the effective compliance matrix, and these can be found using the three equations comprising equation (4.72).

$$\hat{S}_{12} = \frac{1}{\overset{=(1)}{\sigma}_{y'}}\left(\epsilon^{\circ}_{x'} - S_{11}\overset{=(1)}{\sigma}_{x'}\right) \tag{4.79}$$

$$\hat{S}_{22} = \frac{1}{\overset{=(1)}{\sigma}_{y'}}\left(\epsilon^{\circ}_{y'} - \hat{S}_{12}\overset{=(1)}{\sigma}_{x'}\right) \tag{4.80}$$

$$\hat{S}_{66} = \frac{\gamma^{\circ}_{x'y'}}{\overset{=(1)}{\tau}_{x'y'}} \tag{4.81}$$

Finally, the effective engineering constants (i.e., Young's moduli, shear moduli, Poisson's ratios - all being described in the secant manner) for the damaged layer can be determined from the effective compliance matrix. The definitions for the compliance terms as functions of the engineering constants are given below,

$$S_{11} = \frac{1}{E_1} \qquad S_{12} = -\frac{\nu_{12}}{E_1}$$

$$S_{22} = \frac{1}{E_2} \qquad S_{66} = \frac{1}{G_{12}}$$

Substituting the effective compliance terms into the above relations, and solving for the engineering constants yields

$$\hat{E}_1 = E_1 \qquad \hat{E}_2 = \frac{1}{\hat{S}_{22}}$$

$$\hat{G}_{12} = \frac{1}{\hat{S}_{66}} \qquad \hat{\nu}_{12} = -\frac{\hat{S}_{12}}{\hat{S}_{11}}$$

These engineering constants describe how the damaged layer effectively behaves within the laminate system. In the next section, the ability to model the effective behavior of the damaged material will be used to perform progressive failure studies for example laminates.

EXAMPLES

In this section, specific example problems are investigated to verify that the generalized shear-lag model and the traditional shear-lag model agree for simple cross-ply systems, as well as to look at the more complex material and load configurations which the generalized model is capable of examining. The computer code (PFRAC, see Appendix D) used in the analyses models the progressive failure of composite laminates under strain-controlled conditions. The material strengths are considered to be random variables of known distri-

TABLE 4.1
Material Properties for Graphite/Epoxy
(Lee and Daniel, 1990)

Longitudinal modulus	144.8 GPa
Transverse modulus	10.7 GPa
In-plane shear modulus	7.2 GPa
Out-of-plane shear modulus	3.8 GPa
In-plane major Poisson's ratio	0.285
Longitudinal tensile strength	2167.7 MPa
Transverse tensile strength	54.5 MPa
Longitudinal compressive strength	-1440.3 MPa
Transverse compressive strength	-227.5 MPa
In-plane shear strength	82.0 MPa
Interlaminar shear strength*	113.0 MPa
Ply thickness	0.000127 m

*Agarwal and Broutman, 1980

bution, and multiple modes of failure (i.e., longitudinal, transverse, and shear) are considered within each layer. As individual modes fail, corresponding stiffness reductions are made via the methods of the previous section as well as by traditional ply drop-off (or in this case *mode drop-off*) techniques. Monte Carlo methods are employed to determine the cumulative distribution function for the laminate.

In the first example, agreement between a conventional shear-lag model (Lee and Daniel, 1991; Tsai, et al., 1990) and the generalized model developed in Chapters 3 and 4 is demonstrated for simple cross-ply laminates. The above referenced work examined a $[0/90_4]_s$ graphite/epoxy (Gr/Ep) laminate. The material strengths were assumed to be deterministic, and thus the four 90° layers were considered to behave as one, resulting in

the conventional two-layer system. The material parameters can be found in Table 4.1. The Lee and Daniel analysis was performed for a load-controlled system, as opposed to the strain-controlled system mentioned above for the PFRAC code. Therefore, a modified version of the code is used for this example problem to allow for a direct comparison.

This material system is examined for two laminate configurations, the $[0/90_4]_s$ laminate studied by Lee and Daniel, and additionally, a $[0_{1/2}/90_4/0_{1/2}]_s$ laminate which is explored to review the three layer capability of the generalized model. The analysis simulates a monotonic loading in the 0° direction. The $[0/90_4]_s$ laminate was analyzed using both the generalized and the conventional shear-lag models, and the $[0_{1/2}/90_4/0_{1/2}]_s$ laminate was analyzed using the generalized model. The resulting stress/strain curves are shown in Figure 4.6. As can be seen by the nearly coincident curves, very good agreement between the models is found. Additionally, it can be noted that a higher load to failure is predicted for the $[0_{1/2}/90_4/0_{1/2}]_s$ laminate. This can be attributed to the three-layer system's generating lower interlaminar shear stresses than the two-layer system, and thus allowing efficient load transfer up to a higher applied load level.

For the remaining examples, a four problem test matrix is established by examining two different material geometries as well as two different material systems (Gr/Ep and SiC/RBSN). The ability of the generalized shear-lag model to handle more complex laminate configurations is explored using laminate lay-ups of $[0/15/80/-15/-80]_s$ and $[0/30/60/-30/-60]_s$. In order to perform the reliability analysis for the Gr/Ep material, Weibull strength parameters are needed, and are listed in Table 4.2 (note that it is assumed that the tensile and compressive strengths are equivalent). Experimentally determined values for the out-of-plane material properties of the SiC/RBSN system were not available.

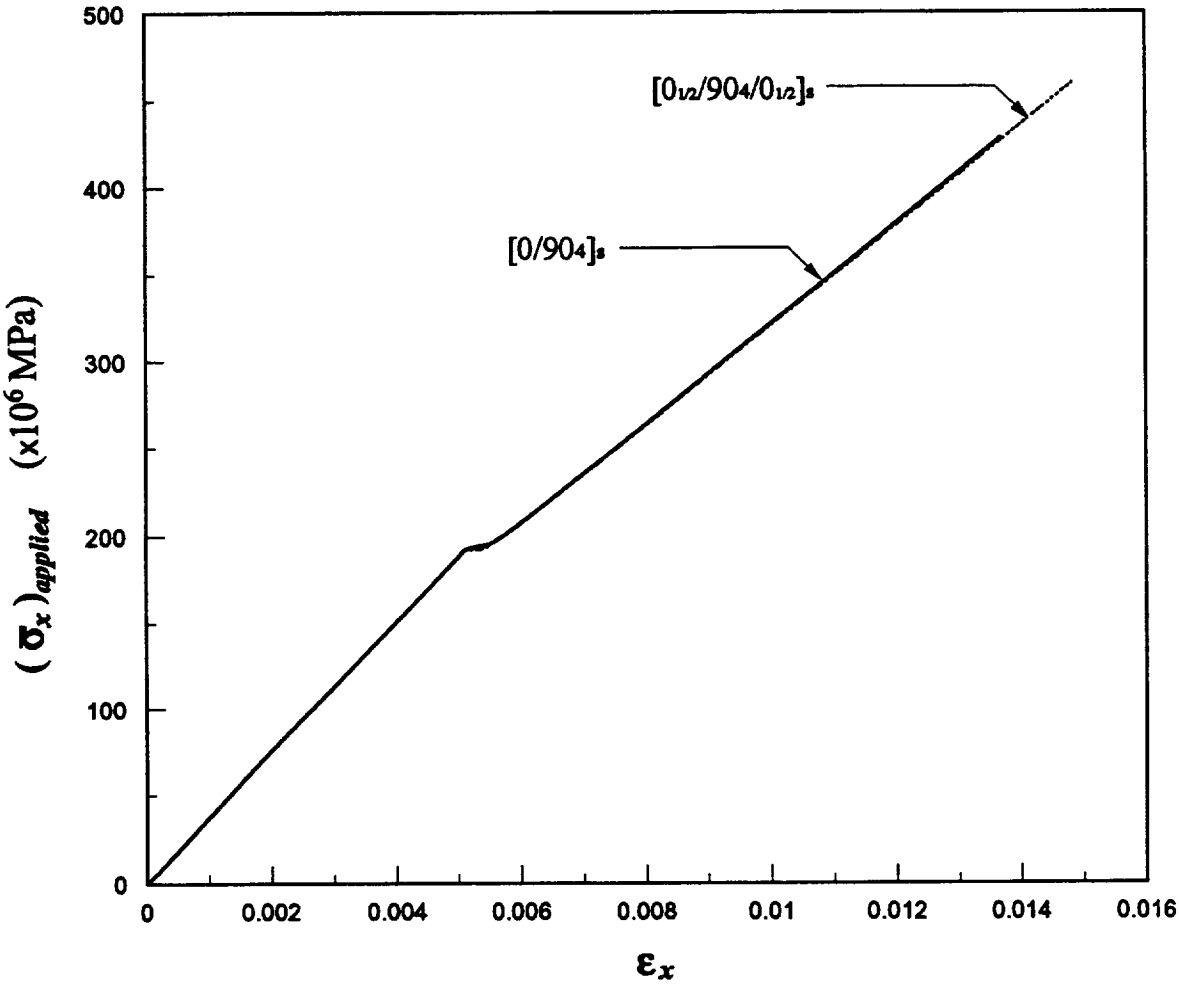

Figure 4.6: Predicted stress-strain behavior for [0/90$_4$]$_s$ and [0$_{1/2}$/90$_4$/0$_{1/2}$]$_s$ laminates.

For demonstration purposes, values of 130 MPa for the interlaminar shear strength and 27.5 GPa for the out-of-plane shear modulus were assumed.

The example problems will be conducted for cases of applied longitudinal strain, $(\epsilon_x)_{applied}$ with free-edge conditions in the y direction (see Appendix D). Even for this relatively simple applied strain state, the off-axis layers will still be experiencing states of full in-plane loading. Therefore, examining the occurrences of transverse matrix cracking

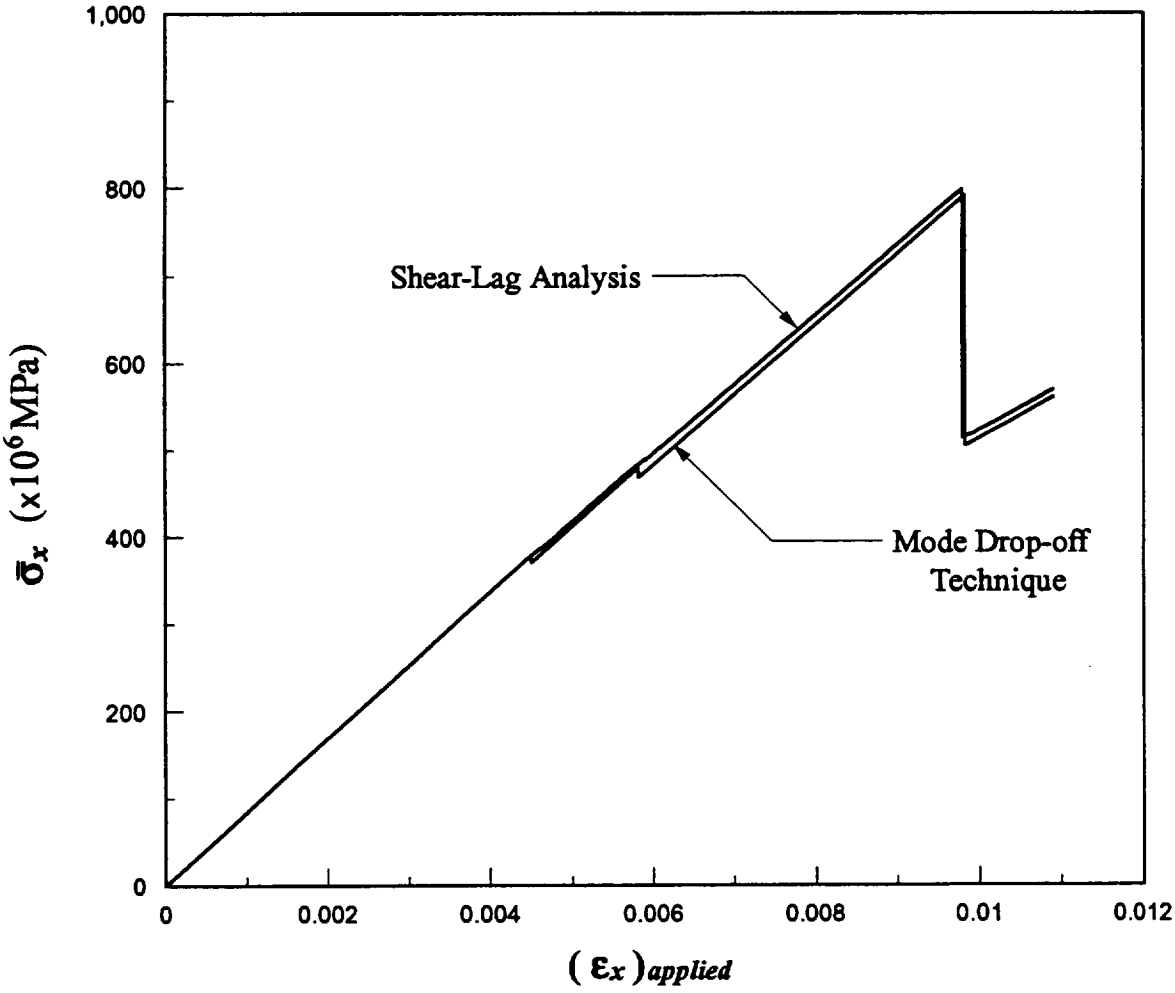

Figure 4.7: Realization of the stress-strain behavior for a $[0/15/80/-15/-80]_s$ Gr/Ep laminate.

TABLE 4.2
Weibull Strength Parameters for Gr/Ep
(Wetherhold, 1986)

	α	β
Longitudinal strength	25	1516.8 MPa
Transverse strength	10	51.7 MPa
In-plane shear strength	15	68.9 MPa

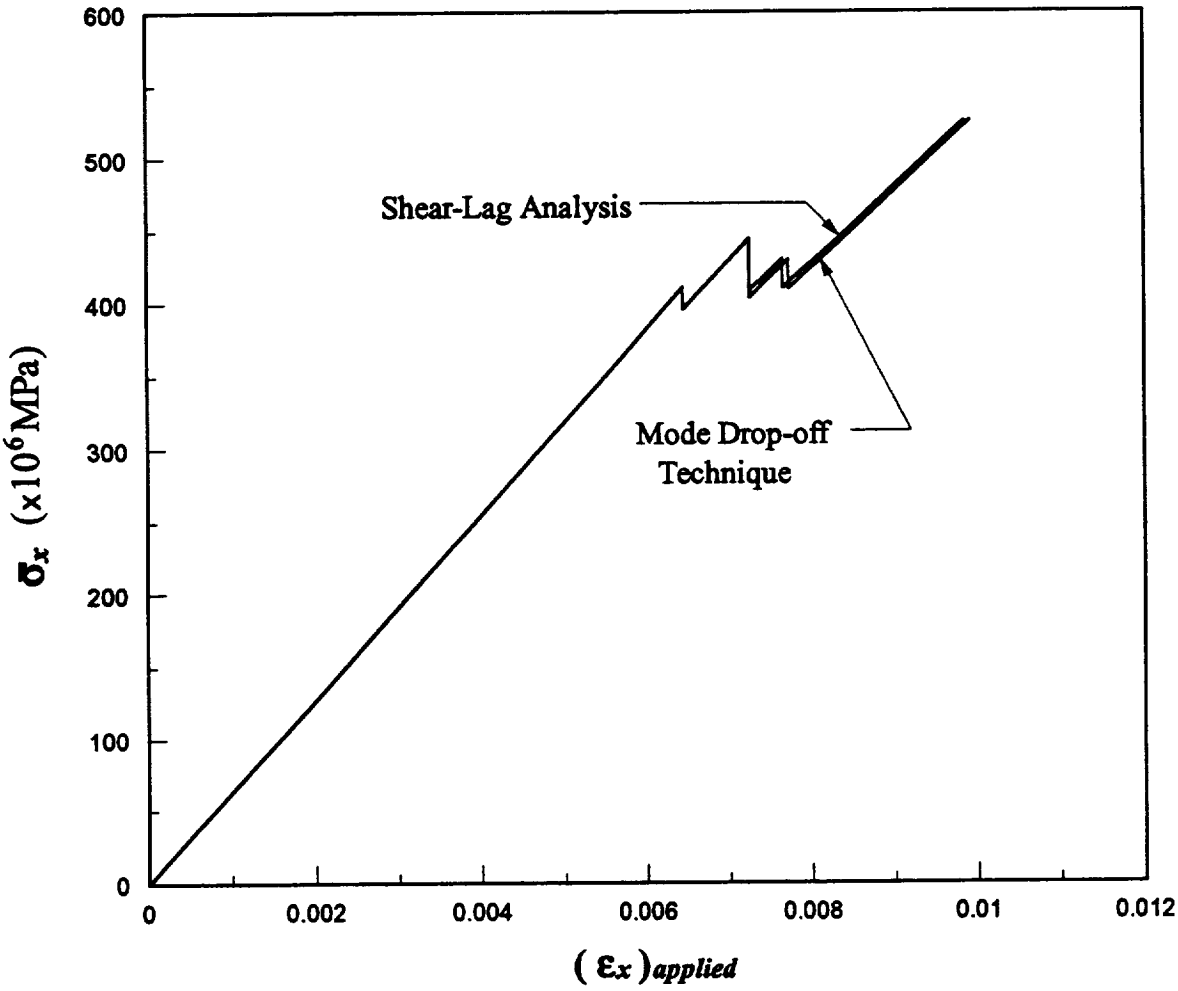

Figure 4.8: Realization of the stress-strain behavior for a $[0/30/60/-30/-60]_s$ Gr/Ep laminate.

in any of the off-axis layers will require taking full advantage of the generalized shear-lag model.

In the first set of figures, Figures 4.7 through 4.10, characteristic stress-strain responses are presented for each of the example problems. Each of these response curves are for one set of *realizations* of the material strengths. Contained within each figure are two curves comparing the results of the shear-lag model and the mode drop-off model.

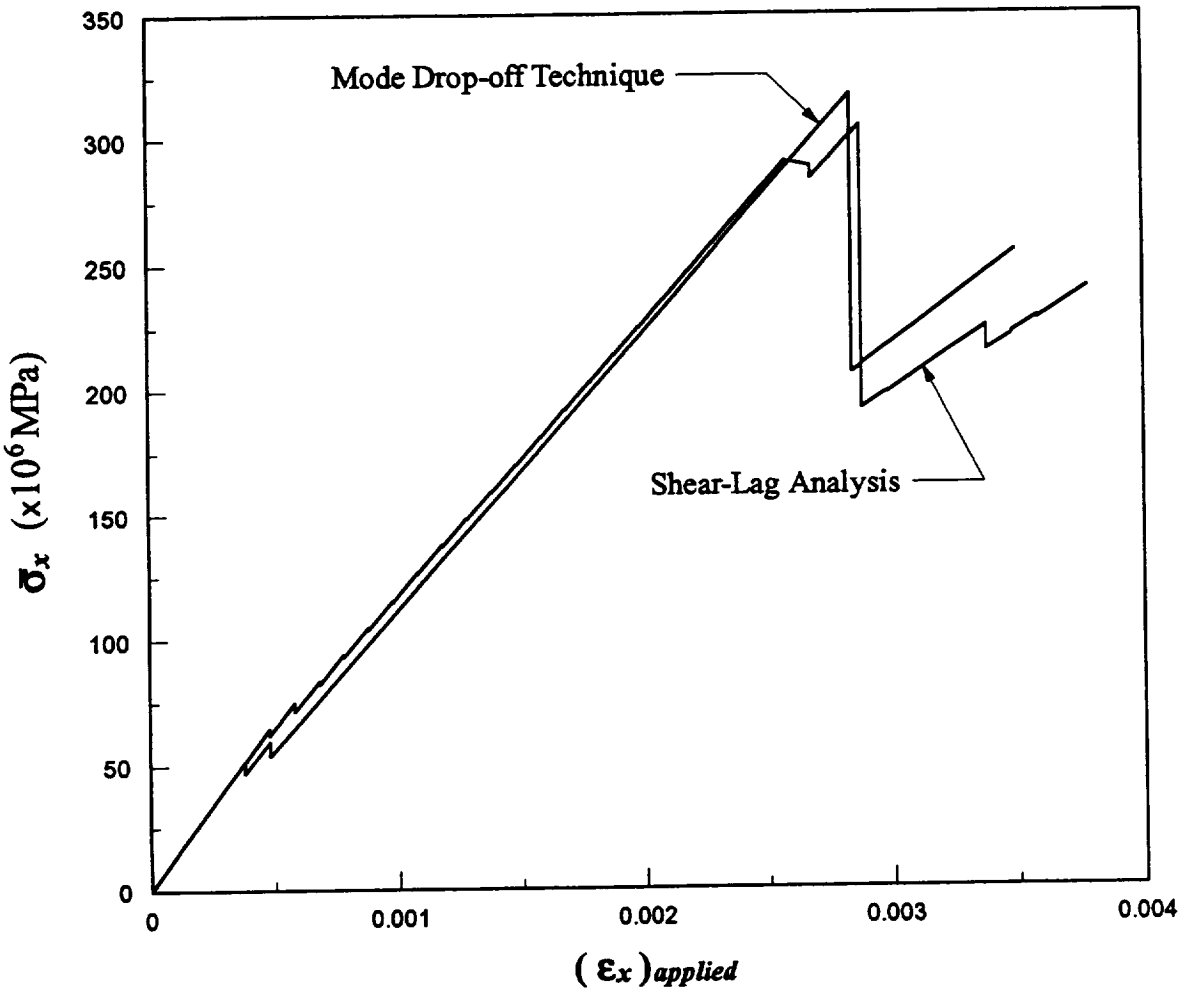

Figure 4.9: Realization of the stress-strain behavior for a $[0/15/80/-15/-80]_s$ SiC/RBSN laminate.

The algorithms for generating each of the curves use a drop-off technique for modeling stiffness reductions due to longitudinal and shear failures. However, for transverse failures (i.e., transverse matrix cracking), one algorithm uses the shear-lag model to determine the effective elastic properties of the damaged layer, and the other algorithm uses the drop-off method and removes that mode from future computations. In general, both the shear-lag and mode drop-off techniques produced comparable results, especially for the Gr/Ep

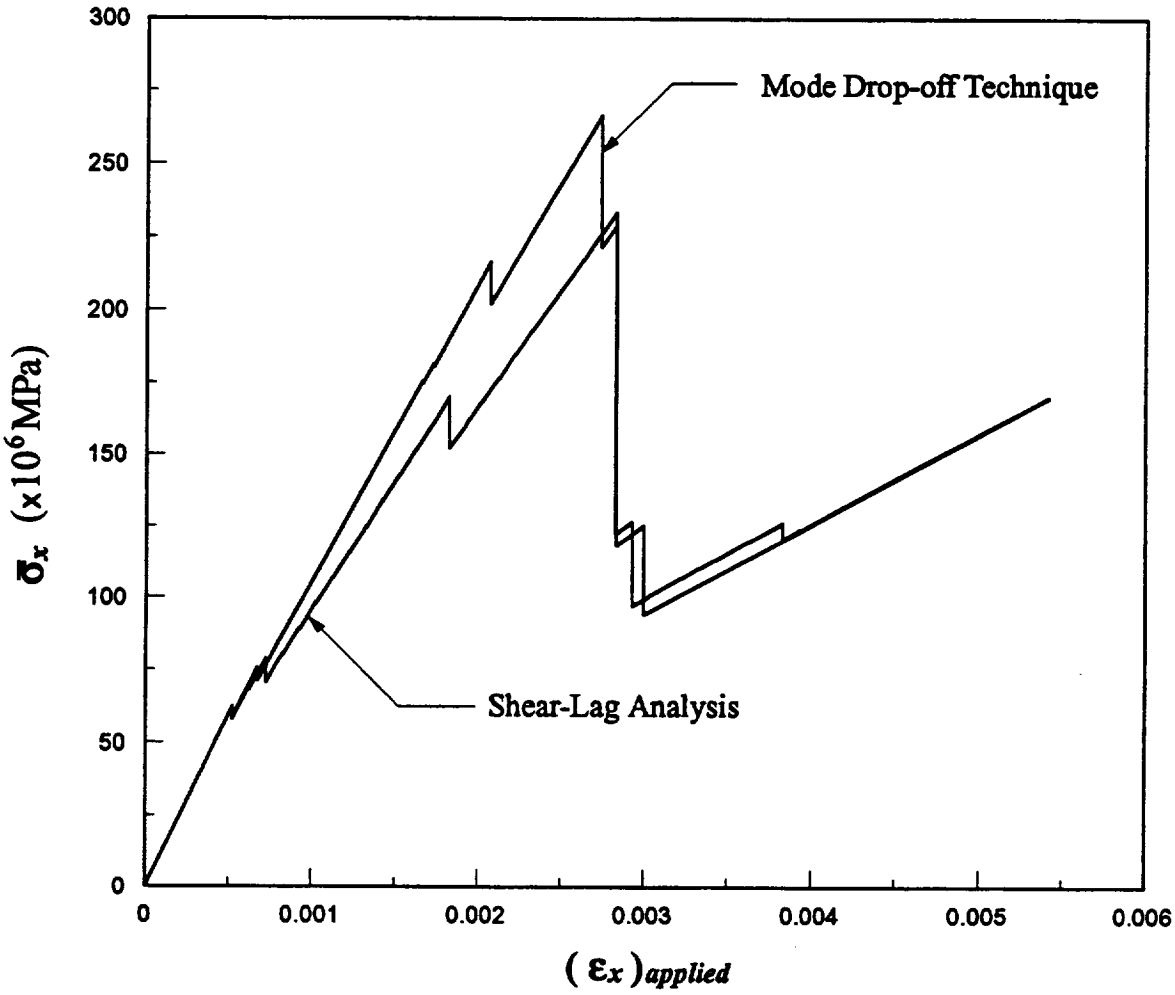

Figure 4.10: Realization of the stress-strain behavior for a $[0/30/60/-30/-60]_s$ SiC/RBSN laminate.

analyses. This may be partially due to the fact that, to avoid singularity problems with the computer program, the stiffnesses were not exactly zero when using the drop-off technique. Thus, a damaged mode retained some load bearing capacity in both models. The stress-strain curves for all four examples demonstrate the evolution of damage in the material and the corresponding change in the global level constitutive behavior.

Figures 4.11 through 4.14 contain characteristic plots of the crack density, ρ [$= (2s)^{-1}$,

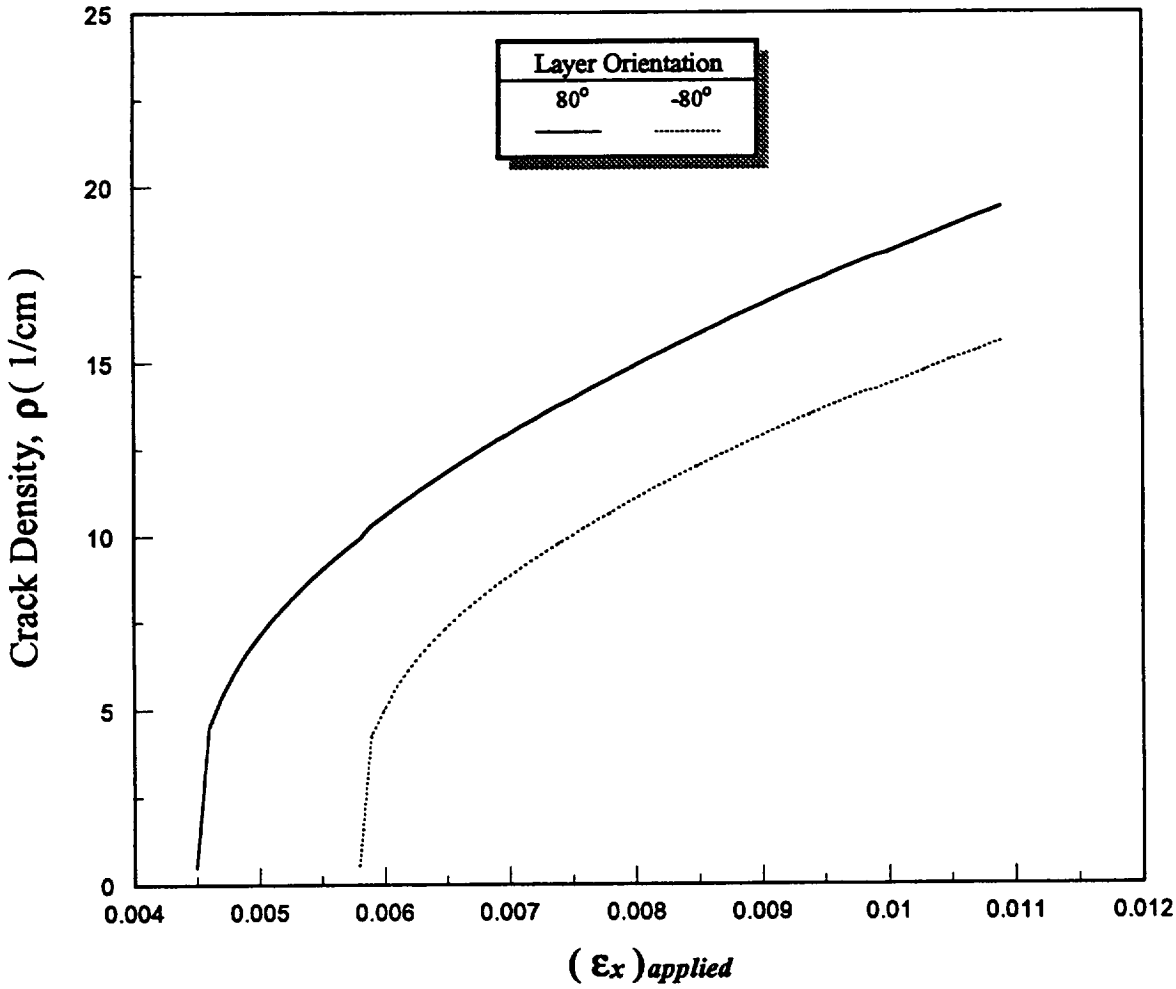

Figure 4.11: Crack density as a function of applied longitudinal strain for realization of [0/15/80/-15/-80]$_s$ Gr/Ep laminate.

where $2s$ is the crack spacing], in the damaged layers as a function of the applied strain. Note once again, these plots are for a particular realization of material strengths. For the Gr/Ep examples, it is only the far off-axis layers ($\pm 80^{\circ}$ and $\pm 60^{\circ}$) in each case which experience transverse matrix cracking. In the SiC/RBSN laminates, cracking is seen in the 15° and 30° near off-axis layers in addition to those further off-axis. The curves for all four examples are similar in nature, with increasing density and decreasing slope associated

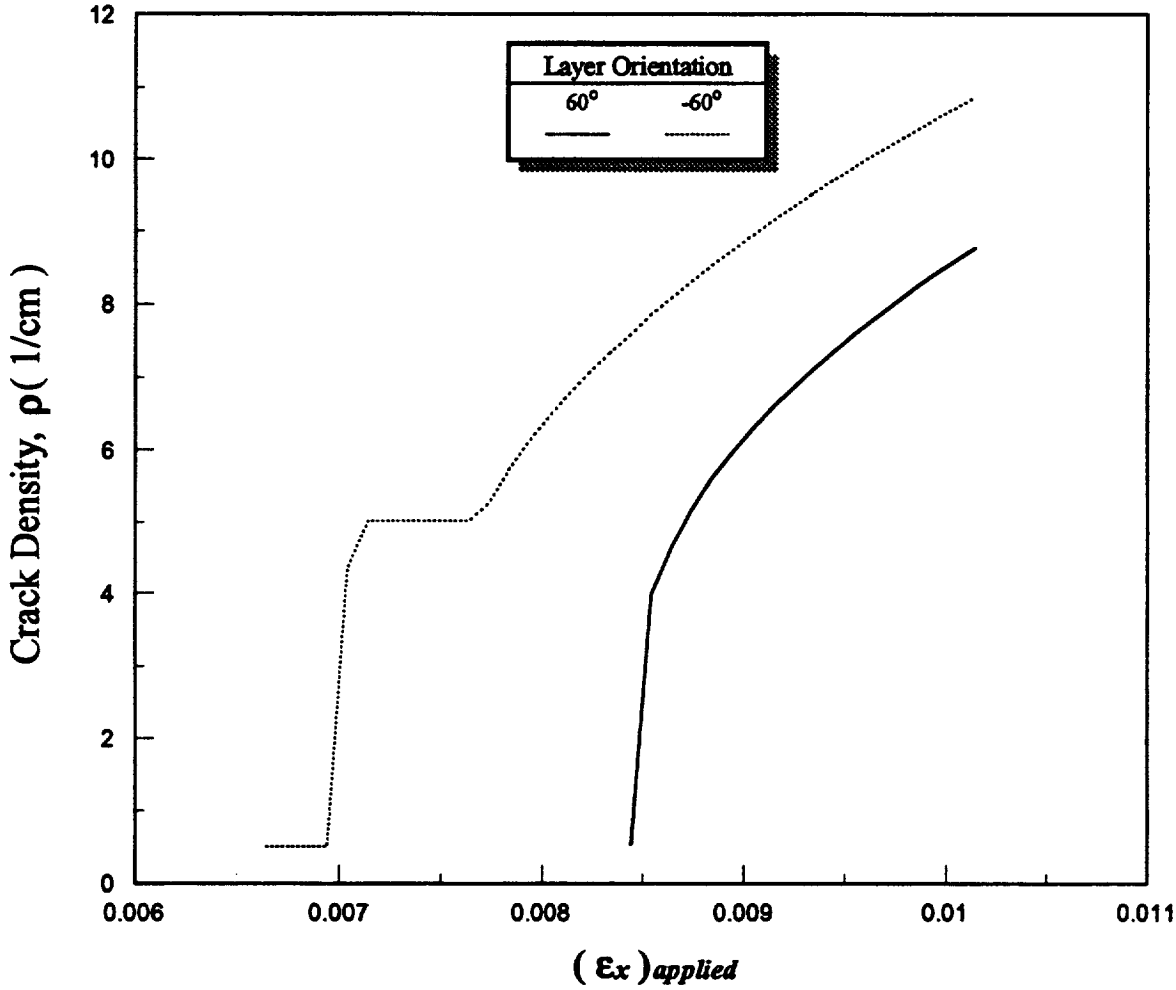

Figure 4.12: Crack density as a function of applied longitudinal strain for realization of [0/30/60/-30/-60]$_s$ Gr/Ep laminate.

with increasing strain. Plateau regions are present in some of the curves, and these can be attributed to times when there was a sufficient enough decrease in the far-field stress, due to the failure of various internal modes, that the stress transferred into the damaged layers was not great enough to cause additional cracking.

The last set of figures, Figures 4.15 through 4.18, contain the cumulative distribution curves for each of the example problems, with the probability of failure plotted as a

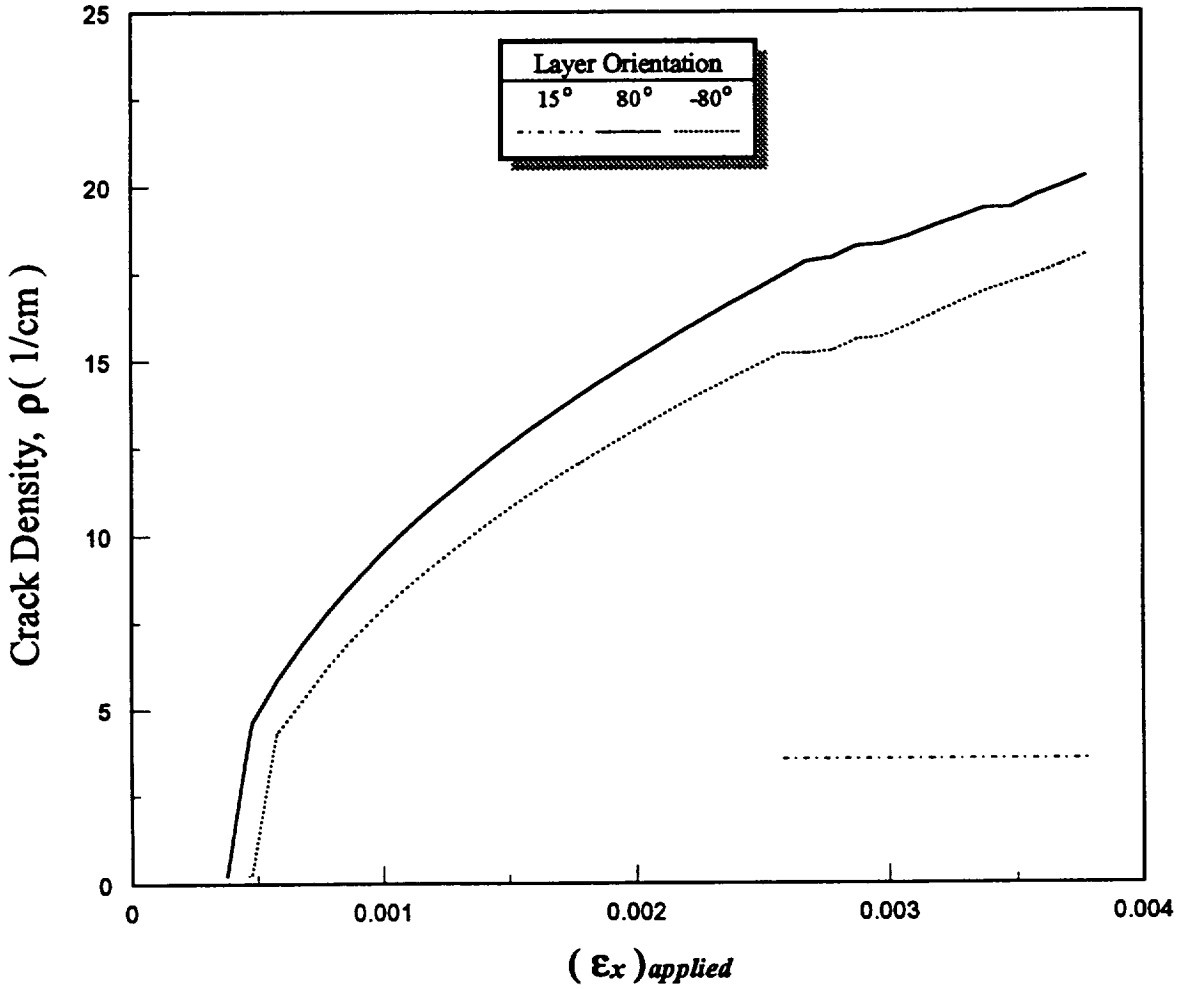

Figure 4.13: Crack density as a function of applied longitudinal strain for realization of [0/15/80/-15/-80]$_s$ SiC/RBSN laminate.

function of the applied strain. The curves for the Gr/Ep laminates have the typical "S" shape common to cumulative distribution curves. The SiC/RBSN curves show a very large scatter in the ultimate strain (i.e., the strain to failure), with the maximum failure strain occurrence having a magnitude of approximately four times that of the minimum. The distribution curve for the failure of the [0/15/80/−15/−80]$_s$ SiC/RBSN example in Figure 4.17 levels off at approximately 0.003 strain and then begins increasing again at 0.0035

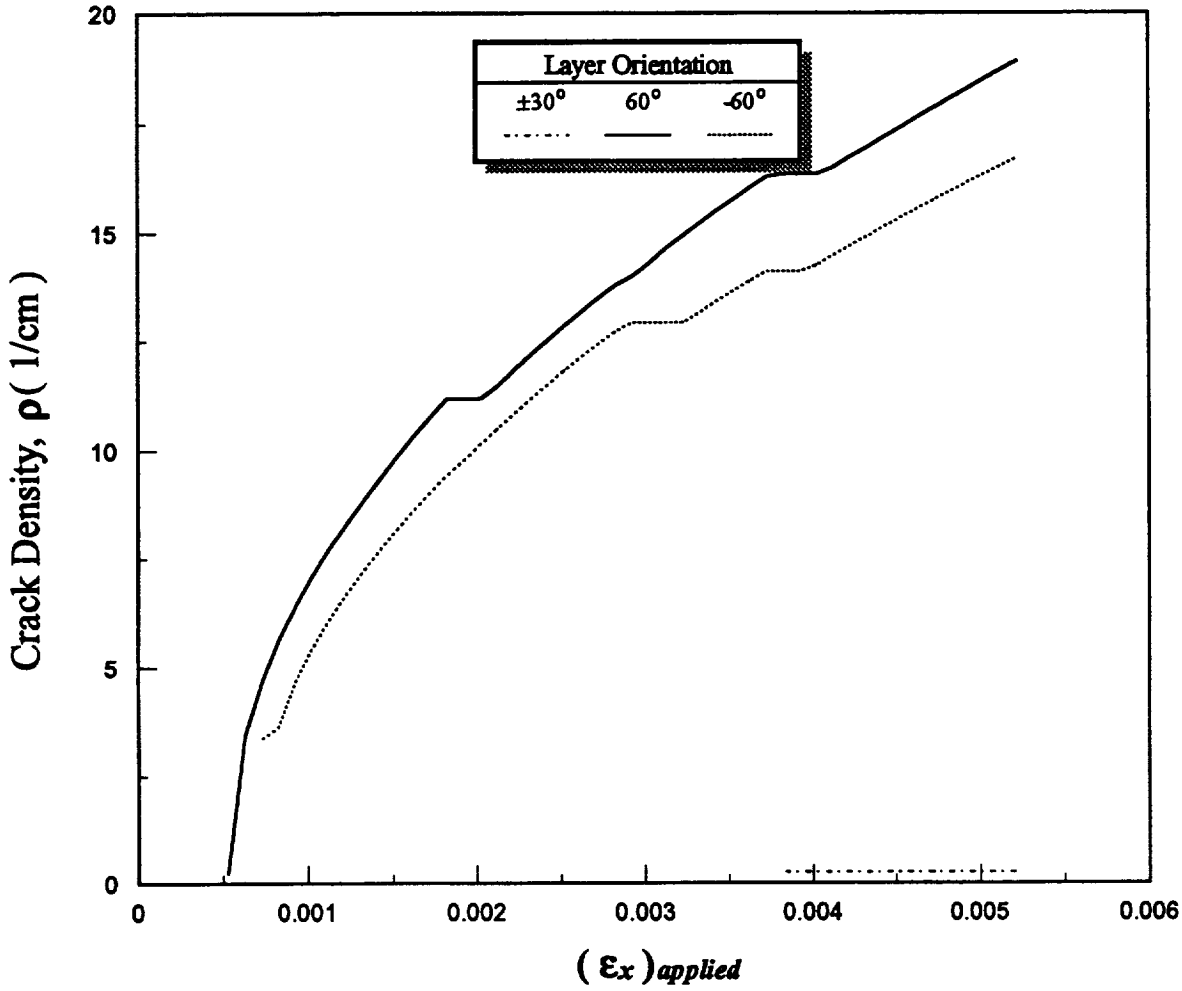

Figure 4.14: Crack density as a function of applied longitudinal strain for realization of [0/30/60/-30/-60]$_s$ SiC/RBSN laminate.

strain. This is characteristic of a bi-modal distribution. Further examination of the Monte Carlo results showed that in fact this is so, with the lower end of the distribution curve representative of those laminate realizations which failed due to the stiffness matrix violating the positive definiteness requirement, and the higher end of the distribution curve representative of those laminate realizations which failed due to a sudden 50% drop in the load carried by the laminate (these two failure criteria are explained in greater detail in

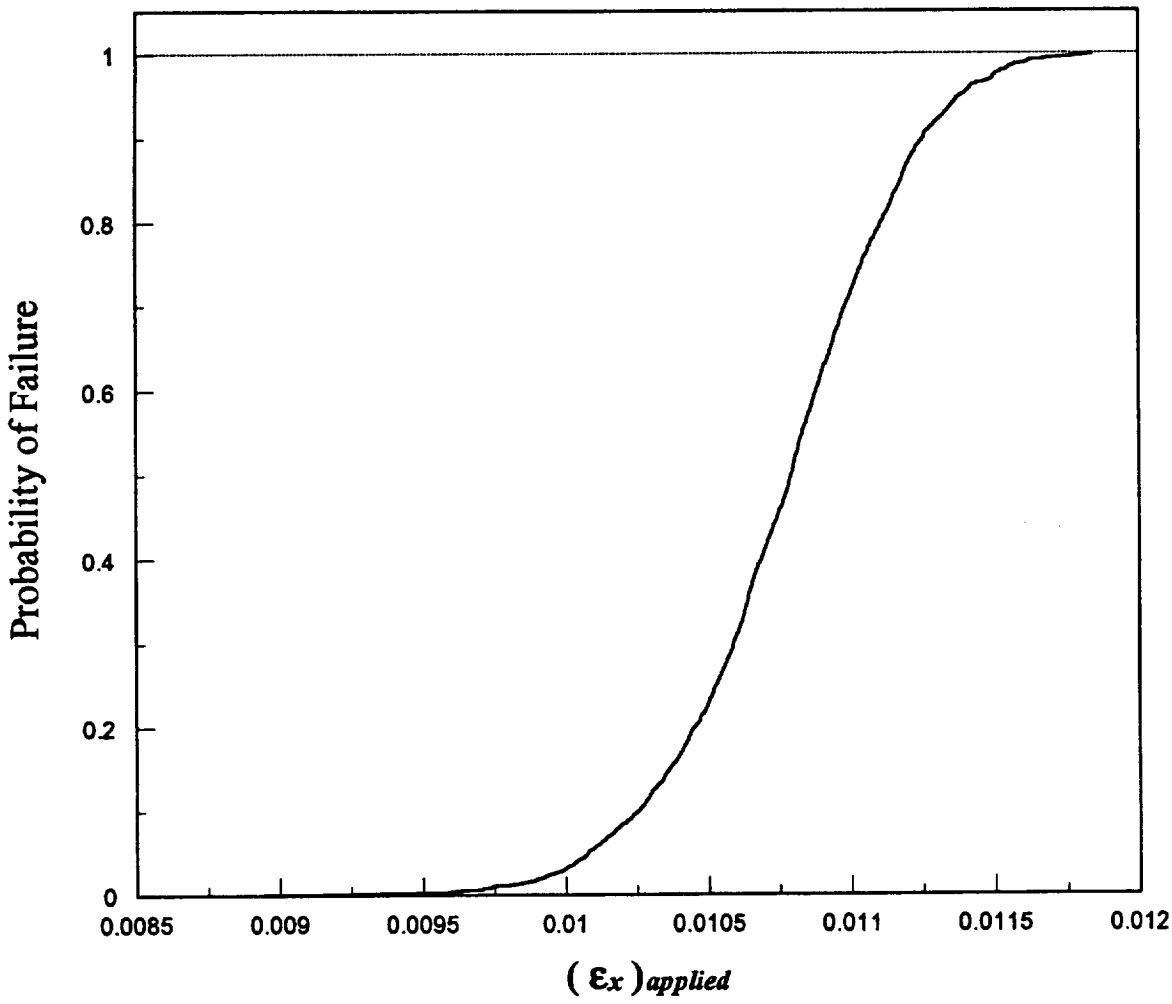

Figure 4.15: Cumulative distribution curve for [0/15/80/-15/-80]$_s$ Gr/Ep laminate.

Appendix D).

SUMMARY

A generalized shear-lag model has been derived to determine the average through-the-thickness stress state present in a layer undergoing transverse matrix cracking. The model

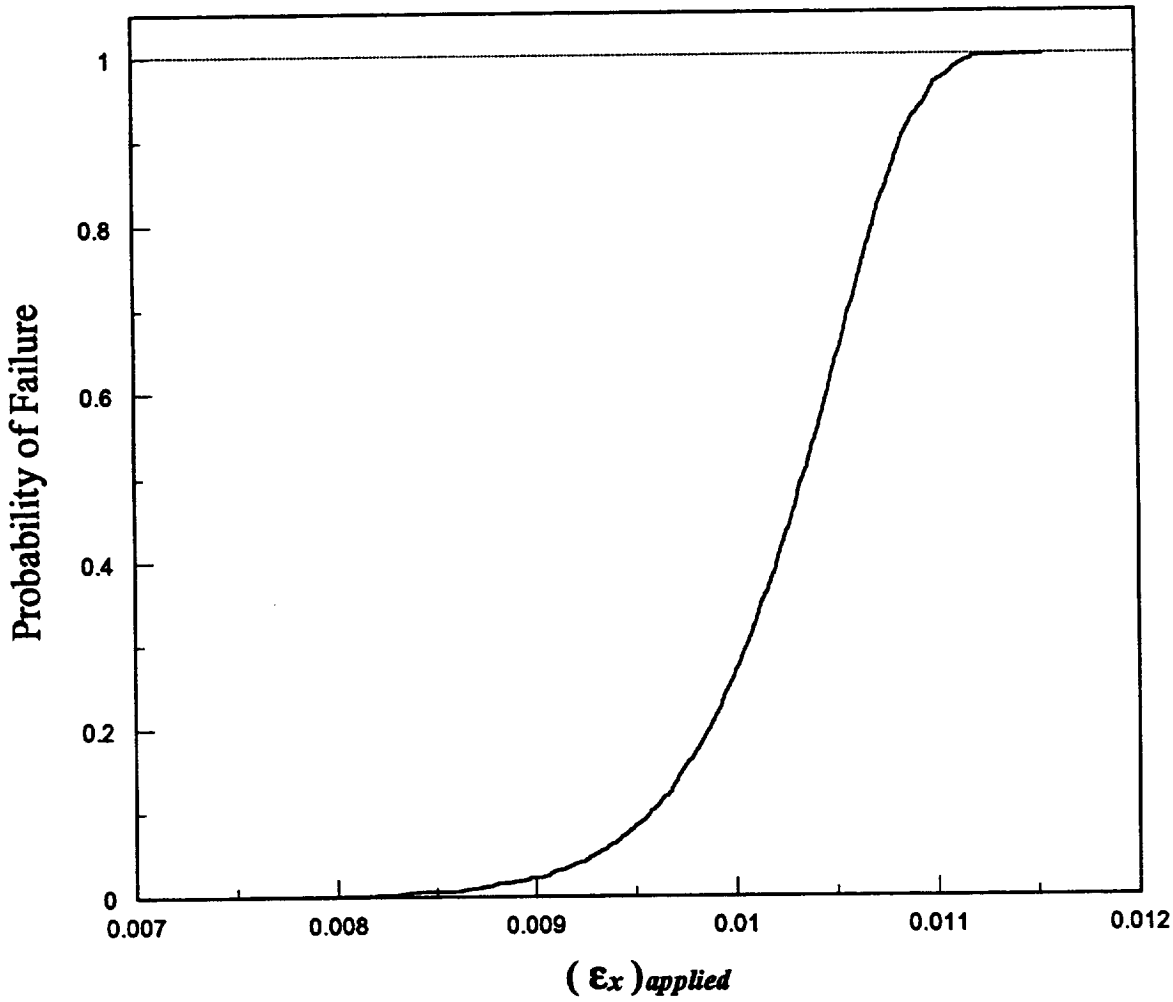

Figure 4.16: Cumulative distribution curve for $[0/30/60/-30/-60]_s$ Gr/Ep laminate.

is capable of considering cracking in layers of arbitrary orientation, states of general in-plane applied loading, and laminates having a general symmetric stacking sequence. The model has been shown to agree with a conventional model for the case of a simple cross-ply laminate. Agreement was also found for the slightly more general three layer cross-ply system. Example problems were carried out for more general laminate configurations, namely $[0/15/80/-15/-80]_s$ and $[0/30/60/-30/-60]_s$ laminates, with results showing the

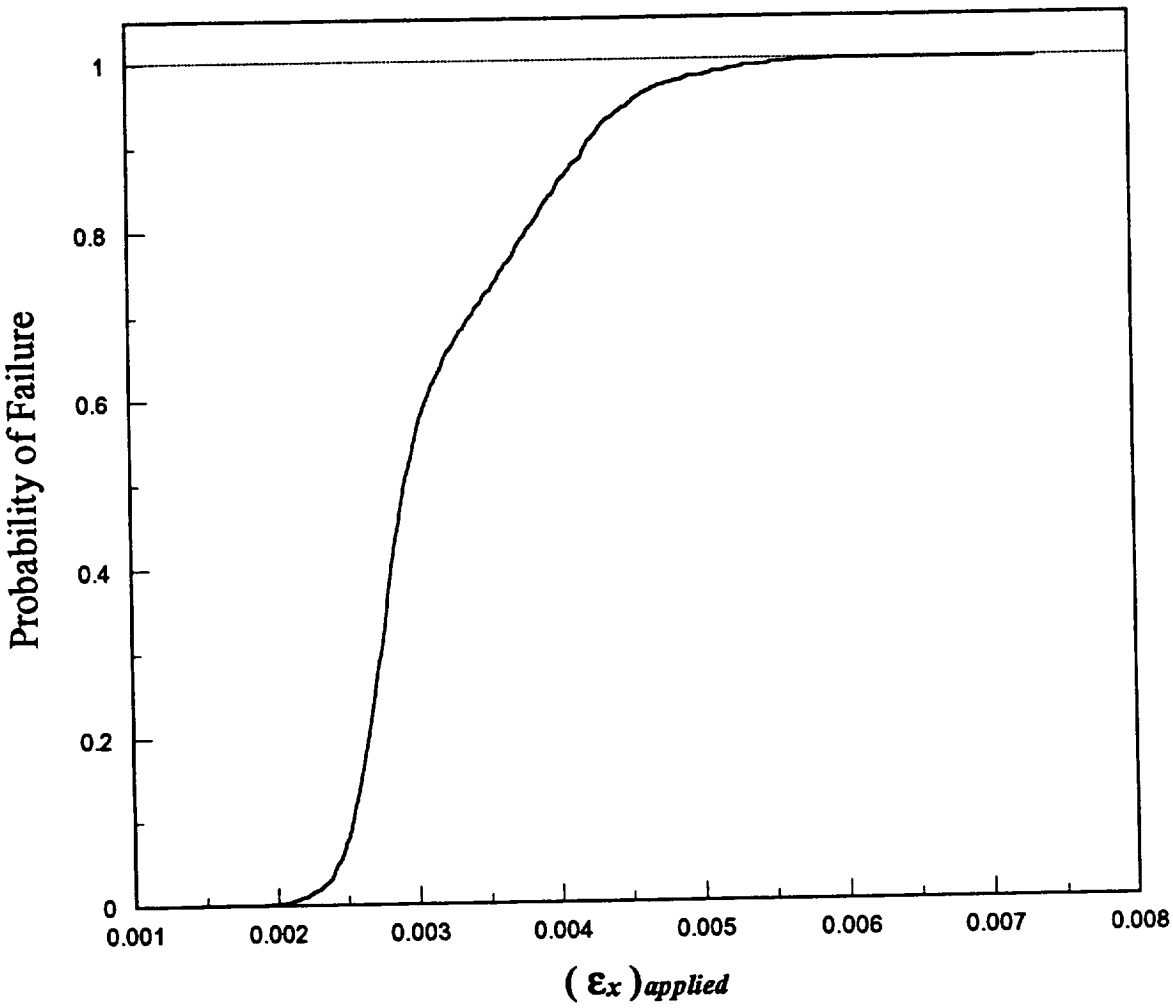

Figure 4.17: Cumulative distribution curve for $[0/15/80/-15/-80]_s$ SiC/RBSN laminate.

evolution of damage in the material and the corresponding change in the global level constitutive behavior of the laminate.

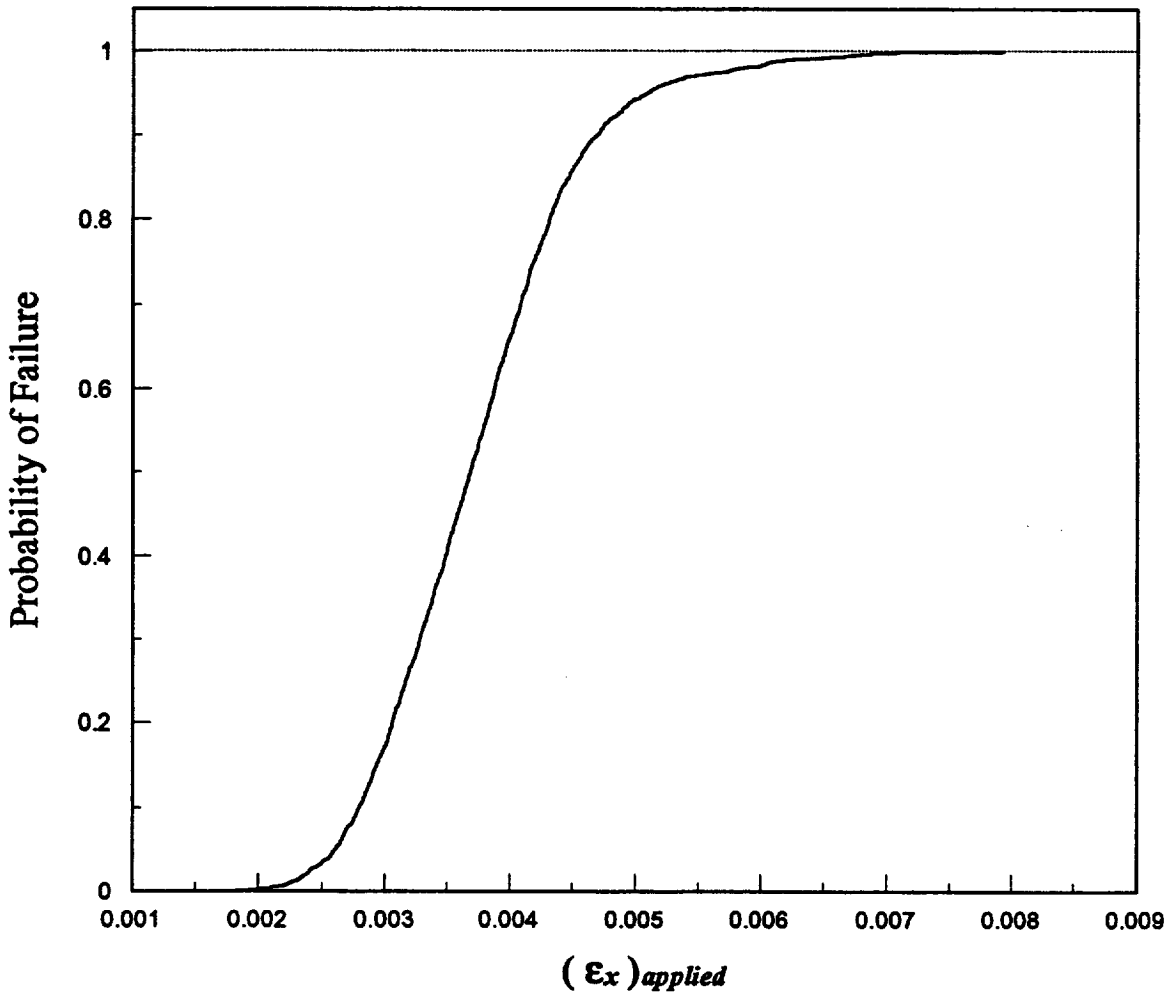

Figure 4.18: Cumulative distribution curve for $[0/30/60/-30/-60]_s$ SiC/RBSN laminate.

CHAPTER 5

Location of Next Transverse Crack in Crack Bounded Region

In the solution of Chapter 4, it was implicitly assumed that during damage progression, the transverse matrix cracks occurred at regularly spaced intervals. This assumption allowed the solution of the stress state of the damaged layer to be reduced to the solution of a characteristic volume bounded by two transverse cracks and having a length equal to the crack spacing ($2s$). In this chapter the validity of this assumption will be investigated qualitatively by examining the probability density function for transverse crack location.

In a classic paper by Oh and Finney (1970), the traditional Weibull analysis was extended to model the characteristics of the location of failure for brittle materials. It was demonstrated that for cases where the stress state present in the solid can be stated as a function of a far field reference stress as well as location, the probability density function (pdf) for the location of failure can be determined analytically. In this chapter, Wetherhold's (1991) treatment of Oh and Finney's work will be followed, and combined with the solution from Chapter 4 for the stress state present in the region between two transverse matrix cracks to arrive at the pdf for the next crack (i.e., failure) location.

STRESS SOLUTION

Assuming that failure due to transverse cracking can be modeled using a probabilistic version of the maximum stress criterion (equation (2.3)), the critical stress which must be considered is the in-plane transverse stress. In Chapter 4, the solution was presented (equation (4.61-4.63)) for the state of in-plane stress of a damaged layer for the region between two transverse matrix cracks. As opposed to the general laminate configuration studied in Chapter 4, the laminate studied here is simplified for heuristic purposes. A uniaxially loaded, two layer cross-ply configuration (see Figure 5.1.) is investigated. Corresponding to this simplified system, several reductions can be made to the general solution of Chapter 4. Due to the cross-ply configuration, the term ψ_{12} becomes identically zero (see Appendix C). Because this is only a two layer problem, the thickness of the third layer is obviously zero, and drops out of all of the calculations. The uniaxial loading condition results in only the P_x load ($P_{y'}$ in the transformed coordinates) being present. Taking the above effects into account and dividing the in-plane load (equation (4.62)) by the layer thickness, the average through-the-thickness transverse stress for the damaged layer can be written as

$$\bar{\sigma}_{y'}(y') = \frac{A_2 P_{y'}}{h_1 \alpha}\left[\frac{1-\cosh(2\lambda s)}{\sinh(2\lambda s)}\sinh(\lambda y') + \cosh(\lambda y') - 1\right] \qquad (5.1)$$

The functional dependence on the location variable y' for this equation can be separated and defined by a new function r,

This separation of variables allows the average stress to be expressed as a function of the applied load and the position.

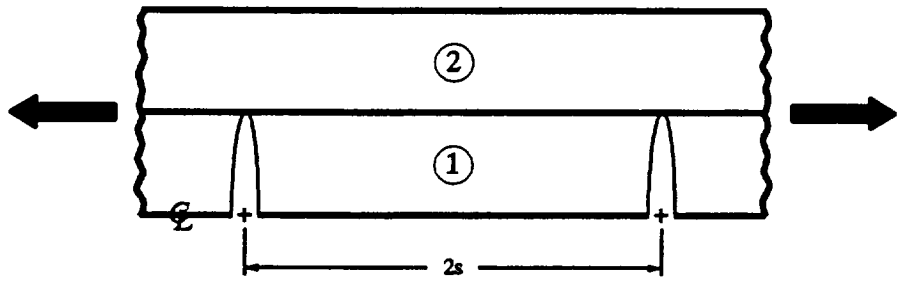

Figure 5.1: Two-layer cross-ply system with matrix cracks in layer 1.

$$r(y') = \frac{A_2}{h_1 \alpha}\left[\frac{1-\cosh(2\lambda s)}{\sinh(2\lambda s)}\sinh(\lambda y') + \cosh(\lambda y') - 1\right] \tag{5.2}$$

$$\bar{\sigma}_{y'}(y') = r(y') \cdot P_{y'} \tag{5.3}$$

CRACK LOCATION

Consider that the region between the two transverse cracks consists of n elements. Each element may be uniquely specified by its position, y_i', and its volume, $\Delta y_i'$, where $i = 1,...,n$. The probability that element i fails under the transverse stress present on the element is defined as (Oh and Finney, 1970; Wetherhold, 1991)

$$Pr[\text{transverse failure of element } i] \equiv G_{\Delta y_i'}\left((\bar{\sigma}_{y'})_i, \Delta y_i'\right) \tag{5.4}$$

From equation (5.3), the stress present on the element is a function of the position and the applied load, therefore

$$G_{\Delta y_i'} = G_{\Delta y_i'}(P_{y'}, y_i', \Delta y_i') \tag{5.5}$$

If the stress is considered to be constant over the volume of the element, then this equation can be restated using a failure density function.

$$G_{\Delta y_i'} = \psi_i(P_{y'}, y_i')\,\Delta y_i' \tag{5.6}$$

The function ψ_i is a measure of the probability of failure per unit volume, and is a function of the reference load and the position.

The conditional probability of failure for an element can also be studied. The probability that element $\Delta y_i'$ fails on the load interval $(P_{y'}, P_{y'} + dP_{y'})$ given that the element has already survived a reference load of $P_{y'}$ can be expressed using the following event statement,

$$Pr[\Delta y_i' \text{ fails for load} \in (P_{y'}, P_{y'} + dP_{y'}) \mid \Delta y_i' \text{ survived } P_{y'}] = \frac{Pr[(\Delta y_i' \text{ fails for load} \in (P_{y'}, P_{y'} + dP_{y'})) \cap (\Delta y_i' \text{ survived } P_{y'})]}{Pr[\Delta y_i' \text{ survived } P_{y'}]} \tag{5.7}$$

The probability that $\Delta y_i'$ survived a load of $P_{y'}$ is a subset of the event that it fails on the interval $(P_{y'}, P_{y'} + dP_{y'})$. Thus, if the condition that the element fails for a load $\in (P_{y'}, P_{y'} + dP_{y'})$ is met, the condition that it survived load $P_{y'}$ will automatically have been satisfied. Therefore, the conditional probability in equation (5.7) takes on the ensuing form.

$$Pr[\Delta y_i' \text{ fails } \in (P_{y'}, P_{y'} + dP_{y'}) \mid \Delta y_i' \text{ survived } P_{y'}] = \frac{Pr[\Delta y_i' \text{ fails } \in (P_{y'}, P_{y'} + dP_{y'})]}{Pr[\Delta y_i' \text{ survived } P_{y'}]}$$

$$= \frac{\dfrac{\partial G_{\Delta y_i'}}{\partial P_{y'}}\, dP_{y'}}{1 - G_{\Delta y_i'}(P_{y'}, y_i', \Delta y_i')} \tag{5.8}$$

The failures of each of the n elements comprising the entire damaged region are assumed to be independent events. Thus, the probability of survival for the whole region is given as the product of the individual survival probabilities. Combining this with equation (5.8) allows the determination of the probability that the next failure in the region occurs at element $\Delta y_i'$ for the interval $(P_{y'}, P_{y'} + dP_{y'})$.

$$Pr\left[\Delta y_i' \text{ fails } \in (P_{y'}, P_{y'} + dP_{y'}) \cap \text{whole region survives } P_{y'}\right]$$

$$= \frac{\partial G_{\Delta y_i'}}{\partial P_{y'}}\, dP_{y'} \frac{\prod_{j=1}^{n} \left(1 - G_{\Delta y_j'}(P_{y'}, y_j', \Delta y_j')\right)}{1 - G_{\Delta y_i'}(P_{y'}, y_i', \Delta y_i')} \tag{5.9}$$

$$= \frac{\partial \psi_i}{\partial P_{y'}}\, \Delta y_i' dP_{y'} \frac{\prod_{j=1}^{n} \left(1 - G_{\Delta y_j'}(P_{y'}, y_j', \Delta y_j')\right)}{1 - G_{\Delta y_i'}(P_{y'}, y_i', \Delta y_i')}$$

As the number of elements is allowed to increase, with n approaching infinity in the limit and the norm of the elemental volumes approaching zero, the finite volume $\Delta y_i'$ can be replaced with the differential sized volume dy_i'. Additionally, the denominator of equation (5.9) approaches one,

$$\lim_{\Delta y_i' \to 0} \left(1 - G_{\Delta y_i'}\right) = 1$$

and the numerator, via the classical first order expansion employed by Weibull, can be written in the limit as having the following exponential form

$$\lim_{n\to\infty}\left[\prod_{i=1}^{n}\left(1-G_{\Delta y_i'}\right)\right] = \exp\left(-\int_{y'}\psi(y')dy'\right)$$

Thus, the probability of equation (5.9) can be written as,

$$Pr[\text{element } dy' \text{ fails} \in (P_{y'}, P_{y'}+dP_{y'}) \cap \text{whole region survives } P_{y'}] = h(P_{y'}, y')\,dy'\,dP_{y'} \tag{5.10}$$

where h is the joint density function for variables y' and $P_{y'}$, and is given below.

$$h(P_{y'}, y') = \frac{\partial \psi}{\partial P_{y'}}\exp\left(-\int \psi\, dy'\right) \tag{5.11}$$

Integrating equation (5.11), either with respect to $P_{y'}$ or y' yields the marginal density functions for the location of failure, $\phi(y')$, or for the reference load at failure, $g(P_{y'})$, respectively.

$$\phi(y') = \int_{P_{y'}} h(P_{y'}, y')\,dP_{y'} \tag{5.12}$$

$$g(P_{y'}) = \int_{y'} h(P_{y'}, y')\,dy' \tag{5.13}$$

In evaluating the joint density function, it is assumed that the probability of failure per unit volume has a Weibull distribution,

$$\psi(P_{y'}, y') = \left(\frac{\bar{\sigma}_{y'}(P_{y'}, y')}{\sigma_o}\right)^m = \left(\frac{r(y')\,P_{y'}}{\sigma_o}\right)^m \tag{5.14}$$

where σ_o is the Weibull scale parameter and m is the Weibull modulus. The following variable substitution is introduced in order to normalize the location variable,

$$y' \in [0, 2s] \quad \rightarrow \quad \xi = \frac{y'}{2s} \quad ; \xi \in [0, 1] \tag{5.15}$$

The joint density function then becomes,

$$h(P_{y'}, \xi) = \frac{m}{\sigma_o}\left(\frac{P_{y'}}{\sigma_o}\right)^{m-1} r^m(\xi) \exp\left[-2sq\left(\frac{P_{y'}}{\sigma_o}\right)^m\right] \tag{5.16}$$

where the constant q has been introduced to represent the following integral,

$$q \equiv \int_0^1 r^m(\xi) d\xi \tag{5.17}$$

The marginal density function for location which is being sought is then found by substituting expression (5.16) into equation (5.12), and integrating over the full range of the loading spectrum, i.e. $(0, \infty)$.

$$\phi(\xi) = \int_0^\infty h(P_{y'}, \xi) dP_{y'} = \frac{r^m(\xi)}{2sq} \tag{5.18}$$

By definition, if integration is carried out over all possible values of ξ, thereby guaranteeing that all possible outcomes of ϕ have been considered, this integral must be equal to one (this is a requirement of a pdf). Integration of equation (5.17) yields

$$\int_0^1 \phi(\xi) d\xi = \frac{1}{2s} \neq 1 \tag{5.19}$$

The density function must therefore be normalized in order to insure that the integral equals one. Denoting the normalized density function as $\hat{\phi}$, the final form for the marginal density function for location of the next transverse matrix crack between two existing matrix cracks takes the following form

$$\hat{\phi}(\xi) = \frac{r^m(\xi)}{q} \tag{5.20}$$

EXAMPLES

In this section, the probability density functions describing the location of the next transverse crack are examined for two material systems, the $[0_2/90_2]_s$ SiC/RBSN laminate presented in Chapter 2 (Table 2.2) and the $[0/90_4]_s$ Gr/Ep laminate described in Chapter 4 (Table 4.1). For each of these cases, pdf's are generated for a range of crack spacings. The evaluation of the constant q (equation (5.17)) contained in the final form of the solution requires numerical integration; all other calculations are capable of being determined in closed form.

Figure 5.2 contains the results of the (normalized) pdf, $\hat{\phi}$, plotted as a function of the location, ξ, for the SiC/RBSN system. Five pdf's are depicted, each corresponding to a selected value of the crack spacing, $2s$. These values range from a minimum of 2.5 mm to a maximum of 50 mm. Results for the Gr/Ep system, analogous to those just described for SiC/RBSN, are presented in Figure 5.3.

Similar results are found for both material systems. The pdf's calculated for large crack spacings show large central regions of equal probability of failure. This corresponds to these regions being far enough away from the crack face to have uniformly reloaded. However, as the crack spacing gets smaller, the distribution narrows. This demonstrates the tendency towards cracking in the more highly stressed central regions. Consequently, in the early stages of damage, when the matrix crack density is relatively low, it appears

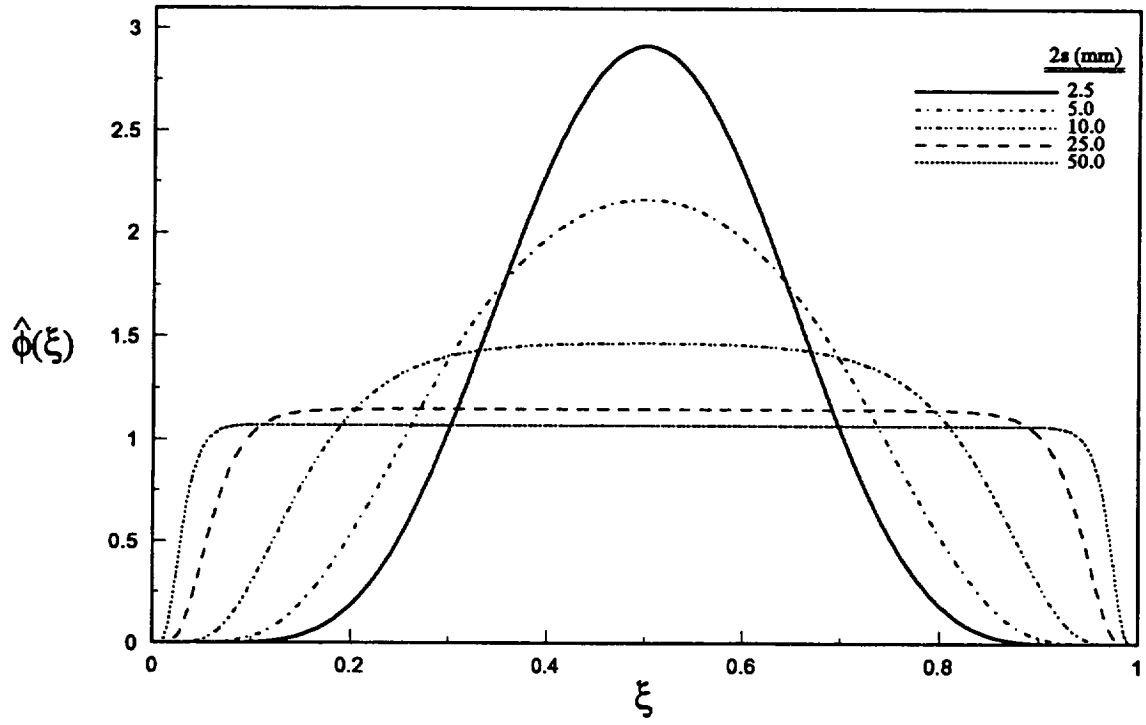

Figure 5.2: pdf's for next failure location for a $[0_2/90_2]_s$ SiC/RBSN laminate.

that the assumption of regularly spaced transverse cracks may be unrealistic (although the average crack location will always be the midpoint!). However, the global effects of the damage in these early stages are relatively minor. As damage progresses, and the crack density increases, the validity of the regular spacing assumption gains credence. Therefore, the assumption of a regular spacing throughout the damage development, which in turn allows the problem to be modeled via the analysis of a characteristic volume, would appear to be justified from an engineering standpoint.

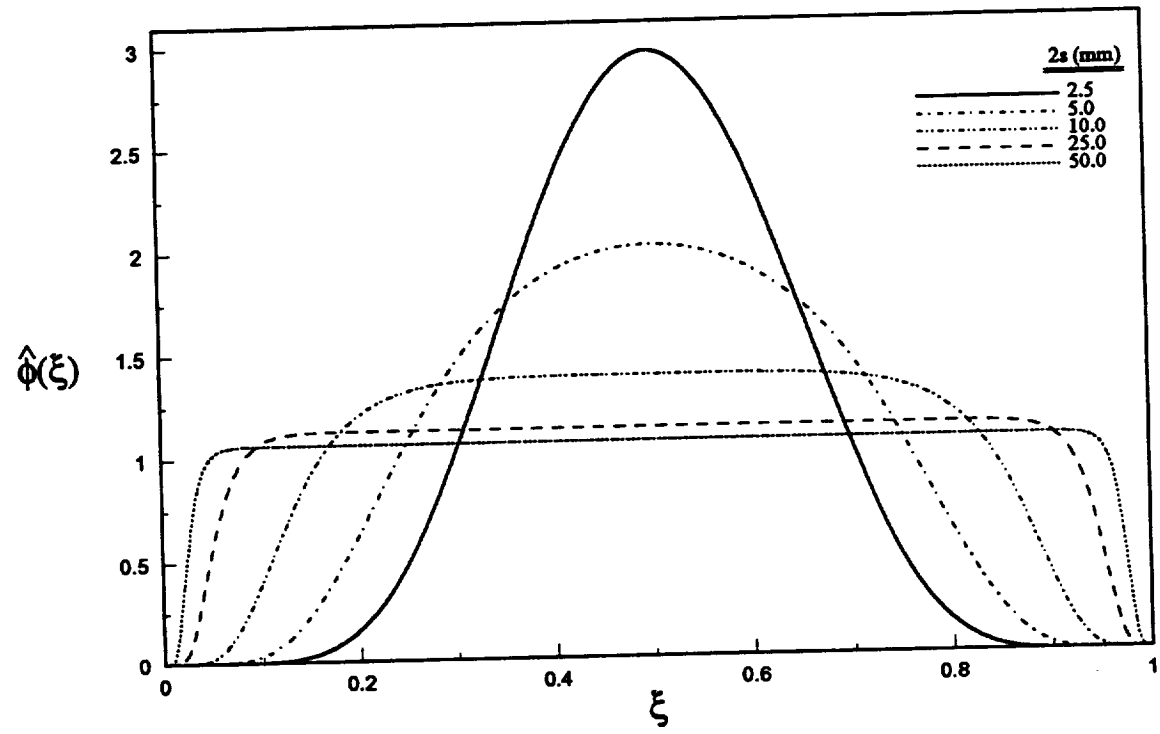

Figure 5.3: pdf's for next failure location for a $[0/90_4]_s$ Gr/Ep laminate.

SUMMARY

In this chapter, the method developed by Oh and Finney for modeling the characteristics of the location of failure has been revisited. Reworking the stress solution from Chapter 4 to accommodate the less general cross-ply system, an analytical expression was developed for the probability density function of the next failure location in a region of a cross-ply laminate bounded by two existing transverse matrix cracks. In exercising this model, it was found that, from a qualitative standpoint, the assumption of regularly spaced transverse matrix cracks is valid.

CHAPTER 6

Summary and Conclusions

Methods for probabilistically modeling the progressive failure of brittle matrix composite laminates were investigated in order to more accurately model the failure process. Failure was approached from a non-interactive standpoint in which each of the in-plane stresses present in a composite layer were assumed to act independently of one another towards correspondingly separate and independent failure modes.

A *modified bundle theory* which had been proposed in the literature to be a good model for the post-matrix-cracking strength of a periodically cracked composite was examined and found to poorly predict the distribution in strength which has been commonly observed for these materials. Extensions to the model were introduced to allow for various material imperfections, in an effort to expand the predicted distribution of strength. These remedies were insufficient to solve the problem. Other possible extensions were indicated, but not investigated.

A *generalized shear-lag theory* for analyzing the stress state of a transversely cracked layer having a general off-axis orientation and subjected to a state of full in-plane loading

was derived. This represents a major step in the development of shear-lag models, which prior to this had been limited in application to cross-ply laminates under in-plane normal or shear loads (but not both). A method for utilizing this theory to model the effective behavior of a transversely cracked layer within the laminate environment was established and a computer program was written to fully exercise the model. Results showing the characteristic stress-strain response, damage accumulation (in terms of the density of transverse matrix cracks) as a function of applied strain, and cumulative distribution curves for the probability of failure as a function of applied strain were presented for a variety of example problems.

An analytical expression for the probability density function for the location of the next transverse crack occurrence within a crack bounded region was developed for a cross-ply laminate. The results of this investigation provided qualitative proof that the uniform crack spacing which had been assumed in the shear-lag analysis was a valid engineering assumption.

This report has looked in detail at various ways by which macro-level behavior of composites may be extrapolated from micro-level analyses of representative damage regimes. An approach of this manner should capture enough of the actual physics of the failure process to provide insight into the best ways to design with these material systems (this is sacrificed in a truly phenomenological model). At the same time the problem should be computationally simple enough to allow application of the model to practical sized components (this not possible with a true micro-level, i.e. fiber/matrix, approach).

In the area of future work, experimental verification of the generalized shear-lag model is needed. The results of Chapter 4 appear good qualitatively, but quantitative results are

necessary. Also, pertaining to the generalized shear-lag model, thermal stress effects need to be included.

APPENDIX A

Global Equilibrium Equations for Three Layer System

The global equilibrium equations for a three-layer system were stated without proof in Chapter 4 (equations 4.44, 4.45 and 4.46). In this Appendix, the equilibrium conditions are derived in order to verify that the forms of these equations are in fact correct.

The derivation begins by considering an undamaged three-layer laminate with dimensions L_x, L_y and L_z (see Figure A.1). This system is assumed to be subjected to an applied in-plane displacement field. The applied displacements results in a far-field loading which is uniform (i.e., the loads are independent of x, y and z) and has a general in-plane nature (i.e., longitudinal, transverse and shear terms may be present). The far-field loads are specified in units of force per unit length. Due to the undamaged condition of the plate and St. Venant's principle, the stress field which arises within the laminate as a result of the far-field loads is independent of x and y. However, because elastic properties can change from layer to layer, the stresses may vary from layer to layer as

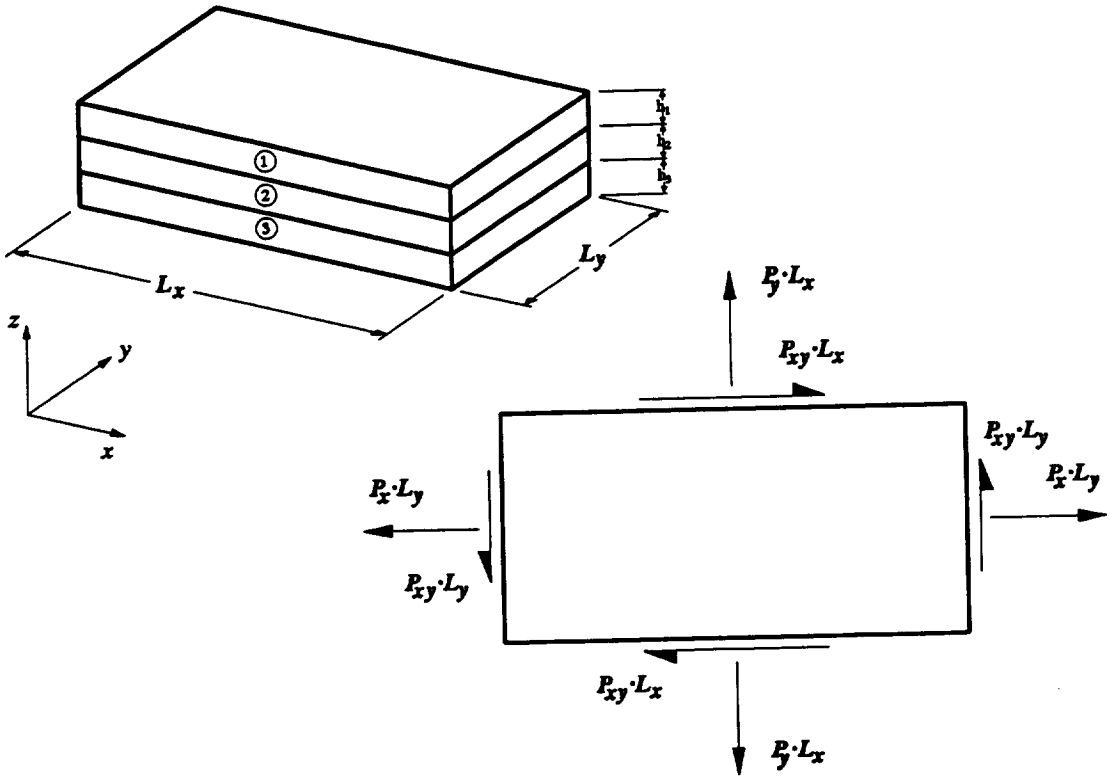

Figure A.1: Three layer laminate with general in-plane loads applied.

well, and are thus a function of z. Within each of these layers, in-plane loading terms are defined as the integrated stress through the layer thickness.

$$N_x^{(i)} = \int_{h_i} \sigma_x^{(i)}(z)dz \tag{A.1}$$

$$N_y^{(i)} = \int_{h_i} \sigma_y^{(i)}(z)dz \tag{A.2}$$

$$N_{xy}^{(i)} = \int_{h_i} \tau_{xy}^{(i)}(z)dz \tag{A.3}$$

This integration has the effect of "smearing out" the z dependence of the stress, producing effective in-plane loads.

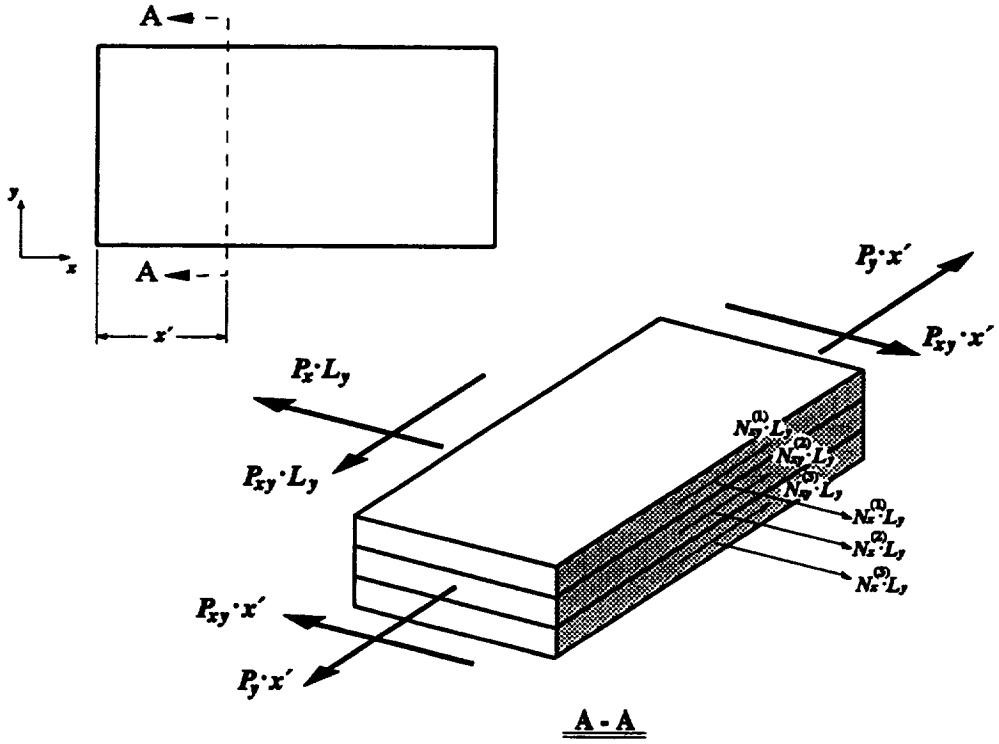

Figure A.2: Free body diagram for section along the plane $x = x'$.

Consider the segment of the laminate resulting from slicing the laminate along the plane $x=x'$. A free body diagram, showing the far-field loads on the free edges and the resultant in-plane loads on the exposed section for each of the layers, is presented in Figure A.2. Summing the forces in the x and y directions separately, yields,

$$\sum F_x = 0 = -P_x \cdot L_y - P_{xy} \cdot x' + P_{xy} \cdot x' + N_x^{(1)} \cdot L_y + N_x^{(2)} \cdot L_y + N_x^{(3)} \cdot L_y \quad \text{(A.2)}$$

$$P_x = N_x^{(1)} + N_x^{(2)} + N_x^{(3)} \quad \text{(A.3)}$$

$$\sum F_y = 0 = -P_y \cdot x' + P_y \cdot x' - P_{xy} \cdot L_y + N_{xy}^{(1)} \cdot L_y + N_{xy}^{(2)} \cdot L_y + N_{xy}^{(3)} \cdot L_y \quad \text{(A.4)}$$

$$P_{xy} = N_{xy}^{(1)} + N_{xy}^{(2)} + N_{xy}^{(3)} \quad \text{(A.5)}$$

Similarly, sectioning the laminate along the plane $y=y'$ (see Figure A.3) and summing

C-2.

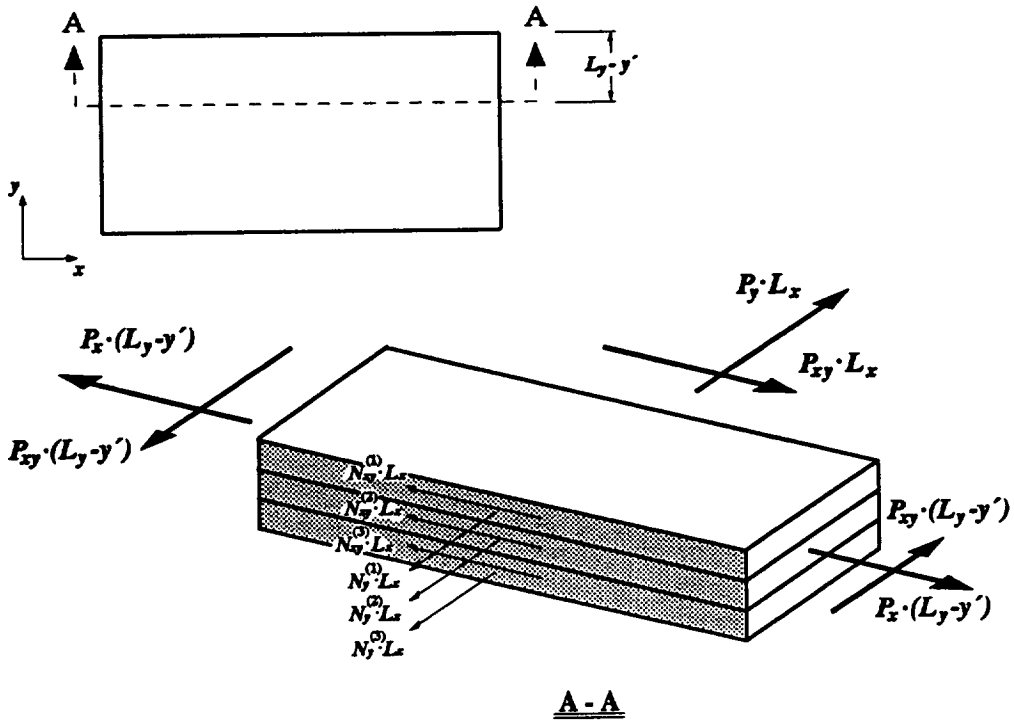

Figure A.3: Free body diagram for section along the plane $y = y'$.

forces yields the equilibrium equation for the forces in the y direction.

$$\sum F_y = 0 = P_y \cdot L_x + P_{xy} \cdot (L_y - y') - P_{xy} \cdot (L_y - y') - N_y^{(1)} \cdot L_x - N_y^{(2)} \cdot L_x - N_y^{(3)} \cdot L_x \tag{A.6}$$

$$P_y = N_y^{(1)} + N_y^{(2)} + N_y^{(3)} \tag{A.7}$$

Equations (A.3), (A.5) and (A.7) comprise the global equilibrium equations, relating the far-field loads to the resultant in-plane loads on each layer, for an undamaged laminate. The question which remains to be answered is whether or not these equations still apply for a laminate containing transverse matrix cracking.

Due to the system being under a state of displacement control, the onset of damage will effect the magnitude of the far-field loads (as governed by the constitutive law), however

they are assumed to remain constant with respect to position (i.e., independent of x, y and z). Locally, the presence of damage within the laminate produces a stress field within each of the layers which is no longer independent of position. The assumption from Chapter 4 that damage effects are direction specific is continued here. For the case of transverse matrix cracks running in the x direction, damage is induced in the y direction. This implies that the stresses within the layers are functions of y and z, (i.e., $\sigma_j^{(i)} = \sigma_j^{(i)}(y,z)$),

$$N_x^{(i)}(y) = \int_{h_i} \sigma_x^{(i)}(y,z)dz \tag{A.8}$$

$$N_y^{(i)}(y) = \int_{h_i} \sigma_y^{(i)}(y,z)dz \tag{A.9}$$

$$N_{xy}^{(i)}(y) = \int_{h_i} \tau_{xy}^{(i)}(y,z)dz \tag{A.10}$$

and thus, the loading terms are functions of the y position at which they are evaluated.

Returning to Figure A.3, a cut-away section of the laminate along the plane $y=y'$ is examined. However, now the resultant in-plane loads are functions of y, $N_y^{(i)}(y)$ and $N_{xy}^{(i)}(y)$, due to the transverse matrix cracks. Summing the forces on this segment in the x and y directions yields equilibrium equations for the transverse and shear forces.

$$P_y = N_y^{(1)}(y') + N_y^{(2)}(y') + N_y^{(3)}(y') \tag{A.11}$$

$$P_{xy} = N_{xy}^{(1)}(y') + N_{xy}^{(2)}(y') + N_{xy}^{(3)}(y') \tag{A.12}$$

With regard to the equilibrium in the x direction, a segment of finite length x' in the$x$ direction, and differential length dy in the y direction (see Figure A.4) is examined. The far-field loads remain independent of position. The reaction forces on the faces $y = y'$ and

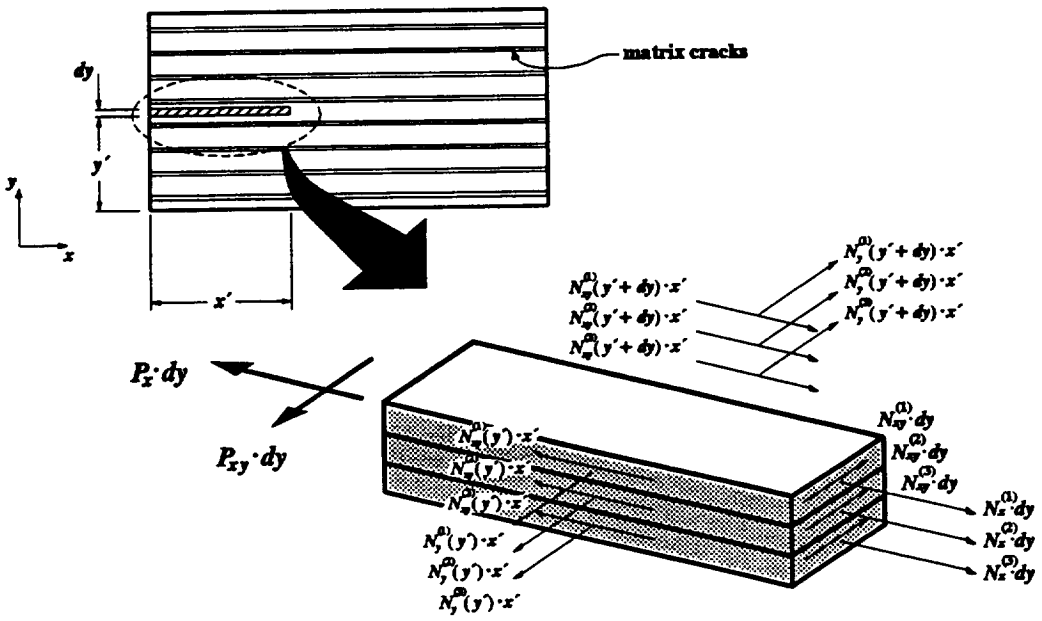

Figure A.4: Free body diagram for section of length x' and width dy.

$y = y' + dy$ are constant due to y being constant on these faces. The reaction forces on the exposed edge of this segment, $x = x'$, vary with y. The average value of the in-plane load $N_x^{(i)}(y)$ over this region can be expressed in integral form as,

$$\bar{N}_x^{(i)} = \frac{1}{dy} \int_{y'}^{y'+dy} N_x^{(i)}(y) dy \tag{A.13}$$

Evaluating this integral using a first-order Taylor series expansion in y', it is found that

$$\bar{N}_x^{(i)} = N_x^{(i)}(y') \tag{A.14}$$

If higher order terms are neglected, the load may be considered constant over the differential span. Similarly, the shear forces acting on this face can also be considered constant.

$$\bar{N}_{xy}^{(i)} = N_{xy}^{(i)}(y') \tag{A.15}$$

Utilizing equations (A.14) and (A.15) and summing forces in the x direction yields the final equilibrium equation,

$$P_x = N_x^{(1)}(y') + N_x^{(2)}(y') + N_x^{(3)}(y') \tag{A.16}$$

Equations (A.11), (A.12) and (A.16) are the final form for the global equilibrium equations for a three layer system with damage present due to transverse matrix cracking.

APPENDIX B

Load Transformation of In-plane Loads

Load terms are typically thought of as vectors (or first order tensors) and are usually specified in units of force [FORCE]. Accordingly, they transform via the first order tensor transformation equation,

$$\begin{Bmatrix} P_{1'} \\ P_{2'} \\ P_{3'} \end{Bmatrix} [\text{FORCE}] = \begin{bmatrix} a_{1'1} & a_{1'2} & a_{1'3} \\ a_{2'1} & a_{2'2} & a_{2'3} \\ a_{3'1} & a_{3'2} & a_{3'3} \end{bmatrix} \begin{Bmatrix} P_1 \\ P_2 \\ P_3 \end{Bmatrix} [\text{FORCE}] \tag{B.1}$$

where the transformation matrix is comprised of the direction cosines $a_{i'j} = \cos(\hat{n}_{i'}, \hat{n}_j)$. However, when referring to laminated plates, and plates in general, in-plane loads are usually specified in units of force per unit length of edge [FORCE/LENGTH]. These *"loads"* are actually stress terms which have been integrated over a linear distance (specifically, the thickness of either the entire plate or an individual layer within the plate).

$$P_x \left[\frac{\text{FORCE}}{\text{LENGTH}}\right] = \int_h \sigma_x(z)dz \tag{B.2}$$

$$P_y \left[\frac{\text{FORCE}}{\text{LENGTH}}\right] = \int_h \sigma_y(z)dz \tag{B.3}$$

$$P_{xy}\left[\frac{\text{FORCE}}{\text{LENGTH}}\right] = \int_h \tau_{xy}(z)dz \tag{B.4}$$

Thus, what is typically referred to as the *applied loading vector*, $\{P_x, P_y, P_{xy}\}$, is actually a convenient grouping in column matrix form of elements which are actually members of a second order tensor, and must therefore be transformed accordingly.

The transformation equation for a second order tensor is given in index notation as,

$$\sigma_{i'j'} = a_{i'k}a_{j'l}\sigma_{kl} \tag{B.5}$$

and in matrix notation as,

$$[\sigma'] = [A][\sigma][A]^T \tag{B.6}$$

The transformation matrix, $[A]$, is defined as

$$[A] = \cos(\hat{n}_{i'}, \hat{n}_j) \equiv \begin{bmatrix} m_1 & n_1 & p_1 \\ m_2 & n_2 & p_2 \\ m_3 & n_3 & p_3 \end{bmatrix} \tag{B.7}$$

For an in-plane rotation as shown in Figure B.1, evaluation of the direction cosines yields,

$$m_1 = n_2 \equiv m = \cos(\theta)$$

$$n_1 = -m_2 \equiv n = \sin(\theta)$$

$$p_1 = p_2 = m_3 = n_3 = 0$$

$$p_3 = 1$$

and results in the following form for the transformation matrix,

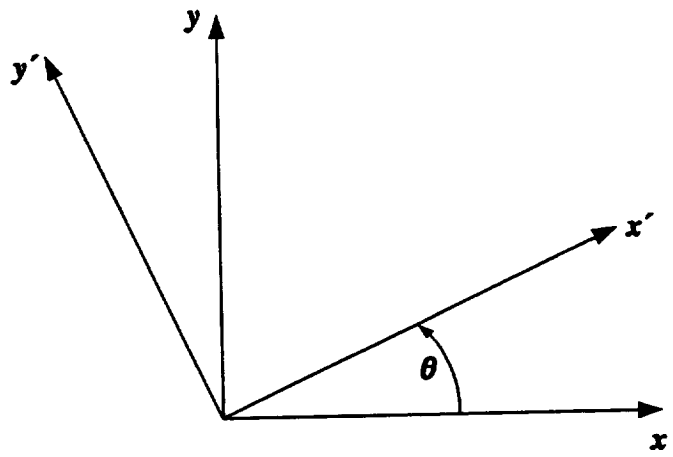

Figure B.1: In-plane transformation of axes.

$$[A] = \begin{bmatrix} m & n & 0 \\ -n & m & 0 \\ 0 & 0 & 1 \end{bmatrix} \tag{B.8}$$

Expanding the matrix multiplications of equation (B.6) for the case of an originally in-plane stress state, the transformed stress tensor is given by

$$\begin{bmatrix} \sigma_{x'} & \tau_{x'y'} & \tau_{x'z} \\ \tau_{x'y'} & \sigma_{y'} & \tau_{y'z} \\ \tau_{x'z} & \tau_{y'z} & \sigma_z \end{bmatrix} = \begin{bmatrix} m & n & 0 \\ -n & m & 0 \\ 0 & 0 & 1 \end{bmatrix} \begin{bmatrix} \sigma_x & \tau_{xy} & 0 \\ \tau_{xy} & \sigma_y & 0 \\ 0 & 0 & 0 \end{bmatrix} \begin{bmatrix} m & n & 0 \\ -n & m & 0 \\ 0 & 0 & 1 \end{bmatrix}^T$$

$$= \begin{bmatrix} \left(m^2\sigma_x + 2mn\tau_{xy} + n^2\sigma_y\right) & \left(-mn\sigma_x + (m^2-n^2)\tau_{xy} + mn\sigma_y\right) & 0 \\ \left(-mn\sigma_x + (m^2-n^2)\tau_{xy} + mn\sigma_y\right) & \left(n^2\sigma_x - 2mn\tau_{xy} + m^2\sigma_y\right) & 0 \\ 0 & 0 & 0 \end{bmatrix} \tag{B.9}$$

We are only concerned with those terms having non-zero values, i.e., $\sigma_{x'}$, $\sigma_{y'}$ and $\tau_{x'y'}$. These non-zero terms can be expressed in the following matrix equation,

$$\begin{Bmatrix} \sigma_{x'} \\ \sigma_{y'} \\ \tau_{x'y'} \end{Bmatrix} = \begin{bmatrix} m^2 & n^2 & 2mn \\ n^2 & m^2 & -2mn \\ -mn & mn & (m^2-n^2) \end{bmatrix} \begin{Bmatrix} \sigma_x \\ \sigma_y \\ \tau_{xy} \end{Bmatrix} \tag{B.10}$$

Similarly, the transformation relation for the in-plane loads is given by,

$$\begin{Bmatrix} P_{x'} \\ P_{y'} \\ P_{x'y'} \end{Bmatrix} \left[\frac{\text{FORCE}}{\text{LENGTH}}\right] = \begin{bmatrix} m^2 & n^2 & 2mn \\ n^2 & m^2 & -2mn \\ -mn & mn & (m^2-n^2) \end{bmatrix} \begin{Bmatrix} P_x \\ P_y \\ P_{xy} \end{Bmatrix} \left[\frac{\text{FORCE}}{\text{LENGTH}}\right] \tag{B.11}$$

The reader should note that a matrix is simply a mathematical grouping device. It is not a tensor, and does not possess the physical characteristics of a tensor. As a result, the transformation of the in-plane loads must be carried out via equation (B.11) and not through the first order tensor transformation equation.

APPENDIX C

Limitations of Generalized Shear-Lag Solution

In Chapter 4, when equation (4.48) was reached in the derivation of the elasticity solution for the damaged region, the problem had been reduced to a second order ordinary differential equation containing two unknowns, $N_{y'}^{(\tilde{1})}$ and $N_{x'y'}^{(\tilde{1})}$. (Note: this appendix reverts back to using the tilde notation to designate the homogenized system). This equation is repeated below in equation (C.1).

$$\frac{d^2 N_{y'}^{(\tilde{1})}}{dy'^2} = \psi_{22}\left(\alpha N_{y'}^{(\tilde{1})} + \eta N_{x'y'}^{(\tilde{1})} + \beta\right) \tag{C.1}$$

In order to solve this equation, an additional independent equation was needed. For this purpose, the local equilibrium equation for layer $\tilde{1}$ in the x' direction (equation (4.15)) was used, and combined with the shear-lag equations, and the thickness correction terms. This resulted in equation (4.53) (rewritten below as equation (C.2)) relating the second derivative of the shear load to the *"difference in strain"* term by the proportionality

constant ψ_{12},

$$\frac{d^2 N_{x'y'}^{(1)}}{dy'^2} = \psi_{12}\left(\bar{\epsilon}_{y'}^{(2)} - \bar{\epsilon}_{y'}^{(1)}\right) \tag{C.2}$$

where

$$\psi_{12} = \frac{1}{2(h_2+h_3)}\left[h_2\left(H_{12}-K_{12}\right) + h_3\left(J_{12}-L_{12}\right)\right] \tag{C.3}$$

By introducing global equilibrium considerations and displacement continuity in the x' direction, this differential equation can be reformulated such that the strain terms are replaced by load terms (equation (4.55/C.4))

$$\frac{d^2 N_{x'y'}^{(1)}}{dy'^2} = \psi_{12}\left(\alpha N_{y'}^{(1)} + \eta N_{x'y'}^{(1)} + \beta\right) \tag{C.4}$$

where α, η and β have been defined in equations (4.49 - 4.51).

For equation (C.4) to provide non-trivial information (i.e., for $\frac{d^2 N_{x'y'}^{(1)}}{dy'^2} \neq 0$), it is necessary to have a non-zero value for ψ_{12}. Therefore, in order to determine the limitations of the solution given in Chapter 4 it must known under what conditions, if any, $\psi_{12} = 0$.

Looking at equation (C.3) the first obvious way in which a zero answer could be achieved is if $h_2 = h_3 = 0$. However, this is not a physical possibility for this problem set and can be disregarded. The second possibility would be if $H_{12} = J_{12} = K_{12} = L_{12} = 0$. To examine whether or not this occurrence is possible, the $[H]$, $[J]$, $[K]$ and $[L]$ matrices are examined in greater detail. These matrices, originally defined in equations (3.28-31) of Chapter 3, are repeated below,

$$[L] = \left[[D]-[C][A]^{-1}[B]\right]^{-1} \tag{C.5}$$

$$[H] = [A]^{-1}+[A]^{-1}[B][L][C][A]^{-1} \tag{C.6}$$

$$[J] = -[A]^{-1}[B][L] \tag{C.7}$$

$$[K] = -[L][C][A]^{-1} \tag{C.8}$$

where $[A]$, $[B]$, $[C]$ and $[D]$ are further defined in terms of the inverses of the layer stiffnesses.

$$[A] = -\frac{h_1}{3}[Q]_1^{-1} - \frac{h_2}{3}[Q']_2^{-1} \tag{C.9}$$

$$[B] = -\frac{h_1}{6}[Q]_1^{-1} \tag{C.10}$$

$$[C] = \frac{h_1}{6}[Q]_1^{-1} \tag{C.11}$$

$$[D] = \frac{h_1}{3}[Q]_1^{-1} + \frac{h_3}{3}[Q']_3^{-1} \tag{C.12}$$

The stiffness matrices appearing in the above equations relate the out-of-plane shear stress to strain for each of the layers, i.e.,

$$\begin{Bmatrix}\tau_{x'z}\\ \tau_{y'z}\end{Bmatrix}_i = \begin{bmatrix}Q'_{55} & Q'_{45}\\ Q'_{45} & Q'_{44}\end{bmatrix}_i \begin{Bmatrix}\gamma_{x'z}\\ \gamma_{y'z}\end{Bmatrix}_i \qquad i=\tilde{1},\tilde{2},\tilde{3} \tag{C.13}$$

with the primes signifying that the terms have been transformed to the $x'-y'$ coordinate system.

If each of the stiffness matrices involved in the above computations were to become diagonal matrices, i.e.,

$$[Q']_i = \begin{bmatrix}Q'_{55} & 0\\ 0 & Q'_{44}\end{bmatrix}_i \qquad i=\tilde{1},\tilde{2},\tilde{3} \tag{C.14}$$

then in all subsequent calculations $\left([Q']\rightarrow[Q']^{-1}\rightarrow[A],[B],[C],[D]\rightarrow[H],[J],[K],[L]\right)$, the off-

diagonal terms would also be zero. Therefore, in order to determine under what conditions $H_{12} = J_{12} = K_{12} = L_{12} = 0$, it is necessary to determine the circumstances leading to the Q'_{45} terms taking on zero values for all three layers at the same time.

The transformed coordinates $x'-y'$ are aligned with the material coordinates of layer $\tilde{1}$, therefore $[Q']_{\tilde{1}} = [Q]_{\tilde{1}}$. Since the material is orthotropic, $Q'^{(\tilde{1})}_{45} = 0$ will always hold true.

Layers $\tilde{2}$ and $\tilde{3}$ are homogenized layers. Their elastic properties come from averaging the elastic properties of all the layers (except for layer i, the layer being analyzed for transverse matrix cracking) from the original system.

$$[Q']_{\tilde{2}} = [Q']_{\tilde{3}} = \frac{1}{\sum_{j=1}^{n} h_j}\left(\sum_{j=1}^{n} h_j [Q']_j\right) \quad ; \quad j \neq i \tag{C.15}$$

The stiffness term Q'_{45} is an odd function of the angle of orientation, that is to say $Q'_{45}(+\theta) = -Q'_{45}(-\theta)$. Therefore, if in the transformed coordinate system the orientations of the undamaged layers are balanced with respect to layer i, the summation of the Q'_{45} for the individual layers will cancel each other out and sum to zero. Thus, if the laminate configuration is balanced with respect to the damaged layer, the off diagonal stiffness term will equal zero. As a result, ψ_{12} will take on a zero value for this case.

Additional possibilities for which ψ_{12} could achieve a zero value are if either $h_2(H_{12} - K_{12}) = -h_3(J_{12} - L_{12})$ or $(H_{12} - K_{12}) = (J_{12} - L_{12}) = 0$ were to occur. Using the symbolic manipulator MACSYMA*, these expressions can be evaluated in terms of the inverted stiffness matrices for each layer. The resulting expressions are extremely complicated in an algebraic sense. The complexity of these expressions makes it

impossible to say without reservation whether either of the above conditions could occur, although it can be stated that it appears unlikely.

Thus, the limitation to the solution of Chapter 4 is that it is not applicable to laminates whose configuration is such that the undamaged layers are balanced with respect to the damaged layer.

APPENDIX D

The PFRAC Algorithm for Laminate Analysis

The computer code PFRAC, Progressive Failure and Reliability Analysis of Composites, which is used in this report models the progressive failure of composite laminates under strain-controlled conditions. The material strengths are considered to be random variables of known distribution, and multiple modes of failure (i.e., longitudinal, transverse, and shear (see Chapter 1)) are considered within each layer. As individual modes fail, corresponding stiffness reductions are made via the shear-lag methods of Chapters 3 and 4, as well as traditional ply drop-off (or in this case *mode drop-off*) techniques. Monte Carlo methods are employed to determine the cumulative distribution curves for the laminate's probability of failure as a function of the applied strain. This Appendix provides an overview of theory and logic behind the PFRAC code.

SIMULATING THE STRAIN CONTROLLED TEST

The PFRAC code simulates a strain-controlled environment. The laminated plate in-

plane constitutive relationship is given by (Jones, 1975)

$$\begin{Bmatrix} \epsilon^{\circ} \\ \kappa \end{Bmatrix} = \begin{bmatrix} A' & B' \\ H' & D' \end{bmatrix} \begin{Bmatrix} N \\ M \end{Bmatrix} \tag{D.1}$$

with ϵ° being the mid-plane strains, κ being the plate curvatures, and N and M being the in-plane loads and moments, respectively. The prescribed conditions on the system to be modeled are: a known value for the applied axial strain, $(\epsilon_x)_{applied}$, stress-free states for the in-plane transverse and shear loads ($N_y = 0$ and $N_{xy} = 0$), and moment-free in-plane conditions ($M_x = M_y = M_{xy} = 0$). Substituting these known conditions into equation (D.1), the unknown strains and loads are given by the following expressions,

$$N_x = A'_{11} \cdot (\epsilon_x)^{-1}_{applied} \tag{D.2a}$$

$$\epsilon_y = A'_{21} \cdot N_x \tag{D.2b}$$

$$\gamma_{xy} = A'_{31} \cdot N_x \tag{D.2c}$$

Thus, all in-plane strains and loads can be determined as a function of the applied longitudinal strain.

With the full in-plane strain vector known, the stresses within each layer can be determined

$$\begin{Bmatrix} \sigma_x \\ \sigma_y \\ \tau_{xy} \end{Bmatrix}_i = [\bar{Q}]_i \begin{Bmatrix} \epsilon_x \\ \epsilon_y \\ \gamma_{xy} \end{Bmatrix} \tag{D.3}$$

In equation (D.3), $[\bar{Q}]_i$ represents the stiffness matrix of layer i transformed to the global coordinate system. These individual layer stresses can, in turn, be transformed back to the

material coordinate systems for a specified layer, and these stresses can be compared to the corresponding material strengths, $\hat{X}$, in order to evaluate failure (i.e., $f \geq 1$).

$$f_{1_i} = \left(\frac{\sigma_1}{\hat{X}_1} \right)_i \qquad f_{2_i} = \left(\frac{\sigma_2}{\hat{X}_2} \right)_i \qquad f_{6_i} = \left(\frac{\sigma_6}{\hat{X}_6} \right)_i \qquad \text{(D.4a,b,c)}$$

Based on the stress solution for a very small applied strain, the program can determine which failure mode will be the first to fail and step to the applied strain level corresponding to its failure. This is possible due to the linear behavior of the undamaged composite. The strain is increased incrementally from this point forward.

Once a failure state has been attained in an individual mode, steps must be taken to reduce the stiffness of that mode in an appropriate manner. Failure of modes 1 and 6 are one time occurrences; that is, once they fail, their corresponding stiffnesses (E_1 for mode 1 and G_{12} for mode 6) are reduced and they are dropped from future computations all together. (Note, the stiffnesses are reduced by a factor of 10^{-7} rather than being set equal to zero. This is done to avoid encountering singularity problems in succeeding computations.) A mode 2 failure is modeled using the shear-lag theory which allows for the damage evolution to be included rather than having complete damage being imposed immediately as is done with the drop-off techniques.

The shear-lag model determines the effective elastic properties of the damaged layer based on the homogenized elastic properties of the rest of the laminate and the present value of the in-plane strain vector $\{\epsilon_x, \epsilon_y, \gamma_{xy}\}^T$. However, referring to equations (D.2), it is apparent that the in-plane strains are calculated as a function of the laminate stiffness. The new predicted values for the effective stiffness of the damaged layer will influence the

updated values for the in-plane strains. Thus, an iterative process is required. The following cost function is set up,

$$C = \sqrt{\left(\epsilon_y - \epsilon_y^*\right)^2 + \left(\gamma_{xy} - \gamma_{xy}^*\right)^2} \tag{D.5}$$

where ϵ is the previous strain value, and ϵ^* is the updated strain value. Note that ϵ_x does not appear in the cost function because its value is known and remains fixed until incremented to the next strain level. Theoretically, the correct solution has been reached when the cost function equals zero. Within PFRAC, the convergence criteria has been set to $C < 1\times10^{-8}$. Experience indicates convergence to this value happens quickly, and this particular value returns relatively good accuracy for the corresponding strain values.

When the interfacial shear stress reaches its limit, and no increase in load transfer is possible, then this mode is considered to be finally failed. However, while no additional load can be sustained by the layer, it is assumed that the layer continues to carry the load that it presently bears. This assumption is accounted for by storing the current layer load in a buffer and reducing the stiffnesses of the layer by a factor of 10^{-7}, so as to effectively remove the layer from all future computations. The loads contained in the buffer are then appended to the computed laminate loads when evaluating the total load supported by the laminate.

After all the necessary stiffness reductions have been completed, the $[A]$, $[B]$ and$[D]$ matrices of the laminate constitutive equation are reformulated, and subsequently the stress solution is updated. If additional failures are encountered under the updated stress state (as in a "domino effect"), the appropriate stiffness reductions are made in the manner just presented. If no additional failures have arisen, the applied strain is incremented, and the

stress state is evaluated for the new applied strain. The whole process continues until total laminate failure is reached. There are two criteria by which total laminate failure is judged. The first criterion accounts for a sudden drop in the load bearing capacity of the laminate. If, for a given applied strain, internal failures occur resulting in a decrease in the load by 50% or greater, criterion 1 has been met. A gradual decrease (i.e., over a range of strain values) of 50% is allowable, only a sudden decrease fails the laminate. The second criterion deals with the positive definiteness of the material stiffness matrix. The stiffness matrix for any material is required to be positive definite in order to ensure that the strain-energy density function be closed and convex. Thus if the effective stiffness matrix calculated to satisfy the shear-lag model no longer abides by this requirement, the laminate is considered failed.

PROBABILISTIC CONSIDERATION

It is assumed that the material strengths, X_i (i = 1, 2 and 6) corresponding to each of the individual failure modes are characterized by a Weibull distribution, i.e.,

$$F_{X_i}(\sigma_i) = 1 - \exp\left[-\left(\frac{\sigma_i}{\beta_i}\right)^{\alpha_i}\right] \tag{D.6}$$

where the distribution parameters (α_i, β_i) characterizing each failure mode can be obtained from strength data. Due to the random nature of the strengths, the reliability for an individual *hypothetical* sample will have a value between zero and one inclusive such that

$$F_{X_i} = 1 - u \tag{D.7}$$

where u is a uniform random variable contained on the interval [0,1].

Substituting equation (D.7) into equation (D.6) and inverting the distribution function yields the following realization of the random strength variable,

$$\hat{X}_i = \beta_i[-\ln(1-u)]^{-\alpha_i} \tag{D.8}$$

Here $\hat{X}_i$ represents a sample value of X_i. By utilizing a uniform random number generator to obtain values of u, realizations of the strength can be obtained. Within the Monte Carlo procedure, this is done many times in order to achieve a sample population for the material. This sample population is analyzed for failure in the manner described in the previous section, and the applied strain present at failure is saved. The recorded failure strains are then ranked and assigned a corresponding probability of failure, p, using a median ranking

$$p_j = \frac{j - 0.3}{n + 0.4} \quad ; \quad j = 1,2,3,...,n \tag{D.9}$$

where n is the total number of samples.

BIBLIOGRAPHY

Agarwal, B. and Broutman, L., **Analysis and Performance of Fiber Composites**, John Wiley and Sons Publishing, New York (1980).

Aveston, J., Cooper, G.A. and Kelly, A.,"The Properties of Composite Materials," IPC Sci Tech (1971), p.15-26.

Bhatt, R.T. and Phillips, R.E.,"Laminate Behavior for SiC Fiber-Reinforced Reaction-bonded Silicon Nitride Matrix Composites,"J Compos Tech Res(ASTM) 12(Spring 1990), pp.13-23; also NASA TM 101350 (1988).

Daniels, H.E.,"The Statistical Theory of the Strength of Bundles of Threads. I," Proc. Royal Soc London 183A (1945), pp.405-435.

Evans, A.G. and Marshall, D.B.,"The Mechanical Behavior of Ceramic Matrix Composites," Acta metall 37 (1989), pp.2567-2583.

Garrett, K.W. and Bailey, J.E., "Multiple Transverse Fracture in 90° Cross-ply Laminates of a Glass Fiber-reinforced Polyester," J Matl Sci 12 (1977), pp.157-168.

Jones, R.M., **Mechanics of Composite Materials**, Hemisphere Publishing Corporation, New York (1975).

Kerans, R.J., "Dependence of Composite Properties Upon Statistical Variations in Fiber Length," Ceram Eng Sci Proc 9 (1988), pp.613-620.

Laws, N. and Dvorak, G.J., "Progressive Transverse Cracking in Composite Laminates," J Comp Matl 22 (1988), pp.900-916.

Lee, J.W. and Daniel, I.M., "Progressive Transverse Cracking of Crossply Laminates,"

J Compos Matl 24 (1991), pp.1225-1243.

Nuismer, R.J. and Tan, S.C., "Constitutive Relations of a Cracked Composite Lamina," J Comp Matl 22 (1988), pp.306-321.

Oh, H.L. and Finnie, I., "On the Location of Fracture in Brittle Solids - I: Due to Static Loading," Int J of Frac Mech 6 (1970), pp.287-300.

Petit, P.H. and Waddoups, M.E.,"A Method for Predicting the Nonlinear Behavior of Laminated Composites," J Compos Matl 3(1969), pp.2-19.

Reifsnider, K.L., "Mechanics of Failure of Composite Materials," Proc of the 10th Symposium on Naval Structural Mechanics, George Washington University, Washington D.C., (1978), pp.317-331.

Reifsnider, K.L. and Highsmith, A.,"The Relationship of Stiffness Changes in Composite Laminates to Fracture Related Damage Mechanisms," Frac of Compos Matl, Proc. of 2nd USA-USSR Symposium, Bethlehem, PA, 1981. ed. G.C. Sih, V.P. Tamuzs, pp.279-290.

Reismann, H. (and Wetherhold, R.C.), **Elastic Plates: Theory and Application**, John Wiley and Sons Publishing, New York (1988).

Talreja, R., "Transverse Cracking and Stiffness Reduction in Composite Laminates," J Comp Matl 19 (1985), pp.355-375.

Thomas, D.J. and Wetherhold, R.C.,"Reliability Analysis of Continuous Fiber Composite Laminates," Compos Struc 17 (1991(a)), pp.277-293.

Thomas, D.J. and Wetherhold, R.C.,"Reliability Analysis of Composite Laminates with Load Sharing," J Compos Matl 25 (1991(b)), pp.1459-1475.

Tsai, C.-L., Daniel, I.M., and Lee, J.-W., "Progressive Matrix Cracking of Crossply

Composite Laminates Under Biaxial Loading," Microcracking Induced Damage in Composites, AMDIII/MD22, ed. G.J. Dvorak, D.C. Lagoudas, ASME (1990), pp. 9-18.

Tsai, C.-L., personal communication (1993).

Walls, D.J., M.S. Thesis, Univ. of California, Berkeley (1986).

Wetherhold, R.C., "Statistical Distribution of Strength of Fiber-Reinforced Composite Materials," Polymer Compos 7 (1986), pp.116-123.

Wetherhold, R.C., "The Sensitivity of Fracture Location Distribution in Brittle Materials," Int J of Frac 49 (1991), pp.305-315.

REPORT DOCUMENTATION PAGE

Form Approved
OMB No. 0704-0188

1. AGENCY USE ONLY (*Leave blank*)	2. REPORT DATE	3. REPORT TYPE AND DATES COVERED
	February 1995	Final Contractor Report

4. TITLE AND SUBTITLE

Analysis of the Progressive Failure of Brittle Matrix Composites

5. FUNDING NUMBERS

WU–537–04–22
G–NAG3–862

6. AUTHOR(S)

David J. Thomas

7. PERFORMING ORGANIZATION NAME(S) AND ADDRESS(ES)

S.U.N.Y. at Buffalo
Department of Mechanical and Aeronautical Engineering
Jarvis Hall
Buffalo, New York 14260–1700

8. PERFORMING ORGANIZATION REPORT NUMBER

E–9337

9. SPONSORING/MONITORING AGENCY NAME(S) AND ADDRESS(ES)

National Aeronautics and Space Administration
Lewis Research Center
Cleveland, Ohio 44135–3191

10. SPONSORING/MONITORING AGENCY REPORT NUMBER

NASA CR–195415

11. SUPPLEMENTARY NOTES

Project Manager, John P. Gyekenyesi, Structures Division, NASA Lewis Research Center, organization code 5250, (216) 433–3210.

12a. DISTRIBUTION/AVAILABILITY STATEMENT

Unclassified - Unlimited
Subject Categories 24, 27, 39, and 65

This publication is available from the NASA Center for Aerospace Information, (301) 621–0390.

12b. DISTRIBUTION CODE

13. ABSTRACT ***(Maximum 200 words)***

This report investigates two of the most common modes of localized failures; namely, periodic fiber-bridged matrix cracks, and transverse matrix cracks. A modification of Daniels' bundle theory is combined with Weibull's weakest link theory to model the statistical distribution of the periodic matrix cracking strength for an individual layer. Results of the model predictions are compared with experimental data from the open literature. Extensions to the model are made to account for possible imperfections within the layer (i.e., non-uniform fiber lengths, irregular crack spacing, and degraded in-situ fiber properties), and the results of these studies are presented. A generalized shear-lag analysis is derived which is capable of modeling the development of transverse matrix cracks in material systems having a general multilayer configuration and under states of full in-plane load. A method for computing the effective elastic properties for the damaged layer at the global level is detailed based upon the solution for the effects of the damage at the local level. This methodology is general in nature and is therefore also applicable to $[0_m/90_n]_s$ systems. The characteristic stress-strain response for more general cases is shown to be qualitatively correct (experimental data is not available for a quantitative evaluation), and the damage evolution is recorded in terms of the matrix crack density as a function of the applied strain. Probabilistic effects are introduced to account for the statistical nature of the material strengths, thus allowing cumulative distribution curves for the probability of failure to be generated for each of the example laminates. Additionally, Oh and Finney's classic work on fracture location in brittle materials is extended and combined with the shear-lag analysis. The result is an analytical form for predicting the probability density function for the location of the next transverse crack occurrence within a crack bounded region. The results of this study verified qualitatively the validity of assuming a uniform crack spacing (as was done in the shear-lag model).

14. SUBJECT TERMS

Fiber bridging; Transverse matrix cracks; Weibull; Shear lag; Composite materials; Ceramics; Reliability

15. NUMBER OF PAGES

120

16. PRICE CODE

A06

17. SECURITY CLASSIFICATION OF REPORT	18. SECURITY CLASSIFICATION OF THIS PAGE	19. SECURITY CLASSIFICATION OF ABSTRACT	20. LIMITATION OF ABSTRACT
Unclassified	Unclassified	Unclassified	

National Aeronautics and
Space Administration

Lewis Research Center
21000 Brookpark Rd.
Cleveland, OH 44135-3191